TECHNISCHE UNIVERSITÄT WIEN
Vienna University of Technology

DIPLOMARBEIT

Development of a bioprocess for recombinant protein production with a *Pichia pastoris och1* knock-out strain

Ausgeführt am Institut für Biochemical Engineering

der Technischen Universität Wien

unter der Anleitung von

Univ.Prof. Dr. Christoph Herwig

und

Univ.Ass. Dipl.-Ing. Dr.nat.techn. Oliver Spadiut

durch

Christoph Gmeiner

Weidmanngasse 15/46, 1170 Wien

Wien, 23.05.2014

Abstract

The methylotrophic yeast *Pichia pastoris* is a widely used host organism for recombinant protein production in biotechnology and biopharmaceutical industry. However, if the target product describes a glyco-protein, the yeast has the tendency for hypermannosylation triggered by the enzyme α-1,6-mannosyltransferase. The resulting heterogeneous and vast glycosylation pattern on the surface of the recombinant protein hampers traditional downstream processes and limits biopharmaceutical applications.

In this Thesis, a controllable bioprocess with a *P. pastoris* strain, where the responsible gene (*och1*) for hyperglycosylation was knocked out, was developed. Due to a drastically altered morphology of the *P. pastoris och1* knock-out strain compared to the wildtype, various unusual effects were observed: cell lysis, foam formation, a risk of overfeeding and low productivity of the medically relevant recombinant enzyme horseradish peroxidase (HRP). In a multivariate Design of Experiments (DoE) approach, three potential productivity-influencing process parameters - temperature, pH and dissolved oxygen concentration - were analyzed to determine a parameter area for high recombinant protein production. Expression, purification and biochemical characterization of the model protein HRP were also part of this Thesis. Finally, the less-glycosylated enzyme variant, which can be also used for targeted cancer treatment, was analyzed for its reactivity with the prodrug indole-2-acetic acid.

A controllable bioprocess for this *P. pastoris och1* k.o. strain was successfully developed and with the aid of it an expression of recombinant proteins in a less-glycosylated form is possible. Furthermore, a potential candidate for targeted cancer treatment studies could be determined by analyzing various HRP samples.

Kurzfassung

Die methylotrophe Hefe *Pichia pastoris* ist ein weitverbreiteter und bislang gut studierter Mikroorganismus für die biotechnologische Herstellung rekombinanter Proteine und spielt daher auch in der biotechnologischen, so wie in der pharmazeutischen Industrie eine wichtige Rolle.

Die rekombinant hergestellten Proteine in dieser Hefe werden aufgrund des Enzyms α-1,6-mannosyltransferase im Sekretionsweg hyperglykosyliert. Diese Hyperglykosylierung ändert den Downstream-Prozess und verhindert den Einsatz rekombinant hergestellter Proteine in der Medizin, beispielsweise als Pharmazeutika, da diese genannte Hyperglykosylierung im menschlichen Körper eine Immunantwort auslöst.

Diese Arbeit präsentiert die Entwicklung eines Bioprozesses für einen *P. pastoris* Stamm, in dem das verantwortliche Gen für die zuvor erwähnte α-1,6-Mannosyltransferase entfernt wurde. Zudem wurde das medizinisch relevante Enzym Meerrettichperoxidase produziert, welches auch in der Krebstherapie eingesetzt werden kann. In einem Design of Experiment Ansatz wurden Prozessparametereinflüsse von Temperatur, pH und gelöster Sauerstoffkonzentration auf die Produktivität untersucht und somit eine Parameterregion erforscht, bei der die Produktion dieses Meerrettichenzyms in dem verwendeten *P. pastoris och1* k.o. Stamm hoch ist. Somit steht diesem gentechnisch veränderten Stamm zum ersten Mal ein kontrollierter Bioprozess zur Verfügung. Zudem wurden die produzierten Enzyme gereinigt und auf ihre kinetischen Konstanten untersucht.

Zuletzt wurden die hergestellten weniger glykosylierter Meerrettichenzyme auf eine mögliche Anwendung für eine gezielte Krebstherapie untersucht und ein möglicher Kandidat für weiter Untersuchungen diesbezüglich aus verschiedenen Meerrettichenzymproben ermittelt.

CONTENTS

1 Motivation & Goals

Recombinant protein production is an extensively studied field in biotechnology and therefore various expression systems - bacteria, fungi and yeast species, insect or mammalian cells - are used in different industrial sectors as in pharmaceutical industry, nutrition technology as well as in chemical industry to produce recombinantly several proteins and substances.

The yeast *Pichia pastoris* is a favored host organism due to its advantages like the absence of endotoxins in the fermentation broth or its ability to perform all post translational modifications.

However, the high glycosylation capacity of this methylotrophic yeast changes downstream processing of the recombinant proteins and may trigger immunogenic reactions when they are injected into the human body [1]. Thus, glycosylation is an important set-screw for therapeutic and pharmaceutical products. One method to reduce the hyperglycosylation of recombinant proteins is the engineering of the glycosylation pathway by knocking out endogenous mannosyltransferases, as for example the gene *och1* (Outer CHain elongation), which initiates the hypermannosylation [2-6]. We could describe batch cultivations with such a *P. pastoris och1* k.o. strain and their corresponding cultivation challenges [2]. Although some studies of recombinant protein production in such a modified *P. pastoris* strain can be found [3-6], a detailed method of a controlled bioprocess is still missing.

As a model protein horseradish peroxidase (HRP), an enzyme derived from the horseradish root (*Armoracia rusticana*), was expressed in this *P. pastoris och1* knock-out strain. Among others, this enzyme can be used for targeted cancer treatment. Earlier studies showed that this heme-peroxidase is able to oxidize the plant hormone indole-3-acetic acid (IAA) without requiring hydrogen peroxide (H_2O_2) as an oxidant, resulting in cytotoxic by-products which

induce cell apoptosis of cancerous cells when both is injected to human bladder carcinoma cells [1, 7-11]. Extraction from the plant - where HRP is present as a mixture of 19 isoenzymes - is the current method to produce HRP, whereby this process is very cost-intensive and time-consuming [12]. To use HRP as pharmaceutical, the final product should be only one purified isoenzyme, because the Food and Drug Association (FDA) would not authorize a pharmaceutical consisting as a mixture of 19 different isoenzymes.

This work describes a new and high-performance bioprocess for this *P. pastoris och1* k.o. strain for the first time, which may be interesting not only for rHRP production but also for less-glycosylated recombinant proteins in general. An easy and simple feeding strategy was applied doing a fed-batch on methanol under controlled conditions. Performing a multivariate Design of Experiments (DoE) screening - a more time-saving procedure compared to univariate studies -, a region for high productivity of this strain was determined. Moreover, the DoE gives an insight into parameter-interactions, which cannot be investigated using traditional one-parameter variations. This Thesis provides a detailed knowledge for recombinant protein production in this *P. pastoris och1* k.o. strain, in which process challenges could be solved and the process itself could be done under controlled conditions.

<u>The goals of this Thesis can be summarized as:</u>

- Development of a bioprocess for the *P. pastoris och1* k.o. strain under controlled conditions to express less-glycosylated recombinant proteins
- Investigation of three potential productivity-influencing process parameters during the induction phase, using a Design of Experiments (DoE) screening to find an area for high production of less-glycosylated rHRP isoenzyme A2A

- Analysis if the different process conditions in the upstream processing(USP) influence the downstream processing of the products (DSP); performing a 2-step purification and biochemical characterization
- Enzyme/prodrug combination studies of several HRP samples for a potential utilization for targeted cancer treatment at the Department of Oncology at the University of Oxford

2 Introduction

2.1 The expression system *Pichia pastoris*

2.1.1 A historical overview

The yeast *Pichia pastoris* had its beginnings during the 1970s when Philips Petroleum Company developed protocols for growing it on methanol at high cell densities (more than 130 g/dry cell weight [13]) and using this yeast as an alternative for animal feed production. One advantage was the ability to exploit methanol which was a cheap carbon source at that time. Due to the oil crisis during the 1970s, the prize for this carbon source increased extensively and simultaneously the price of soybeans fell, resulting in the utilization of the plant source for animal feed production and *P. pastoris* was not competitive any more.

Afterwards, the Philips Petroleum company and the Salk Institute Biotechnology (SIBIA, La Jolla, USA) investigated a potential utilization of this yeast as a expression host for heterologous proteins, in which the promoter for alcohol oxidase (p*AOX*) was isolated and investigated. Moreover, recombinant vector constructions, fermentation and transformation methods as well as selectable markers have been developed in the last 20 years. The *AOX*-promoter system was sold to SLR Research Corporation (Carlsbad, CA), who is the current holder of the patent for the *P. pastoris* expression system and distributes it since 1993 [14].

The methylotrophic yeast *Pichia pastoris* is nowadays an extensively studied host for recombinant protein production in biotechnology. The advantages of this yeast are its potential to grow on methanol, achieving high yields, the absence of endotoxins and the ability to perform all post-translational modifications (PTMs) of higher eukaryotes [13-15].

2.1.2 Methanol metabolism and phenotypes of *P. pastoris*

P. pastoris is one of 4 yeast genera, which can grow on methanol: *Hansenula, Pichia, Candida* and *Torulopsis* [14]. All of them use the methanol utilization pathway (MUT) to exploit the substrate [12]. The initial reaction occurs in the peroxisomes followed by further metabolic steps in the cytoplasm. Three key enzymes of the methanol metabolism exist, alcohol oxidase (AOX), catalase and the enzyme dihydroxyacetone synthase [13, 14].

Focused on the methanol metabolic pathway in this yeast, AOX is produced when *P. pastoris* grows on methanol. In the further methanol pathway, AOX oxidizes methanol and forms formaldehyde with the byproduct hydrogen peroxide, which is then oxidized by the enzyme catalase. Subsequently formaldehyde is condensed with xylulose-5-phosphate to dihydroxy-acetone, a reaction which is catalyzed by the dihydroxyacetone synthase (DAS) [14, 15].

The enzyme AOX is encoded by two genes, *AOX1* and *AOX2*, whereat *AOX2* shows 10-20 times less activity than *AOX 1* [16]. Three different phenotypes of *P. pastoris* are known with regard to their methanol utilization ability: Mut^+, Mut^S, Mut^-.

In a Mut^+ strain (methanol utilization plus), both *AOX* genes are active and intact, resulting in higher growth rates and productivities than the other phenotypes [17]. Due to high cell densities and a sensitivity to transient high methanol concentrations, scale up of bioprocesses are difficult for this phenotype. The Mut^S strain (methanol utilization slow) has an intact *AOX2* gene but a knocked-out *AOX1* gene, which ends up in lower methanol consumption rates, longer induction times and reduced growth rates [15]. However, a few studies showed that Mut^S strains are advantageous over Mut^+ strain for the production of some recombinant proteins [18-20]. The Mut^- strain (methanol utilization minus) has neither an intact *AOX1* nor an *AOX2* gene. Thus this phenotype is unable to grow on methanol but is still inducible on it.

2.1.3 Secretion pathway in *P. pastoris:* N-linked glycosylation

Glycosylation is one of the most important PTMs, but also a very complex mechanism performed in *P. pastoris* [14]. Recombinant proteins expressed in *P. pastoris* show the same *N*-glycosylation steps as mammalian cell cultures, when the proteins are transported from the cytoplasm to the Endoplasmatic reticulum. *N*-glycosylation means the addition of oligosaccharides on the amino acid asparagine resulting in the structure Asn-X-Ser/Thr, whereat X can be any amino acid except proline. The well understood biosynthesis of *N*-glycans is triggered by the transfer of *N*-acetylglucosamine (GlcNAc) from uridine diphosphate to dolichol-phosphate, resulting in a dolichol-phosphate-linked *N*-acetyl-glucosamine (DolP-GlcNAc). Five mannose chains are added to this DolP-GlcNAc, which is subsequently transferred into the Endoplasmatic reticulum by the enzyme flippase. Further, glucose and mannose sugar chains are linked to DolP-GlcNAc ending up in a $Glc_3Man_9GlcNAc_2$ - glycan structure. In the following steps, glucosidase I and II trim three glucose residues and a α-1,2-mannosidase further removes one mannose residue resulting in a $Man_8GlcNAc_2$-glycan structure [2, 21-23]. Up to this point, *N*-glycosylation in mammalians and yeasts is identical.

In the Golgi apparatus of mammalians, another α-1,2-mannosidase trims several mannose residues, which reduces the core glycan to $Man_5GlcNAc_2$. Due to the presence of β-*N*-acetylglucosaminyl-transferase I (GnTI), mannosidase II and different transferases which add GlcNAc, galactose and sialic acid end up in complex *N*-glycosylated protein structures [24].

In contrast, *N*-glycan trimming does not exist in the yeast's Golgi apparatus, but the enzyme α-1,6-mannosyltransferase (Och1p), encoded by the gene **O**uter **CH**ain elongation 1 (*och1*), triggers hyperglycosylation/-mannosylation in yeasts, which was first characterized in the baker's yeast *S. cerevisiae*, where α-1,6-mannosyltransferase links mannose sugar chains to the core glycan by an α-1,6-glycosidic bond [25, 26] (Figure 1). This mentioned enzyme

covers the initial step of hypermannosylation in yeasts. After the addition of one mannose to the transported protein by the α-1,6-mannosyltransferase, hypermannosylation is continued by further phosphomannosyltransferases adding numerous mannose sugars. Consequently, a produced recombinant protein will be surrounded by a high amount of mannose chains, which will change the molecular weight of the protein and maybe therefore its purification or also its functionality, activity or solubility [14, 27, 28].

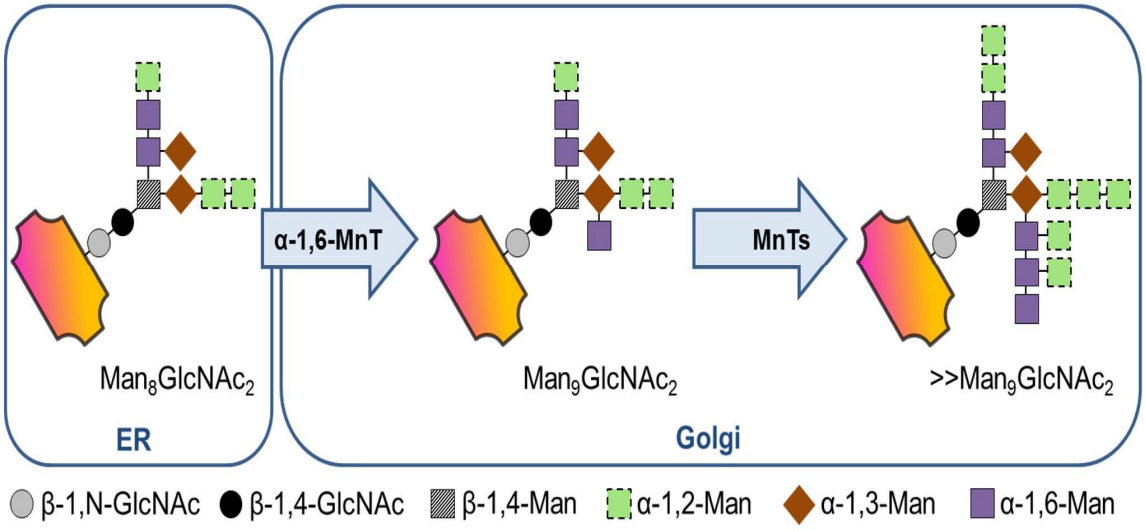

Figure 1: Transport of a protein from the ER to the Golgi apparatus of *P. pastoris*. The enzyme α-1,6-mannosyltransferase adds mannose chains on the protein resulting in a glycan structure >>$Man_9GlcNAc_2$.

2.1.4 Humanization of *P. pastoris*

Due to the hyperglycosylation in *P. pastoris*, recombinantly produced proteins in this yeast cannot be used as pharmaceuticals because they trigger immune responses in humans [14]. This issue turned more attention to the modification of this yeast's glycosylation pathway.

One aim was the humanization of the *N*-glycosylation pathway in *P. pastoris* by knocking out the yeast's initial gene for *N*-glycosylation (*och1*) and inserting the genes for α-1,2-

mannosidase and the human β-1,2-*N*-acetylglucosaminyltransferase I (GnTI). Recombinant expression of a human reporter protein in such engineered strains delivered a glycoprotein with GlcNAc-(Man)(5)-(GlcNAc)(2) as the primary *N*-glycan [28].

Another method described the disruption of the *PNO1* gene of *P. pastoris*, resulting in a reduction of *N*-linked glycosylation of a recombinant human antithrombin. In this study it was shown that the glycosylation could be reduced from 20 % to approx. 1 % using a *P. pastoris* wildtype strain [14].

Hamilton et al. (2006) showed a strategy for the engineering of the glycosylation pathway, in which the yeast's endogenous glycosylation pathways were removed and five key eukaryotic enzymes were localized to obtain a glycosylation pathway, which delivered a complex human sialylated *N*-glycan. This study described a knock-out of four genes to eliminate the yeast's specific glycosylation pathway and the introduction of 14 heterologous genes, which allowed the replication of the sequential steps of human glycosylation. Moreover, it could be shown that recombinantly produced proteins delivered a fully complex terminally sialylated human *N*-glycan [29].

Due to laborious steps to engineer such strains, where numerous genes are knocked-out and others are introduced, the growth of those strains may be influenced and hampered, which would be a disadvantage for an industrial approaches.

2.2 Horseradish peroxidase

2.2.1 Origin and structure

The enzyme horseradish peroxidase (HRP; EC 1.11.1.7) is a heme-containing enzyme, originated in the root of the horseradish (*Armoracia rusticana*). This peroxidase can oxidize various substrates such as aromatic phenols, indoles, amines or phenolic acids [30, 31].

The horseradish peroxidase extract from the plant consists as a mixture of 19 isoenzymes, whereat isoenzyme C1A is the most studied one and captures approximately 70 % of the plant HRP [12].

The 3-dimensional structure of HRP C1A expressed in *E. coli* was solved by X-ray crystallography based on the work of Smith et. al [32]. This isoenzyme consists of a single polypeptide chain of 308 amino acids with a molecular weight of 35 kDa. Furthermore, this enzyme forms 4 disulfide bridges between cysteine residues (11-91, 44-49, 97-301, 177-209) and a buried salt bridge between Asp99 and Arg123. Two different metal centers are present in HRP C1A. The first one is the iron(III) protoporphyrin IX, which represents the heme group, and the second metal centre consists of two calcium ions (Figure 2). The heme group is linked to the enzyme at His170 and the two calcium binding sites are located at positions distal and proximal to the heme plane. However, both metal centers are very important for the biological activity of the enzyme as well as for the structure [30].

Furthermore, the plant HRP offers 9 potential *N*-glycosylation sites and 8 of those are occupied in the plant (N13, N57, N158, N186, N198, N214, N250, N268) showing the motif Asn-X-Ser/Thr, where X can be any amino acid but proline (Figure 3).

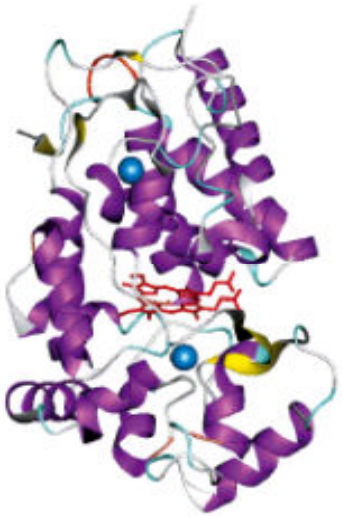

Figure 2: 3-dimensional structure of HRP C1A. A heme plane (red) and two calcium ions (blue dots) are located in the centre. The structure is mainly α-helical with small regions of β-sheets [30].

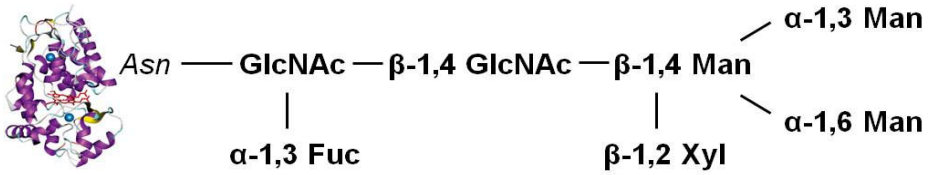

Figure 3: Glycosylation pattern of plant HRP showing a core structure of two N-acetylglucosamines (GlcNAc), a fucose (Fuc), a xylose (Xyl) and 3 mannose molecule (Man)

2.2.2 Catalytic mechanism

The catalytic mechanism of HRP was investigated nearly 15 years ago [31, 33]. Figure 4 shows the catalytic cycle of this heme peroxidase. As mentioned before, HRP is able to oxidize substrates as aromatic phenols, indoles, amines or phenolic acids. These substrates, which can be inorganic or organic compounds, are oxidized in the reaction by HRP, whereas the reaction partner H_2O_2 is reduced to water. The substrate acts in this reaction as electron

donor and H_2O_2 as acceptor. Two one-electron reduction steps occur in this catalytic cycle, resulting in the formation of the HRP compound I and II.

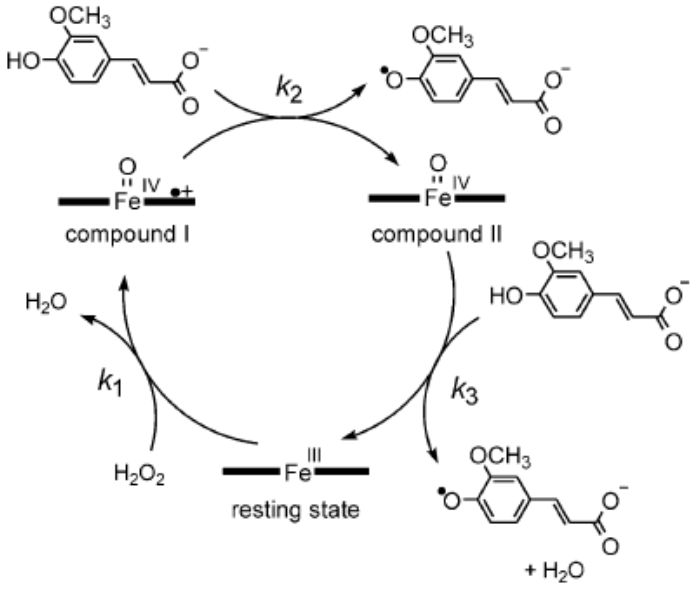

Figure 4: Catalytic cycle of HRP. The reducing substrate ferulate is converted in two intermediates via two one-electron reduction steps forming HRP compound I, II and the resting state, whereby k_1, k_2 and k_3 represent the respective compound formation rates [30].

The first step describes the reaction of H_2O_2 and the Fe(III) to HRP compound I. This intermediate, which is two oxidizing equivalents above the resting state, reacts in a one-electron reduction step to HRP compound II and to a Fe(IV) oxoferryl species. Compound II is one oxidizing equivalent above the resting state. Thus, a second one-electron reduction step occurs, resulting in the resting state of the HRP (Figure 4).

2.2.3 Applications and production of HRP

The traditional HRP production by extracting the enzyme from the plant is a laborious and cost-intensive procedure including ultrasonication, ammonium-sulfate precipitation and/or several chromatographic purification steps [34]. Moreover, the achievable yields are low and the received product is not a single isoenzyme, but a mixture of various isoenzymes, which hampers the application as pharmaceutical due to the needful authorization by the FDA [12, 30].

The HRP mixture derived from the plant consists of varying isoenzyme compositions that are subject to seasonal changes and external influences [35]. Because of the broad range of applications of HRP in biotechnology, industry and medicine, there is an increasing demand of homogenous and highly pure preparation of just 1 single isoenzyme. Thus, several attempts to produce HRP recombinantly in different host organisms were executed in the last decades. Smith et al. (1990) for example expressed rHRP in *E.coli*, which resulted in the formation of inclusion bodies and thus required a cumbersome refolding step ending up with very low yields [32]. However, this study showed that rHRP can be active without sugar chains on it. Also insect and mammalian cells were tested as potential recombinant hosts for HRP, but yields were low and such procedures are expensive and laborious [36, 37].

Another approach was the production in yeasts like *S. cerevisiae* and *P. pastoris,* where the target protein showed extensive hyperglycosylation, but in case of *P. pastoris* less mannose sugar chains are added to the target protein compared to the baker's yeast. For both hyperglycosylated protein species, no efficient downstream strategy was available [38, 39]. Recently, a fast and efficient 2-step purification protocol was developed, allowing a simple purification of hypermannosylated rHRP produced in *P. pastoris* [27]. However, when it comes to medical applications such as targeted cancer therapies or enzyme/prodrug combinations where HRP is injected *in vivo*, no hyperglycosylation must be present because

this triggers immunogenic responses in the human body and the conjugation to antibodies and lectins can be difficult. This is why a recombinant host, that is easy to cultivate and does not hyperglycosylate secreted proteins, is required for a efficient production of HRP that can satisfy the increasing demand of less-glycosylated homogenous enzyme preparations.

HRP is a well studied enzyme that has its applications in a whole range of biotechnological, medical and industrial subjects. It is frequently used in diagnostic and analytical kits or immunoassays because it can be easily conjugated to antibodies and serves as reporter enzyme in several experimental settings [12, 40]. Moreover, it can be used for the removal of phenolic and other substances from waste waters or for detoxification of pesticides from agricultural effluents [41].

2.2.4 Applications for targeted cancer treatment

A more sophisticated application of HRP, which was mentioned before, is the use for targeted cancer treatment in combination with the plant hormone indole-3-acetic acid (IAA). Greco et al. (2000) propose 3 approaches as anti-cancer treatment therapies: GDEPT (Gene-directed enzyme/prodrug therapy), ADEPT (antibody-directed enzyme/prodrug therapy) and PDEPT (polymer-directed enzyme/prodrug therapy) (Figure 5). The concept of GDEPT, which is a controversial method, uses the expression of a enzyme-encoding gene at the location of the tumor, which subsequently converts a usually non-toxic prodrug into a cytotoxic substance. ADEPT and PDEPT both target HRP specifically to the tumor cells by either the use of antibodies that are conjugated to the HRP enzyme or to polymers that act as a shuttle, whereby IAA can be delivered in a common medication type, because the plant hormone is well tolerated in the human body and is not unspecifically activated in healthy tissues [1]. For

that purpose, HRP should be catalytically active at physiological pH-values, show an efficient prodrug activation and have a sufficiently high half-life.

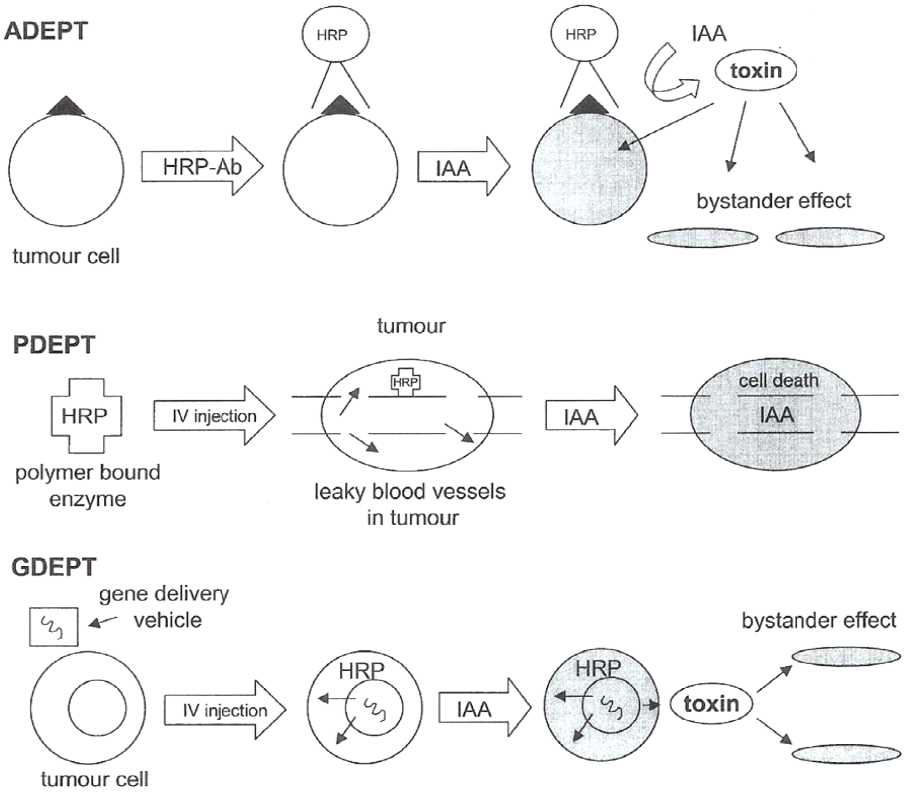

Figure 5: Representation of main targeting strategies of potential value in cancer therapy [10].

Focused on the reaction between HRP and IAA, the heme peroxidase oxidizes the plant hormone, resulting in a radical cation. This radical reacts with oxygen immediately to a peroxyl radical and in a further step to a hydroperoxide (IAA-OOH), which may replace H_2O_2 in forming the HRP compound I [9]. Alcohol (IAA-CH_2OH) and an aldehyde (IAA-CHO) may also be formed via the peroxyl radical. The reaction goes on and ends in the important substance 3-methylene-2-oxindole (MOI), which builds cytotoxins and trigger apoptosis of cancer cells in mammalians [1, 9, 10].

Furthermore various plant hormones, like halogenated indole-3-acetic acids are studied to find an improved enzyme/prodrug combination for targeted cancer treatment [8, 42].

2.3 State of the art: Design and cultivation of a *P. pastoris och1* k.o. strain

One method to prevent a hyperglycosylation of produced recombinant proteins in *P. pastoris* is an intervention in the glycosylation pathway of this yeast. A knock-out of the responsible gene *och1* for the α-1,6-mannosyltransferase was practiced a few times as a first step [4-6]. Production of less-glycosylated recombinant protein was reported with this modified strain. For example, an influenza neuraminidase was expressed in an *och1* defective *P. pastoris* strain and showed a decreased molecular weight due to the reduced glycosylation [3].

There are different strategies to knock out the *och1* gene. One method is based on the deletion of the *URA 3* gene, which encodes orotidine-5'-phosphate decarboxylase, of a *P. pastoris* X-33 strain in a double homologous recombination [4].

Our recent reported study presents the *och1* knock out of a *P. pastoris* Mut^S CBS7435 wildtype strain by using a flipper cassette (34 bp) targeting to the *och1* locus to replace the *och1* open reading frame. The responsible gene for the α-1,6-mannosyltransferase was deleted in a double homologous recombination. Transformation into the *P. pastoris* Mut^S CBS7435 strain was followed by the selection by a Zeocin™ resistance. The double homologous recombination replaced the *och1* open reading frame in the genome with the flipper cassette and growth on methanol induced the production of FLP recombinase, recognizing two *FRT* sites and excising the inner sequence, whereas only one *FRT* site remained in the genome [2].

This knock-out delivered an altered strain morphology of big cell aggregates or clusters instead of normal single *P. pastoris* wildtype cells. This phenomena was described several times, not only in *P. pastoris*, but also in *S. cerevisiae* [2, 43, 44].

We also described the behavior of this *P. pastoris* Mut^S CBS7435 *och1* k.o. strain in the bioreactor running a simple batch cultivation following a methanol pulse feeding strategy [2, 45]. We described that the cultivation of this modified *P. pastoris* strain under common conditions for this yeast (30 °C [14, 28]) underlies several critical aspects: foam formation, cell lysis, methanol accumulation and low productivity of the used model protein HRP isoenzyme A2A. Moreover, this modified *P. pastoris och1* knock-out strain showed decreasing yield parameters, $Y_{CO2/S}$ and $Y_{X/S}$, during the induction phase with methanol, while these parameters during a cultivation with a *P. pastoris* Mut^S CBS7435 wildtype strain stayed constant. The C-balance closed to 1 in the wildtype strain cultivation, but was constantly decreasing in the bioprocess of the *P. pastoris och1* knock-out strain caused by a loss of metabolic activity over time.

However, we showed in our study that a batch cultivation of this engineered strain is possible, but various bottlenecks still exist:

- No fed-batch process for this strain is developed
- Foam formation, cell lysis, risk of overfeeding
- Decreasing C-balances due to loss of metabolic activity over time

Due to the still missing controllable bioprocess of this genetically modified strain, this strain including HRP isoenzyme A2A was used in this Thesis to develop such a process for less-glycosylated recombinant protein production.

3 Roadmap of this Thesis

Following figure (Figure 6) gives a short overview of the practical parts of this Thesis. Upstream processing (USP) includes the bioprocess development for the *P. pastoris och1* k.o. strain by using a Design of Experiments approach, on-line and off-line data analysis during the processes. In this DoE-screening we want to determine an area for high rHRP A2A production by investigating the three process parameters temperature, pH and dissolved oxygen concentration and also their influence on the productivity. For this investigation 13 bioprocesses were done, including 11 DoE experiments plus 2 verification runs.

The downstream processing (DSP) includes enzyme purifications of the expressed rHRP isoenzyme A2A according to a previous established 2-step purification for hyperglycosylated rHRP expressed in *P. pastoris* [27].

The third part describes product analysis, including biochemical characterization, thermal stability as well as a enzyme/prodrug combination for potential targeted cancer treatment.

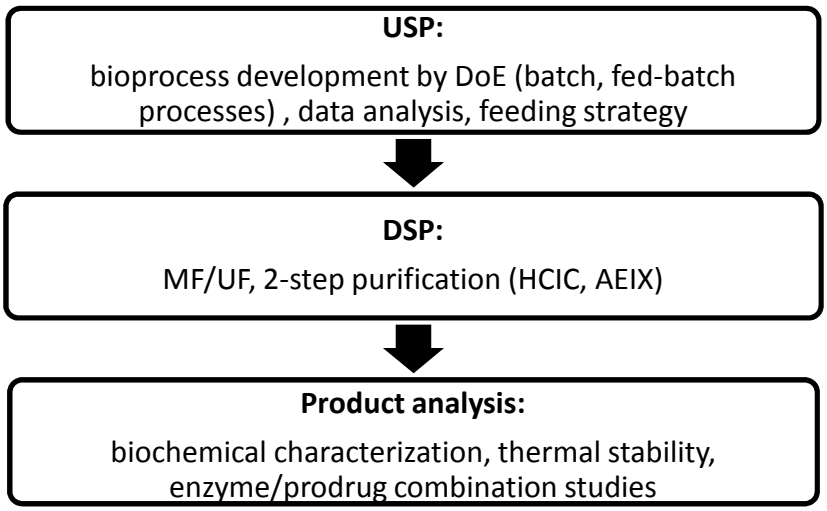

Figure 6: Roadmap; represented overview of the practical steps of the Thesis; USP = upstream processing; DSP = downstream processing; MF/UF = micro- and ultrafiltration; HCIC = hydrophobic charge induction chromatography; AEX = anionic exchange chromatography;

4 Materials & Methods

4.1 Bioprocess development for a *P. pastoris och1* k.o. strain

4.1.1 Bioreactor set up

The description of the bioreactor set-up applies for all of the performed bioprocesses. The experiments were carried out with an identical set up consisting of two 3 L working volume Labfors glass bioreactors with double-wall jackets for temperature control (Infors, Switzerland), which was measured by a PT 100 temperature sensor (Infors, Bottmingen). The double-wall jacket was filled with water, which was forwarded by an peristaltic pump of the bioreactor tower control (Infors, Switzerland).

Dissolved oxygen concentration (pO_2) was measured with a sterilizable fluorescence dissolved oxygen electrode (Visiferm DO425, Hamilton, Germany) and the pH was measured with a sterilizable pH-electrode (Mettler Toledo, Switzerland). The pH was regulated using diluted ammonia solution, which was connected to the bioreactor and forwarded by a peristaltic pump of the bioreactor tower control (Infors, Switzerland). pH as well as pO_2 electrodes were calibrated with a 2-point calibration. The pH probe was calibrated before the sterilization step with two solutions having a pH of 4.0 and 7.0. The pO_2 electrode was calibrated after the sterilization step, when the bioreactor was completely prepared for the experiment. The calibration was adjusted with dry air (100 %) and pure nitrogen (0 %). The bioreactors were sterilized with the basal salt medium (BSM) inside at 122 °C for 30 minutes.

Feeding bottles were used only in the fed-batch fermentations. Therefore a 2 L glycerol feed was prepared and sterilized together with the bioreactor. The feeding bottle was connected via sterilizable tubes and plastic quick fit connectors to the feeding pipe. The feed was forwarded

by a preciflow peristaltic pump (Lambda laboratory instruments, Switzerland). The weight of the feed was determined gravimetrically and recorded by the process information management system (PIMS, Lucullus, Biospectra, Switzerland). After the growth phase, the glycerol feeding bottle was changed to a 1 L bottle filled with the methanol feeding solution, which was sterile filtered into an autoclaved 1 L bottle. The change of the feeding bottles was done by changing the quick fit connectors in a decontaminated area using ethanol spray (70 % EtOH).

Furthermore, base and bioreactor weights were determined gravimetrically and recorded by the process information management system (PIMS, Lucullus, Biospectra, Switzerland). Aeration was carried out through a sparger. Air and oxygen inlets were equipped with sterile 0.2 µm air filters (PALL Corporation, USA) and flowrates were regulated by mass flow controllers (Vögtlin, Aesch, Switzerland).

A valve for sampling and a feeding pipe - for fed-batch processes only - were installed. The sampling pipe was connected through a by-pass to the sparger and to a 50 mL sampling vessel.

Off-gas was cooled by an offgas-cooler located at the beginning of the off-gas-line and measured by an off-gas-analyzer (MARINO Mueller, Gasanalyzer, Switzerland) using an infrared cell for CO_2 and a paramagnetic cell for O_2. The values were logged in the process information management system (PIMS, Lucullus, Biospectra, Switzerland).

A septum was placed in one port of the bioreactor for the aseptical injection of trace elements, precursor solutions, adaptation pulses and antifoam, if necessary.

Off-gas signals CO_2 and O_2, pH, reactor temperature, pO_2, base, feed and reactor weight as well as agitation, aeration and flow rates of the pumps were automatically recorded by the process information management system (PIMS, Lucullus, Biospectra, Switzerland).

4.1.2 Preculture and culture media

Yeast nitrogen base medium (YNBM): 20g·L^{-1} α-D(+)-glucose monohydrate, 3.4g·L-1 YNB2, 10g·L-1 (NH4)2SO4, 0.4g·L-1 D(+)-biotin, 0.1M potassium phosphate buffer, pH6.0.

Trace element solution (PTM1): 6g·L^{-1} $CuSO_4.5H_2O$, 0.08g·L^{-1} NaI, 3g·L^{-1} $MnSO_4.H_2O$, 0.2g·L^{-1} $Na_2MoO_4.2H_2O$, 0.02·L^{-1} H_3BO_3, 0.5g·L^{-1} $CoCl_2$, 20g·L^{-1} $ZnCl_2$, 65g·L^{-1} $FeSO_4.7H_2O$, 0.2g·L^{-1} D(+)-biotin, 5mL·L^{-1} 95-98% H_2SO_4.

Basal salt medium (BSM) - 2x concentrated: 40g·L^{-1} glycerol, 0.36g·L^{-1} $CaSO_4.2H_2O$, 27.24g·L^{-1} K_2SO_4, 4.48g·L^{-1} $MgSO_4.7H_2O$, 8.26g·L^{-1} KOH, 21.58mL·L^{-1} 85% (v/v) o-phosphoric acid, 0.3mL·L^{-1} Antifoam Struktol J650, 4.35mL·L^{-1} PTM1, NH_4OH as N-source

Base: NH_4OH, concentration was determined by titration with 0.25 M potassium hydrogen phthalate.

Glycerol feed: 250g·L^{-1} glycerol, 0.3mL·L^{-1} Antifoam Struktol J650, 4.35mL·L^{-1} PTM1.

Methanol feed: 100g·L^{-1} methanol, 0.3mL·L^{-1} Antifoam Struktol J650, 4.35mL·L^{-1} PTM1.

BMGY: 1 % yeast extract; 2% peptone; 100 mM potassium phosphate buffer, pH6.0; 1,34 % YNB; $4 \cdot 10^{-5}$ % biotin; 1 % glycerol

BMMY: 1 % yeast extract; 2% peptone; 100 mM potassium phosphate buffer, pH6.0; 1,34 % YNB; $4 \cdot 10^{-5}$ % biotin; 0.5 % methanol

A frozen stock (-80 °C) of the *P. pastoris och1* knock-out strain was split into two 1 L Erlenmeyer flasks, filled with 100 mL sterile YNB medium containing 1 µg·mL^{-1} Zeocin™, and the preculture flasks were incubated for 48 h at 30 °C and 230 rpm. After checking the cells under the microscope to exclude contaminations, 112.5 mL preculture (7.5 % of the total batch volume) were inoculated into the bioreactor aseptically.

4.1.3 Batch cultivations with MeOH pulses

Two batch cultivations of the *P. pastoris och1* k.o. strain following a methanol pulse strategy [45] were done at different temperatures. The batch BSM medium was calculated to a volume of 1.5 L and sterilized in the bioreactor. The pH value of BSM was set by using concentrated ammonia solution after sterilization. The agitation was set to 850 – 900 rpm and aeration to a pO_2 concentration above 30 %. Sterile filtered PTM1 was transferred to the reactor aseptically.. After depletion of the carbon-source glycerol in the batch phase, the induction phase was started by injecting an adaption pulse containing methanol (0.5 % v/v) supplemented with the trace element solution PTM1 (12 mL PTM1 per 1 L of methanol). In addition to that, the heme-precursor δ-aminolevulinic acid (1 mM) was also injected into the fermentation broth to support the production of HRP A2A. Furthermore an induction phase, consisting of methanol pulses (1.0 % v/v), was performed.

According to literature [14], one of the two cultivations was done at 30 °C with an induction phase of 8 methanol pulses (1.0 % v/v). The second batch cultivation ran in the same way, whereat the temperature was set to 25 °C and held for 10 methanol pulses (1.0 % v/v) after the adaptation pulse, followed by decreasing the temperature to 20 °C for another 3 pulses.

With this experiments and this feeding strategy the maximal specific substrate uptake rate ($q_{Smax.,}$MeOH) at these different temperatures was determined in a fast and easy process instead of doing repetitive fed-batches [6]. A list of the used equations for the determination of rates, yields and the C-balances is shown in the next chapter.

Moreover, the correlation between dry cell weight (DCW) and optical density, measured at 600 nm (OD_{600}) by using a spectrophotometer (Genesys 20; Thermo Scientific, Austria), during the induction phase was determined and defined as "α-factor" within this Thesis. The fermentation broth of a sample taken at the end of the methanol induction phase was diluted several times (1:2, 1:4, 1:6, 1:8 and 1:10) and the investigated DCWs of the diluted samples

were plotted against their corresponding OD_{600} values, measured photometrically at a final concentration of 1:200. The OD_{600} measurement was done in triplicates and the DCW in duplicates. The gradient of the straight line, meaning the correlation factor between DCW and OD_{600}, illustrates the α-factor and was used for biomass calculation (equation 1). The feeding rate for applying a constant methanol fed-batch as induction phase in further experiments was calculated with this factor. This investigation was done for the *P. pastoris och1* k.o. strain as well as for a *P. pastoris* wildtype strain and describes the correlation of the DCW and OD_{600} in during the induction phase on methanol.

$$X = OD_{600,ave} * \alpha \quad (1)$$

X = calculated biomass [$g \cdot L^{-1}$]
OD_{600} = optical density at 600 nm
α = correlation factor between DCW and OD_{600} value

4.1.4 Equations for the bioprocess interpretation

The relevant equations (Eq.) for the interpretation and analysis of the bioprocesses are shown below in order to determine the uptake rates, specific uptake rates, yields and C-balances of all executed experiments [46].

a) Stoichiometric equations:

$$r_S * CH_m O_l + r_{O_2} * O_2 + r_N * NH_3 \rightarrow r_X * CH_p O_n N_q + r_P * CH_r O_t N_u + r_{H2O} * H_2O + r_{CO2} * CO_2 + Energy\ (\Delta G) \quad (2)$$

CH_mO_l = substrate [$g \cdot L^{-1}$]
NH_3 = base; N-source [$mol \cdot L^{-1}$]

O_2 = oxygen [%]
CO_2 = carbon dioxide [%]
H_2O = water [%]
$CH_pO_nN_q$ = biomass [$g \cdot L^{-1}$]
$CH_rO_tN_u$ = product [$g \cdot L^{-1}$]
ΔG = energy due to reaction [J]
r_i = building rate [$g \cdot h^{-1}$]; i = X (biomass), S (substrate), P (product), N (nitrogen)
r_j = biomass building rate [$mol \cdot L^{-}1 \cdot h^{-1}$]; j = CO_2, H_2O, O_2

***b) General mass balance*:**

Input – output + conversion = accumulation

$$\dot{V}_{i,in} * c_{i,in} - \dot{V}_{i,out} * c_{i,out} + V_R * r_i = V_R * \frac{\partial c_i}{\partial t} + c_i * \frac{\partial V_R}{\partial t} \quad (3)$$

V_R = reactor volume [L]
$c_{i,in}$ = concentration, that goes into the reactor [$g \cdot L^{-1}$]
$c_{i,out}$ = concentration, that comes out of the reactor [$g \cdot L^{-1}$]
$\dot{V}_{i,in}$ = volume of flow that goes into the reactor [$L \cdot h^{-1}$]
$\dot{V}_{i,out}$ = volume of flow that goes into the reactor [$L \cdot h^{-1}$]
r_i = building rate [$g \cdot h^{-1}$]

***c) Conversion rate for r_X*:**

$$r_X = \frac{d(X)}{dt} - \dot{X}_{in} + \dot{X}_{out} = \frac{d(X)}{dt} \quad (4)$$

X = biomass [g]
t = time [h]
r_X = biomass building rate [$g \cdot h^{-1}$]

***d) Conversion rate for r_P*:**

$$r_P = \frac{d(P)}{dt} - \dot{P}_{in} + \dot{P}_{out} = \frac{d(P)}{dt} \quad (5)$$

P = product [U]
t = time [h]
r_P = product building rate [$U \cdot h^{-1}$]

In a fed-batch process the terms $\dot{X}_{in}, \dot{X}_{out}$ as well as $\dot{P}_{in}$ and $\dot{P}_{out}$ are zero (Eqs. 4, 5).

e) Conversion rate for r_S:

$$r_S = \frac{d(s)}{dt} - \dot{S}_{in} + \dot{S}_{out} = \frac{F_{f,in} * S_0}{\frac{\rho_{feed}}{\Delta t}} \quad (6)$$

S_0 = substrate conc. of the feed [g·L^{-1}]
$F_{f,in}$ = consumption of the substrate between the samples [g]
Δt = time from sample to sample [h]
ρ_{feed} = density of the substrate/feed [kg·L^{-1}]
r_S = substrate uptake rate [g·h^{-1}]

The term $\dot{S}_{out}$ (Eq. 5) in a fed-batch mode is zero and the d(S)/dt term can be neglected if μ is lower than $\mu_{max.}$. The consumption of the substrate was determined from sample to sample by measuring the weight of the feed. The amounts of CO2 and O2 in the off-gas were measured by an off-gas analyzer (MARINO Mueller, Gasanalyzer, Switzerland). The corresponding rates for carbon dioxide (CO_2) and oxygen (O_2) were determined by Eq. 7 and 8.

f) Conversion rate for $r_{CO2} = CER$:

$$r_{CO2} = \frac{d(CO_2)}{dt} - \dot{CO}_{2,in} + \dot{CO}_{2,out} = \frac{F_{a,in} * 60 * (y_{CO2,out} * Ra_{inert} - y_{CO2,in})}{V_m} \quad (7)$$

Legend see below at h)

g) Conversion rate for $r_{O2} = OUR$:

$$r_{O2} = \frac{d(O_2)}{dt} - \dot{O}_{2,in} + \dot{O}_{2,out} = \frac{F_{a,in} * 60 * (y_{O2,out} * Ra_{inert} - y_{O2,in})}{V_m} \quad (8)$$

Legend see below at h)

h) Inert gas ratio:

$$Ra_{inert} = \frac{1-y_{O2,in}-y_{CO2,in}}{1-y_{O2,out}-y_{CO2,out}-\frac{y_{wet}}{y_{O2,in}}} \quad (9)$$

r_{CO2} = CO_2 building rate [mmol·L^{-1}·h^{-1}]
r_{O2} = O_2 building rate [mmol·L^{-1}·h^{-1}]
y_{wet} = O_2 concentration, where no bioreaction occurs and relates to to dilution by water stripping [mol·L^{-1}]
$y_{i,in/out}$ = measured components (i = CO_2 or O_2) [mol·L^{-1}]
$F_{a,in}$ = flow in to the bioreactor [L·min^{-1}]
V_m = volume of ideal gas related to 1 mol = 22,415 [L·mol^{-1}]

The term d(O_2)/dt can be neglected because of the low solubility of oxygen in the fermentation broth (Eq. 8). Ra_{inert} depends on the dilution by water stripping and it describes the ratio between in- and outflow term (Eq. 9).

For determination of the specific rates (Eq. 10), the relevant rates are referred to the total biomass, which was investigated by measuring the DCW.

i) Specific rates:

$$q_i = \frac{r_i}{X_i} \quad (10)$$

q_i = specific rates; i = S [C-mmol·g^{-1}·h^{-1}], P [U·g^{-1}·h^{-1}], CO_2 [mmol·g·h^{-1}], O_2[mmol·g·h^{-1}]
X_i = biomass [g] at the corresponding sample; i = 1, 2, 3, etc.
r_i = rates; i = S [g·h^{-1}], X [g·h^{-1}], P [U·h^{-1}]

The substrate uptake rates r_S were divided by the molecular weight of the used substrate ending up in a specific substrate uptake rate q_S which is related to the carbon composition (C-molar). The product building rate divided by the biomass delivers the specific product building rate or also called specific productivity q_P.

The biomass rate r_X related to the biomass results in the specific growth rate μ (Eq. 11).

j) Specific growth rate:

$$\mu = \frac{r_X}{X_i} \quad (11)$$

μ = specific growth rate [h^{-1}]
X_i = biomass [g] at the corresponding sample; i = 1, 2, 3, etc.
r_X = biomass building rate [$g \cdot h^{-1}$]

k) Yields:

$$Y_{\frac{i}{S}} = \frac{r_i}{r_S} \quad (12)$$

$Y_{\frac{i}{S}}$ = yield; i = X [C-mol·C-mol^{-1}], CO_2 [mol·C-mol^{-1}], O_2 [mol·C-mol^{-1}]

The yields were related to the substrate uptake rate r_S (Eq. 12). For defining the product yield a new factor, called efficiency factor, is inserted. It describes the uptake of the substrate and the conversion into product (Eq. 13).

$$\eta = \frac{q_P}{q_S} \quad (13)$$

q_P = specific productivity [$U \cdot g^{-1} \cdot h^{-1}$]
q_S = specific substrate uptake rate [C-$mmol \cdot g^{-1} \cdot h^{-1}$]
η = efficiency factor [$U \cdot C\text{-}mmol^{-1}$]

l) C-balance:

$$C - balance = Y_{\frac{CO_2}{S}} + Y_{\frac{X}{S}} \quad (14)$$

C-balance = [ ]
$Y_{\frac{CO_2}{S}}$ = CO_2 yield related to the substrate [mol·C-mol^{-1}]
$Y_{\frac{X}{S}}$ = biomass yield related to the substrate [C-mol·C-mol^{-1}]

The C-balance of an experiment in a bioreactor must be closed to 1.0. This means, all carbon atoms, which are going into the bioreactor and thus into the reaction, must be found again afterwards.

4.1.5 Development of a fed-batch bioprocess by a Design of Experiments

Design of Experiments:

We chose three parameters for the Design of Experiments to develop a parameter area for high production of rHRP A2A; temperature, pH and pO_2 concentration.

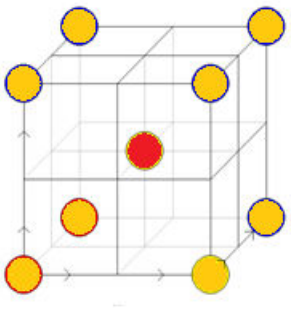

Figure 7: 2-level cubic screening approach using MODDE 10.0 (Umetrics)

On the basis of the previous batch cultivations we could see that the strain shows a higher productivity at 25 °C and 20 °C instead of 30 °C. Hence, the temperatures 20, 25 and 30 °C for this DoE were chosen because we want to gain a high productivity but also cultivations with *P. pastoris* at these temperatures were done and reported before [14].

The pH values 5.0 – 7.0 for the DoE were defined due to the pH-stability of the enzyme HRP A2A, which could be found in literature but were also determined in previous pH-stability experiments [27].

The third parameter for the DoE was the dissolved oxygen concentration, which might have an effect on the strain's productivity. 10, 20 and 30 % pO_2 were chosen because of *P. pastoris* cultivations reported and done before [14].

In this DoE screening, an area for high rHRP A2A production should be found by investigating those three mentioned process parameters. Therefore a 2-level cubic full factorial screening approach with 3 centre points (Figure 7) was set up with the program

MODDE 10.0 (Umetrics AG, Umea, Sweden) to explore the influence of those three parameters, which were varied in the induction phases of all bioprocesses (Table 2). The suggested run order of MODDE 10.0 was done randomly to prevent a systematical error. Furthermore, two verification processes were done to prove the identified results of the experiments and to confirm the parameter area for high rHRP A2A production. A bioprocess with this parameter area was also done for a *P. pastoris* wildtype strain to compare it with the *P. pastoris och1* k.o. strain.

The responses for the DoE were split into **physiology-related** and **product-related** responses (Table 1).

Table 1: Responses of the Design of Experiments separated in physiology- and product related responses

physiology-related responses	product-related responses
$Y_{CO2/S}$ and $Y_{X/S}$ [mol·C-mol^{-1}]	specific activity [U·mg^{-1}] (= product quality)
MeOH accumulation [g·L^{-1}]	specific productivity $\mathbf{q_P}$ [U·g^{-1}.h^{-1}]
$q_{S,adapt}$ [mmol·g^{-1}·h^{-1}]	volumetric productivity [U·L^{-1}.h^{-1}]
	efficiency factor η [U·mmol.$^{-1}$]

Table 2: Induction phase process parameters for the Design of Experiments (DoE) bioprocesses of the *P. pastoris* Mut^S CBS7435 *och1* knock-out strain with the HRP isoenzyme A2A.

Experiment order	Temp. [°C]	pH [-]	pO_2 [%]
DoE 1	20	5	30
DoE 2	20	5	10
DoE 3	30	5	30
DoE 4	30	7	30
DoE 5	30	7	10
DoE 6	25	6	20
DoE 7	20	7	10
DoE 8	20	7	30
DoE 9	25	6	20
DoE 10	25	6	20
DoE 11	30	5	10

Fed-batch cultivation:

The bioreactor for the developed bioprocess was set up as it is described before. The batch run in the same way as the first batch cultivation, which was represented earlier. After the depletion of the carbon source, the fed-batch on glycerol was started following an exponential feeding profile (Eq. 15, 16) with a constant specific growth rate μ of 0.08 h^{-1}. The biomass for the fed-batch on glycerol was calculated by the $Y_{X/S}$ [$g \cdot g^{-1}$] and the substrate concentration at the beginning of the process (S_0) (Eq.17).

$$F_0 = \frac{X * V * \mu * \delta_{Feed}}{Y_{\frac{X}{S}} * c_{Feed}} \quad (15)$$

$$F = F_0 * e^{(\mu * t)} \quad (16)$$

F = feeding rate [$g \cdot h^{-1}$]
F_0 = determined feed [$g \cdot h^{-1}$]
X = calc. biomass [$g \cdot L^{-1}$]
V = volume after batch phase [L]
μ = specific growth rate = 0.08 [h^{-1}]
δ = density of the glycerol feed [$g \cdot L^{-1}$] = 1055 $g \cdot L^{-1}$
c = concentration of the glycerol feed [$g \cdot L^{-1}$]
$Y_{X/S}$ = yield of *P. pastoris* on glycerol = 0.47 [$g \cdot g^{-1}$] (determined in previous studies in the research group)

$$Y_{\frac{X}{S}} = \frac{\Delta c_X}{\Delta c_S} = \frac{c_{X,in} - c_{X,out}}{c_{S,in} - c_{s,out}} = \frac{X_{out}}{40\ g * L^{-1}} \quad (17)$$

$Y_{X/S}$ = yield of *P. pastoris* on glycerol = 0.47 [$g \cdot g^{-1}$] (determined in previous studies in the research group)
$c_{X,in/out}$ = biomass concentration at the beginning and the end of the batch phase [$g \cdot L^{-1}$]
$c_{S,in/out}$ = substrate concentration at the beginning and the end of the batch phase [$g \cdot L^{-1}$]; starting conc. of glycerol = 40 $g \cdot L^{-1}$

The exponential fed-batch run until a total reactor volume of 2.2 L was reached. Temperature and pH value were held at 30 °C and 5.0 as in the batch phase. Agitation stayed at the same

speed of 850 – 900 rpm, but aeration was reduced from 1.0 vvm during the batch to 0.5 vvm during the fed-batch phase to prevent extensive foam formation. Due to a potential oxygen limitation as a consequence of the reduced aeration, the fermentation broth was aerated with 2/3 dry air and 1/3 pure oxygen to stay over 30 % during the whole fed-batch phase.

After the depletion of the carbon-source glycerol in the fed-batch phase, the relevant process parameters (Table 2) were changed. Afterwards an induction phase was started by injecting a 0.5 % (v/v) adaptation pulse, containing methanol supplemented with PTM1 (12 mL PTM1 per 1 L of methanol). Furthermore the heme-precursor δ-aminolevulinic acid (1 mM) was added together with the adaptation pulse supporting the rHRP A2A production.

After the adaptation pulse, a methanol fed-batch running a constant feeding profile with a certain specific substrate uptake rate ($q_{S,MeOH}$) was operated. In consideration of the prior executed batch-cultivations with MeOH pulses (chapter 3.1.3), the $q_{S,MeOH}$ for the methanol fed-batch was set to 0.2 $mmol \cdot g^{-1} \cdot h^{-1}$ to prevent methanol accumulation. The biomass for the calculation of the feeding rate was determined by using the α-factor (Eq.1, chapter 3.1.3). Moreover, the feeding rate (Eq. 18) was set at the beginning of the fed-batch, checked twice a day for a correlation with the optical density and adjusted. The fed-batch ran in a constant mode till the fed-batch was stopped after more or less 100 hours (Figure 8).

$$F = \frac{X * V * q_{S,MeOH} * \delta_{Feed}}{c_{Feed}} \quad (18)$$

F = determined feed $[g \cdot h^{-1}]$
X = calc. biomass with the α-factor $[g \cdot L^{-1}]$
V = volume after the batch phase [L] = 1.5 L
$q_{S,MeOH}$ = specific substrate uptake rate = 0.2 $[mmol \cdot g^{-1} \cdot h^{-1}]$
δ = density of the methanol feed $[g \cdot L^{-1}]$ = 941 $g \cdot L^{-1}$
c = concentration of the methanol feed $[g \cdot L^{-1}]$

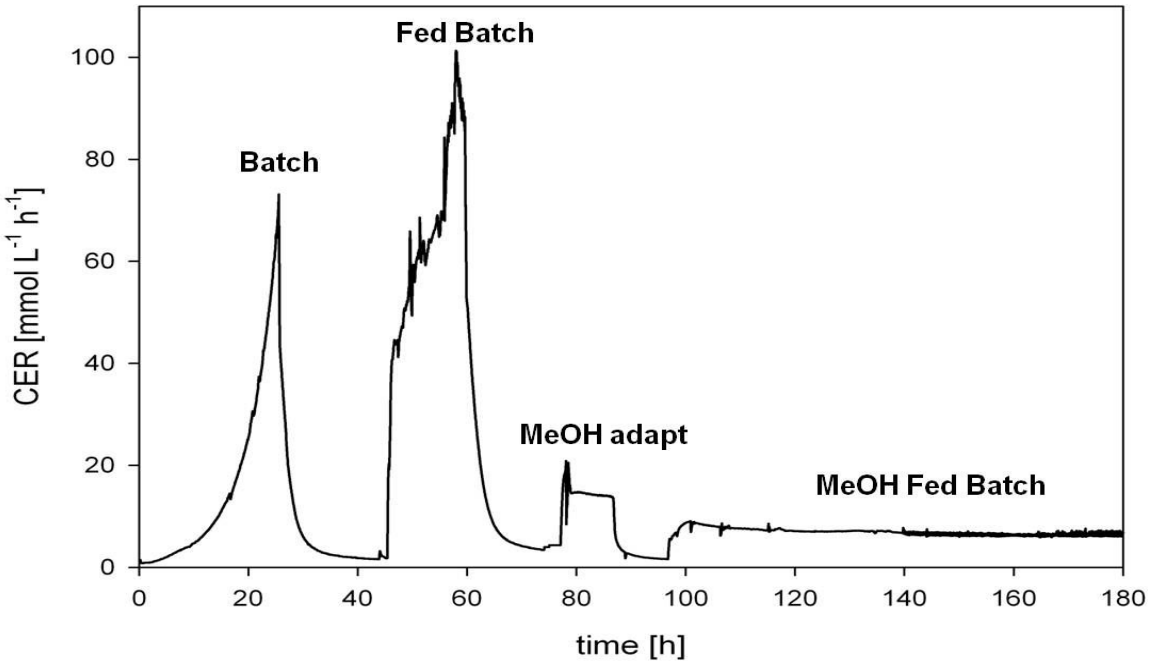

Figure 8: Demonstration of a typical DoE - fermentation, containing a batch and fed-batch phase on glycerol, followed by a 0.5 % (v/v) methanol adaptation pulse and a constant methanol fed-batch using a $q_{S,MeOH}$ of 0.2 mmol·g^{-1}·h^{-1}.

The pO_2 concentration in the induction phase was controlled by a proportional-integral-differential (PID) controller of the process information management system (PIMS Lucullus; Biospectra, Switzerland). The PID controller regulated the pO_2 % concentration through the aeration of dry air, but must not fall under a flow of 0.6 nL·min^{-1} for the offgas analysis. Due to possible shear forces to the cell aggregates of the *P. pastoris och1* knock-out strain, the pO_2 % concentration was not controlled by the stirrer and the agitation was set to a speed of 600 - 650 rpm.

At the end of the bioprocess the fermentation broth was harvested into a 5 L glass bottle through the sample pipe and prepared for the DSP. The bioreactor was decontaminated by using a 2 M potassium hydroxide solution, but the pH and pO_2 electrodes have to be removed from the bioreactor before.

4.1.6 Additional experiments

Precursor experiments:

In shake flask experiments, the best precursor for the *P. pastoris och1* k.o. strain expressing rHRP A2A was analyzed to increase the support of the enzyme's production during the induction phase of the process. Therefore, frozen cell stocks were thawed and cultivated in 250 mL sterile shake flasks filled with 25 mL sterilized BMGY+Zeocin^{TM} medium and incubated at 30 °C and 230 rpm in a shaking incubator. After the cultivation in BMGY+Zeocin^{TM} for 26 hours, the OD_{600} reached a value of approximately 7.0. Afterwards, the amount of cells was calculated to start the cultivation on the BMMY+Zeocin^{TM} medium with an OD of 1.0 and then cells were transferred with sterile pipettes to the inducing medium. Sterile 250 mL shake flasks were used, whereas the total volume of the BMMY+Zeocin^{TM} medium including the cells coming from the cultivation on BMGY+Zeocin^{TM} was 25 mL. The incubation on BMMY+Zeocin^{TM} was done at 20 °C and 230 rpm. During the cultivation in BMMY+Zeocin^{TM}, methanol pulses of 0.5 % (v/v) were injected to the shake flasks. Since the methanolic medium contains 0.5 % methanol, the first pulse was set after two days to prevent an overfeeding of the cells and methanol accumulation. Three different precursors as well as the effect of an absent precursor were analyzed. The precursors δ-aminolevulinic acid (δ-Ala), ferric sulfate ($FeSO_4$) and hemin were used and added to the induction medium BMMY+Zeocin^{TM} to end up in a concentration of 1 mM for δ-Ala and $FeSO_4$ and of 30 µM for hemin. Sampling and pulsing with 0.5 % methanol was done every two days, whereas OD_{600}, protein content [$mg \cdot mL^{-1}$] and vol. activity [$U \cdot mL^{-1}$] were measured in duplicates. The background of the hemin solution was measured by a CuBiAn^{XC} enzymatic robot (Innovatis, Germany).

Protease inhibitor experiments:

In this experiments, the influence of potential existing proteases on HRP production in the *P. pastoris och1* k.o. strain at 30 °C was analyzed. Frozen cell stocks were cultivated on BMGY+Zeocin^{TM}, following the same procedure which was described before. Then the required cell amount was again calculated to start the cultivation on BMMY+Zeocin^{TM} with an OD of 1.0. The temperature was now held on 30 °C and 1mM δ-Ala was used to support HRP production in this shake flasks. Furthermore, a protease inhibitor cocktail tablet (Roche, Switzerland) was dissolved in sterile water and added to the half of all shake flasks. Every two days samples were taken to analyze OD_{600}, protein content [$mg \cdot mL^{-1}$] and extracellular volumetric activity [$U \cdot mL^{-1}$] and 0.5 % methanol pulses were done to induce the expression system. All measurements were done in duplicates. At the end of the experiments, the cells were harvested and homogenized by high pressure homogenization (Emulsiflex-C3 homogenizer). Cell debris were separated by centrifugation (4°C, 5 min, 5.000 rpm) and the enzymatic activity was measured.

4.2 Data Analysis

Samples were taken after the batch and the fed-batch phase on glycerol, immediately after the adaptation pulse and after the exhaustion of the 0.5 % methanol pulse. During the fed-batch on methanol, samples were taken two times a day and analyzed for dry cell weight (DCW), enzyme activity [$U \cdot mL^{-1}$], protein content [$mg \cdot mL^{-1}$], OD_{600} as well as for substrate concentration [$g \cdot L^{-1}$] measured by HPLC.

All measurements were done in duplicates. Figure 9 shows the sampling scheme. The sample was taken by the sampling pipe which was connected through a by-pass to the sparger and to a 50 mL sampling bottle. DCW was determined by centrifugation of 5 mL culture broth

(4.000 x g, 10 min, 4 °C), washing the pellet with 5 mL deionized water and subsequent drying at 110 °C to a constant weight in an oven for 48 hours. OD_{600} of the culture broth was measured by using a spectrophotometer (Genesys 20; Thermo Scientific, Austria) and by diluting samples to be in an absorbance range of 0.2-0.8.

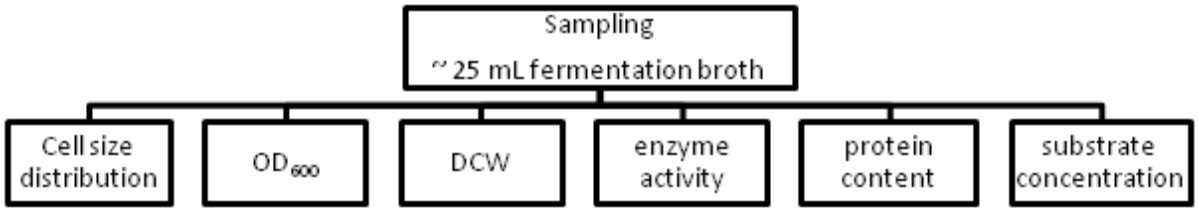

Figure 9: Representation of the sampling pathway

The activity of HRP was determined using a CuBiAn^{XC} enzymatic robot (Innovatis, Germany). Cell free samples (10µL) were added to 140 µL of 1 mM 2,2'-Azino-di-3-ethylbenzthiazolin-6-sulfonsäure (ABTS) in 50 mM potassium phosphate buffer, pH 6.5. The reaction mixture was incubated at 37 °C and was started by the addition of 20 µL of 0.075 % hydrogen peroxide (H_2O_2). Changes of absorbance at 420 nm were measured for 80 seconds and rates were calculated. Calibration was done using commercially available horseradish peroxidase (Type VI-A, Sigma-Aldrich, Austria, P6782, Lot# 118K76734) as standard at six different concentrations (0.02; 0.05; 0.1; 0.25; 0.5 and 1.0 $U \cdot mL^{-1}$).

Protein contents were determined at 595 nm using the Bradford Protein Assay Kit (Bio-Rad Laboratories GmbH, Austria) with bovine serum albumin as standard.

Substrate concentration, which means methanol concentration, was determined in cell free samples by HPLC (Agilent Technologies, USA) equipped with a Supelcoguard column, a Supelcogel C-610H ion-exchange column (Sigma-Aldrich, Austria) and a refractive index detector (Agilent Technologies, USA). The mobile phase was 0.1 % H_3PO_4 with a constant

flow rate of 0.5 $mL \cdot min^{-1}$ and the system was run isocratically. Standard calibration was done by measuring standard samples in the range of 0.5 to 10 $g \cdot L^{-1}$ methanol.

4.3 Strain morphology

According to the altered cell morphology (*vide supra*), a potential effect of the process parameters on the cell structure was investigated and consequently to this an influence on the productivity was analyzed. Therefore, the cell size distribution of all samples of the bioprocesses was analyzed by a Malvern Mastersizer 2000. Frozen cell pellets (stored at -20 °C) with a biomass concentration between 10-20 $g \cdot L^{-1}$ were thawed and resuspended in 10 mL MilliQ® water. After dispersing the samples with the module Hydro 2000S, 6 - 20 drops of this cell-suspension were dropped into a water tank of the Malvern Mastersizer 2000, till the laser diffraction achieved a value between 10-12 %. One measurement took 6 minutes and the samples were analyzed between 0 – 10,000 µm.

Cell sizes itself was analyzed by a light microscope, using a Zeiss Epifluorescence Axio Observer Z1 deconvolution microscopy system (Carl Zeiss, Germany) equipped with LD Plan-Neofluar 63x objective (+ 10x ocular) and the LED illumination system Colibri. A dilution of 1:20 (cells to deionized water) was prepared in a 1.5 mL Eppendorf-tube and samples were dropped onto a microscope slide.

4.4 Enzyme purification

4.4.1 Micro-/Ultrafiltration

The fermentation broths of the different fed-batch bioprocesses which deliver an enzymatic activity > 2 $U \cdot mL^{-1}$ – in total 9 processes – were harvested and centrifuged by a RC-36 refrigerated centrifuge (Servall Instruments) (5000 rpm, 4 °C and 15 min). Microfiltration (MF) was performed at room temperature with a total filter area of 0.3 m² (Omega centramate, T-series; PALL, Austria) and a max. flowrate of 2.1 $mL \cdot min^{-1}$ using the crossflow filtration system Centramate 500S (PALL) to remove cell debris and particles above 0.2 µm.
Ultrafiltration (UF) and diafiltration (DF) were done to concentrate the product and to exchange the buffer. This was done at room temperature and one membrane module was used with a total filer area of 0.1 m² (Omega centramate, T-series; PALL, Austria) and a max. flowrate of 0.8 $mL \cdot min^{-1}$. The product solution was concentrated 15-fold and the buffer was changed to binding buffer (Table 3) for subsequent hydrophobic charge induction chromatography (HCIC). Here a membrane module with a cut-off 10 kDa (Omega T-series; PALL, Austria) was used.
The transmembrane pressure (TMP) was kept below 1 bar during MF and UF/DF to avoid inactivation of HRP. Afterwards, the concentrated and rebuffered product solution was filtered through a 0.2 µm cut-off filter (GE Healthcare, Sweden) before applying it to a chromatography column.

Table 3: Buffer solution for the enzyme purification by doing a 2-step chromatography. HCIC = hydrophobic charged induced chromatography; AEX = anionic exchange chromatography using CIM-DEAE monoliths (BiaSeparations, Slovenia). [12, 27]

HCIC:	Binding buffer:	20 mM NaOAc,500 mM NaCl, pH: 6.0
	Elution buffer:	50 mM TrisHCl, 1M NaCl, pH: 8.0
	Storage buffer:	20 % (v/v) EtOH, 1M NaCl
	Cleaning buffer:	0.8 M NaOH
AEX:	Binding buffer:	50 mM TrisHCl, pH: 8.0
	Elution buffer:	50 mM TrisHCl, 1M NaCl, pH: 8.0
	Storage buffer:	20 % (v/v) EtOH
	Cleaning buffer:	1M NaOH, 1M NaCl

4.4.2 2-step purification: HCIC and AEX

The enzyme purification of the produced proteins followed a 2-step purification protocol, performing a HCIC and AEX chromatography, which was developed for rHRP expressed in *P. pastoris.* Using this method, the product can be found in the flowthrough whereas other proteins interact with the stationary phase [12, 27]. Buffers used for the 2-step purification are shown in Table 3. Both chromatography modes were performed on an ÄKTApurifier^{TM} system (GE Healthcare, Sweden) at room temperature. For HCIC a column with a diameter of 1.6 cm was packed with 25 mL MEP HyperCel (PALL) resin. All loaded protein contents were 10-fold below the maximum binding capacity. The procedures for the HCIC as well as for the AEX with a CIM-DEAE monolith (8 mL) were the same as we described. First, an equilibration step with 5 column volumes (CV) of binding buffer was done, followed by loading of the sample and performing a post-load wash of 4 CV. The elution and cleaning steps were done with 5 CV of elution buffer. The flowrate for all HCIC experiments was approximately 149 $cm \cdot h^{-1}$ and for all AEX using the monolith 5 $mL \cdot min^{-1}$. The product could be found in the flowthrough, whereas eluted proteins during the elution and cleaning steps were collected in fractions. Two UV lamps were used at certain wavelengths to detect the

product and other proteins; 280 nm for proteins and 404 nm for the heme group. The conductivity was measured which was important to follow a correct CIP and regeneration step.

Purification factors and yields were determined by following equations (Eq. 19-22) [27].

$$PF = \frac{specific\ activity_{\ i}}{specific\ activity\ (crude\ extract)} \quad (19)$$

$$Y_A = \frac{(catalytic\ activity_{flowthrough} + catalytic\ activity_{fractions})}{catalytic\ activity_{crude\ extract}} * 100 \quad (20)$$

$$Y_P = \frac{(\ Protein\ concentration_{flowthrough} + Protein\ concentration_{fractions})}{Protein\ concentration_{crude\ extract}} * 100 \quad (21)$$

Y_A = yield of catalytic activity [%]
Y_P= yield of protein concentration [%]
PF = purification factor [ ]
Specific activity = [U·mg^{-1}]
i = fractions or flowthrough

$$Linear\ flowrate\ [cm.h^{-1}] = \frac{volumetric\ flow\ [mL] * 60}{cross\ section\ area\ of\ the\ column\ [cm^2]} \quad (22)$$

4.5 Enzyme characterization

4.5.1 Kinetic characterization

The kinetic constants for the substrate ABTS were determined for all rHRP A2A products expressed in the *P. pastoris och1* k.o. strain. After the purification, the products were filtered through a 0.2 µm sterile filter. The reaction was started by adding 10 µL concentrated enzyme solution to 990 µL reaction buffer containing ABTS in different concentrations (0.01–10 mM), 1 mM H_2O_2 and 50 mM potassium phosphate, pH 6.5. For diluting the samples, ultra purified water was used. The change of absorbance at 420 nm was recorded in a spectrophotometer UV-1601 (Shimadzu, Japan) at 30 °C controlled by a temperature controller (CPS controller 240 A; Shimadzu, Japan). Absorption curves were recorded with the corresponding software program (UVPC Optional Kinetics; Shimadzu, Japan). The software program Sigma-plot was used to diagram a Michaelis-Menten plot and to calculate the kinetic constants; the Michaelis-Menten constant K_M, the maximal reaction rate v_{max} and $k_{cat.}$ (Eq. 23), which describes the substrate turnover. For the determination of k_{cat}, the molecular weight of 35 kDa was chosen, which represents the size of the unglycosylated polypeptide chain, consisting of 308 amino acids. This size was chosen because we did not know the concrete molecular weight of rHRP A2A expressed in the *P. pastoris och1* k.o. strain and we also did not know if the various process parameters would change the glycan pattern on the product and therefore the molecular weight.

$$k_{cat.} = \frac{v_{max} * MW}{t} \quad (23)$$

$k_{cat.}$ = [s^{-1}]
$v_{max.}$ = max. reaction rate [µmol·min^{-1}]
MW = molecular weight [kDa]
t = time [s]

4.5.2 Thermal stability

Enzyme solutions were incubated at 60 °C for 2 hours. At different time points, aliquots were taken, the solutions were centrifuged (14.000 rpm, 15 min) to pellet precipitated proteins and the remaining catalytic activity in the supernatants was measured using the CuBiAn^{XC} photometric robot, which was described earlier. From a semi-logarithmic plot of residual activity over time, inactivation constants were derived. The half-life time was calculated by equation 24 (Eq. 24).

$$\tau_{\frac{1}{2}} = \frac{\ln (2)}{k_{in}} \quad (24)$$

k_{in} = inactivation constant, coming from the negative slope of the inactivation plot
$\tau_{1/2}$ = half-life time [min]

Residuals activities (A_t/A_0, where A_t is the measured activity at time t, and A_0 is the activity at the beginning) were plotted against the incubation time and the inactivation constants were determined by linear regression of (ln activity) versus incubation time [47].

4.5.3 Gel-electrophoresis / SDS-PAGE

The protein content of all purified and concentrated products were determined before analyzing them by electrophoresis. 80 µL of each sample were mixed with 20 µL Laemmli and incubated for 5 min at 95 °C. After loading a SDS-Page, the electrophoresis run vertically for nearly 1.5 hour at 150 Volt in a Mini-PROTEAN Tetra Cell apparatus (Biorad, Austria). The loaded protein content per lane was approximately between 5 – 7 µg protein.

SDS-Page.

separating gel (14 %): 2.7mL dH_2O, 4.7mL Acryl-bis-amid (30 %), 2.5mL 1.5M TrisHCl pH8.8, 0.1mL SDS (10 %), 50µL APS (10 %), 6µL TEMED

stacking gel (7 %): 5.1mL dH_2O, 2.3mL Acryl-bis-amid (30 %), 2.5mL 0.5M TrisHCl pH6.8, 0.1mL SDS (10 %), 50µL APS (10 %), 11µL TEMED

Marker: SeeBlue® Plus2 Pre-stained Protein Standard (Invitrogen)

The gel was visualized by Coomassie Blue G250 staining solution over night, moving on a electric shaker plate. The gel was washed with deionized water and destained with a destaining solution consisting of 50 % (v/v) dH_2O, 40% (v/v) MeOH, 10 % (v/v) HAc.

4.6 Enzyme/prodrug combination for potential targeted cancer treatment

4.6.1 Analysis of the reaction rate between HRP and IAA

The reaction rate (velocity) of the reaction between HRP and the plant hormone IAA was measured by a SF-61 DX2 double mixing stopped-flow-spectrophotometer (HI-TECH scientific, United Kingdom) at 418 nm. Four syringes were used to mix potassium phosphate buffer (PP buffer) (50 mM, pH: 6.5), H_2O_2 (1.54 µM), IAA (50, 100, 150, 200 and 300 µM) and the enzyme diluted in PP buffer (1.54 µM) and the absorbance over time was measured.

All used enzymes were normalized to plant HRP (Sigma), whose concentration was determined by measuring the absorbance at 402 nm and calculating the concentration by using the molar extinction factor ε_{402} ($1.02 \cdot 10^5$ $L \cdot mol^{-1} \cdot cm^{-1}$) [48]. A H_2O_2 stock solution was used to determine the extinction coefficient of ε_{240nm} = 39.4 $L \cdot mol^{-1} \cdot cm^{-1}$ [49]. Indole acetic acid stock solutions (3 mM) were prepared daily in 1% ethanol with 50 mM potassium phosphate buffer, pH 6.5. All used solution except the IAA concentrations were diluted to a concentration of 1.54 µM. Hence, the reaction rate at different IAA concentrations was analyzed not only for plant HRP and rHRP A2A expressed in the *P. pastoris och1* k.o. strain, but also for several others like rHRP C1A and rHRP A2A, both expressed in an unmodified *P. pastoris* wildtype strain. The measured kinetic curves were fitted using the software Kinetic studio (HI-TECH scientific) and the K-value was plotted against the corresponding IAA concentrations, whereas the gradient of the slope showed the reaction rate or the velocity of the reaction. This reaction rate - describing how fast IAA is oxidized by HRP - is called K-value in this Thesis. The determined K-values of all samples were normalized to the protein content of plant HRP of 0.1 $mg \cdot mL^{-1}$.

4.6.2 Measurement of IAA turnover

The IAA turnover was measured at a IAA concentration of 100 µM. Stock solutions of IAA and H_2O_2 were prepared as mentioned before. All measurements were done with and without H_2O_2 (10 µM) at 25 and 37 °C. IAA and potassium phosphate buffer with or without H_2O_2 were mixed in a glass vial. The reaction was initiated by the addition of 15 nM peroxidase. Samples were measured repeatedly for up to 6 h by HPLC analysis (Waters 2695 equipped with a Waters 2996 photodiode array detector). Separation was achieved with a reverse phase RPB column (125 x 3.2 mm, 5µm; Hichrom, Reading, UK) at a flow rate of 1 $ml \cdot min^{-1}$ and a linear gradient comprising 5 mM ammonium acetate buffer pH 5.1 and 75 % acetonitrile. The

products from the reaction were separated with a gradient of 15 - 75 % acetonitrile in 9 min, returning to starting conditions in 0.1 min. The formation of products were measured by calibration with standards. Intermediates due to the oxidation of IAA by HRP were IAA-OOH, IAA-CH_2OH, IAA-CHO and 3-methylene-2-oxindole (MOI), which could be identified by comparison with previously recorded spectra [48].

5 Results & Discussion

5.1 Cell morphology

In this analysis not only a possible influence of the changed process parameters during the induction phase on the morphology of the *P. pastoris och1* k.o. strain was investigated, but also a potential effect of the morphology to the rHRP production. Since the morphology of the strain as well as the behavior in the bioreactor was known from previous batch cultivations, these aspects were analyzed within the framework of the DoE bioprocesses. Therefore, the cell size distribution of all samples during the bioprocesses were analyzed by a Malvern Mastersizer 2000.

The cell size distribution analysis delivered the same results for each bioprocess with the *P. pastoris och1* k.o. strain. During the growth phase the cell clusters increased until the carbon source was changed to methanol. Then, a shift from big cell clusters to smaller clusters and single cells was observed (Figure 10). This shift appeared in all bioprocesses with the *P. pastoris och1* k.o. strain when the carbon source was changed (Figure 11), independent of process parameters such as pH, aeration and temperature.

Defined size ranges were chosen to analyze the distribution of cell sizes, whereas all cells above 15 µm were defined as "clusters" and below 15 µm were defined as single cells and/or cells with budded daughter cells.

As shown in Figure 11, the large peak area (after the growth phase on glycerol; solid line) represents a majority of large cell clusters, which shifts mainly to a cell size of approx.10 µm resulting in a clear and sharp peak during the induction phase when methanol is used as carbon source. A comparison to a *P. pastoris* wildtype strain, cultivating in the same way, showed an altered cell size distribution. Here, nearly all cells were present in a range between

1-10 µm during the whole process and no shift from high cell sizes to smaller ones was observed (Figure 11).

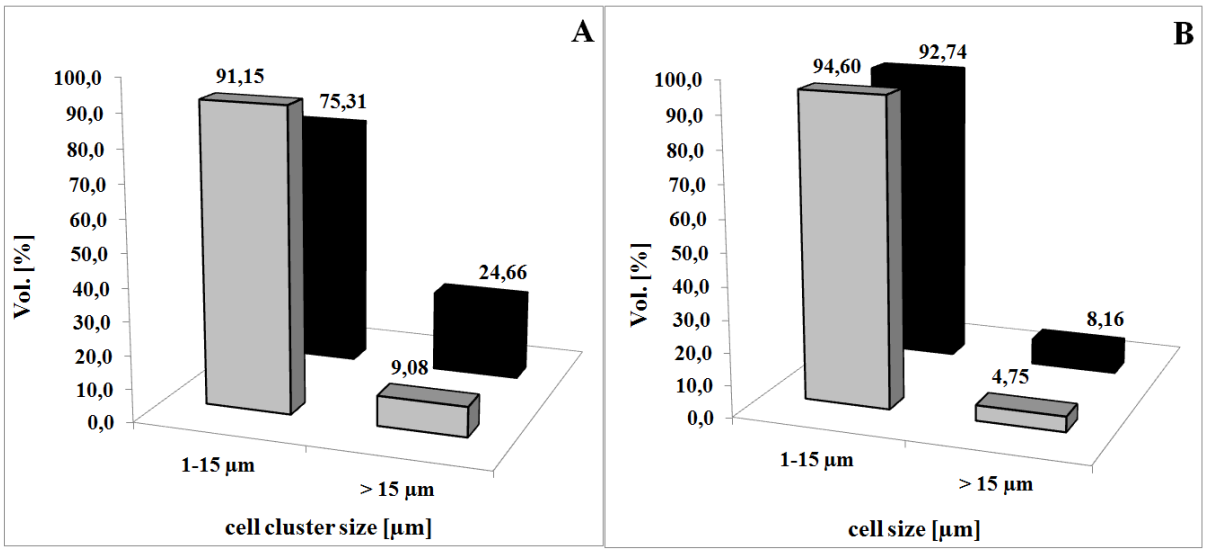

Figure 10: Cell size distribution at 25 °C. A: *P. pastoris och*1 k.o. strain; B: *P. pastoris* wildtype strain; black bar = after growth phase on glycerol; grey bar = fed-batch on methanol after 72 h.

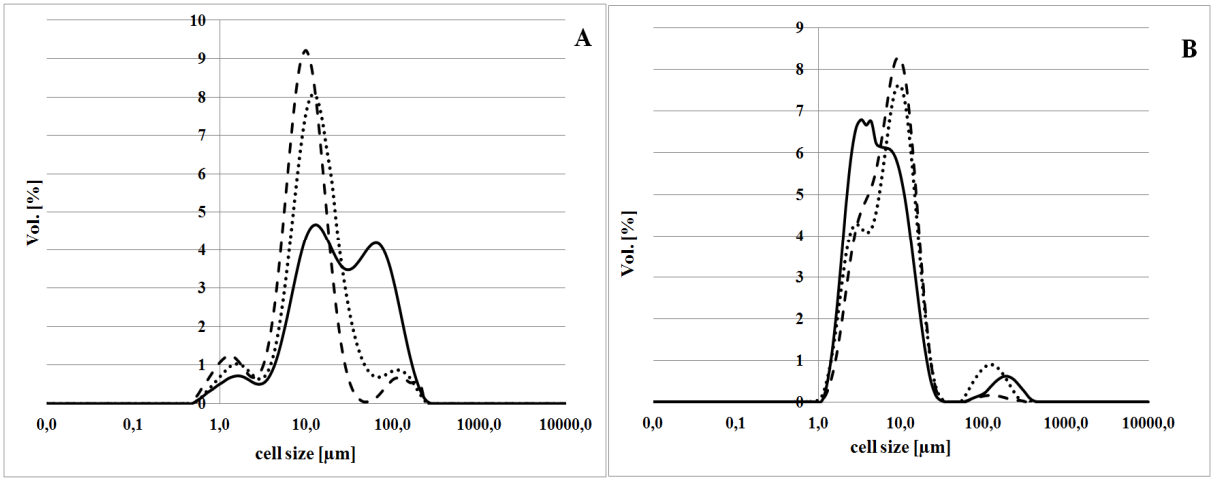

Figure 11: Cell size distribution at 25 °C. A: *P. pastoris och1* k.o. strain; B: *P. pastoris* wildtype strain; solid line = end of growth phase on glycerol; dotted line = methanol fed-batch after 24 h; dashed line = methanol fed-batch after 72 h.

An explanation for this cluster structure might be the effect of the *och1* gene knockout. A loss of mannosyl-phosphate accepting sites in this *P. pastoris och1* k.o. strain might result in reduced charge repulsion between cell surface, which could results in cell aggregates. This

phenomena was described before in *S. cerevisiae* [43, 44]. A hypothesis for the shift in the cell size distribution is, that inner cells of the clusters are substrate limited at the end of the glycerol fed-batch and so they separate or break apart during the fed-batch on methanol. Thus, it may be not an effect of changing the carbon source, it also could be a time effect of cell lysis due to substrate limitation of centre cells. It could be even detected by a light microscope, using a Zeiss deconvolution microscopy system, that inner cells of the clusters became bigger over time during the glycerol fed-batch (Figure 12).

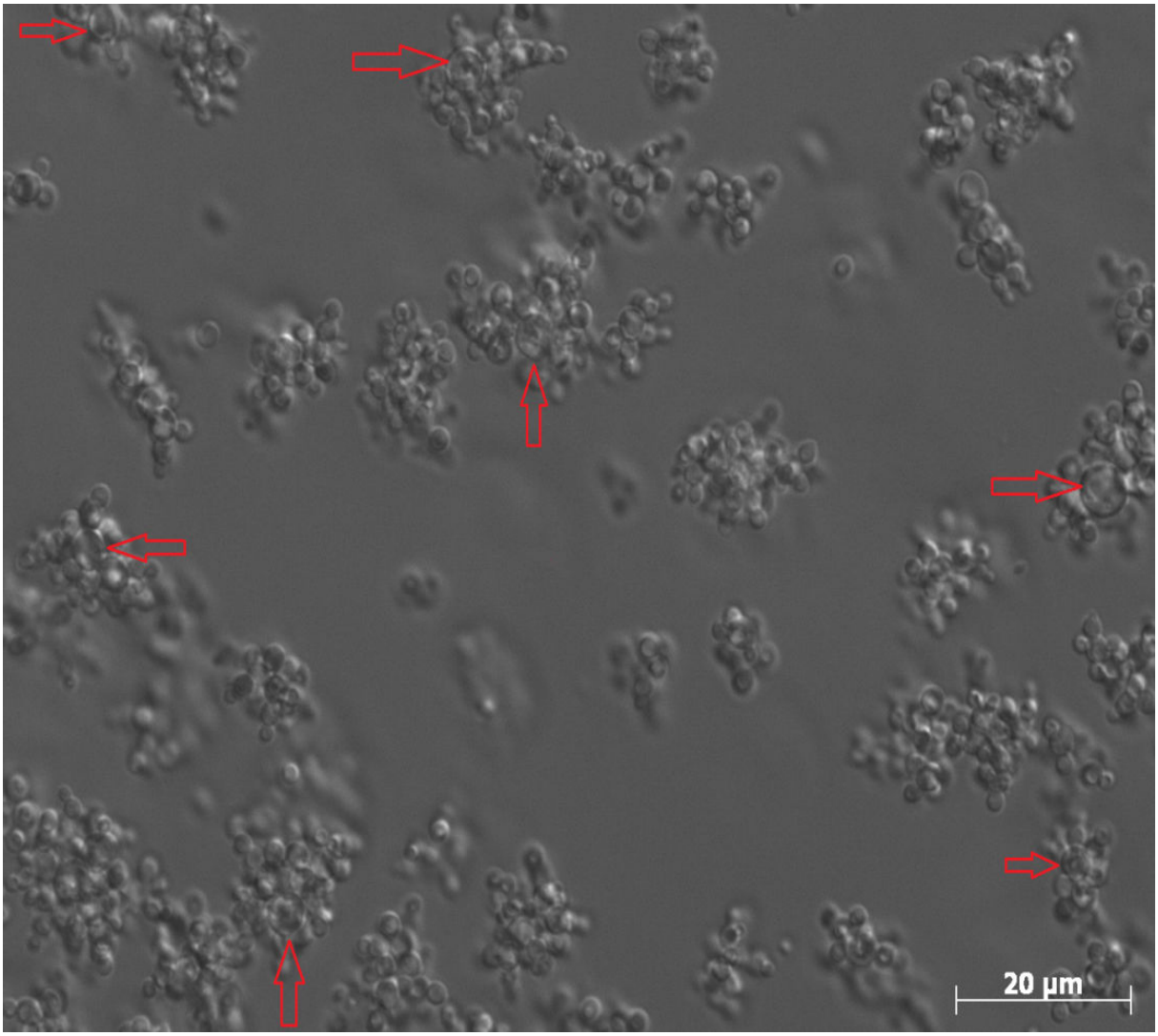

Figure 12: Cell morphology of the *P. pastoris och1* k.o. strain after the beginning of the induction phase on methanol. Centre cells of the cluster are bigger which might be the effect of substrate limitation or higher osmotic pressure. Subsequently these cells lyse and break apart into smaller clusters, which could be recognized and measured with the Malverrn Mastersizer 2000. Huge centre cells are marked with a red arrows.

The volume increase of centre cells might be the fact that water flows inside the cells which results in a higher osmotic pressure. Due to this increasing pressure, stress or substrate limitation these cells may underlie lysis which ends up in smaller cell clusters by breaking apart. Furthermore, there was no cluster formation when the metabolism was changed to the methanol utilization pathway (MUT).

However, the cell size distribution of all bioprocesses of the *P. pastoris och1* k.o. strain showed a similar trend, but no influence on the strain's productivity was observed. Furthermore, no significant influence of the process parameters to the cell morphology could be determined by using the software MODDE 10.0 (Umetrics). It was also analyzed, if this strain specific phenomena is reversible by changing the carbon source again from methanol back to glycerol. Interestingly, it was found out that once the cell size distribution shifted to a smaller size, it did not rise back to higher cell sizes. Thus, this one-way effect is announced to be characteristic for the *P. pastoris och1* knock-out strain, although it does neither influence the productivity nor it is influenced by different process parameters.

The theory mentioned above could be a possible reason for that, although a concrete definition or explanation for this phenomenon cannot be defined. The effect of large cell clusters separating to smaller clusters could also be recognized by a light microscope analysis (Figure 13 and 14). Big cell clusters could be seen during and at the end of the growth phase on glycerol. It is also visible that the single cells of the clusters of the *P. pastoris och1* k.o. strain are smaller compared to the wildtype cells. One single cell of the *P. pastoris* wildtype strain seems to be twofold bigger than a cell of the *och1* k.o. strain. Due to the gene knock out, also the cell size or volume of single cells is degraded (Figure 13 and 14). During the methanol fed-batch, cell clusters became smaller and higher amounts of smaller clusters could be detected under the light microscope. However, as mentioned it is a strain specific phenomenon of this *P. pastoris och1* knock-out strain, but the reason of this shift is not clear to date. Here, only glycerol and methanol were used as carbon sources. Thus, it would be

interesting if the utilization of other carbon sources like glucose or sorbitol also shows this characteristics, or if this is an effect of lysed centre cells instead of changing the carbon source.

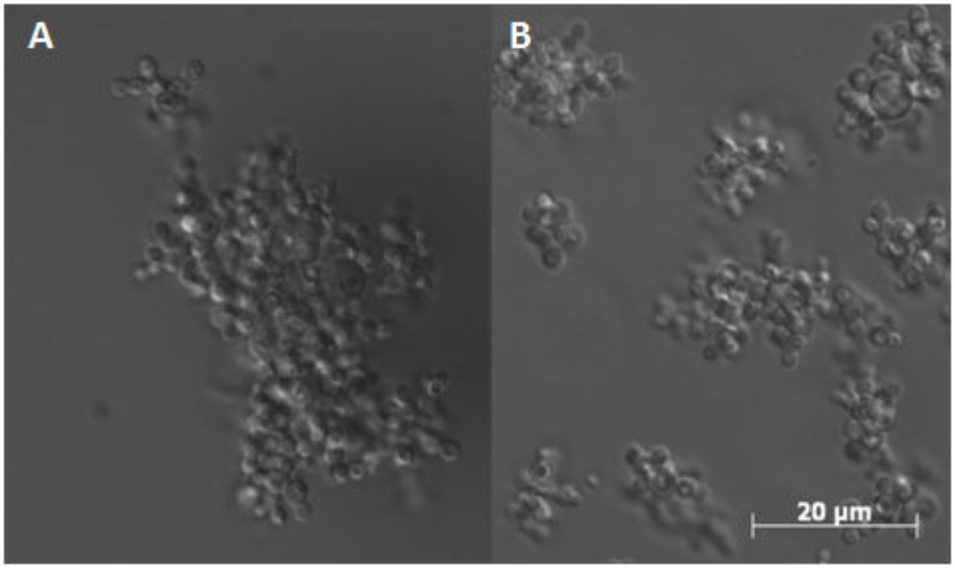

Figure 13: *P. pastoris OCH1* k.o. strain; A: after growth phase on glycerol; B: fed-batch on methanol after 72 h. Big cell clusters appear in the growth phase, whereas smaller cell clusters were present in the methanol fed-batch.

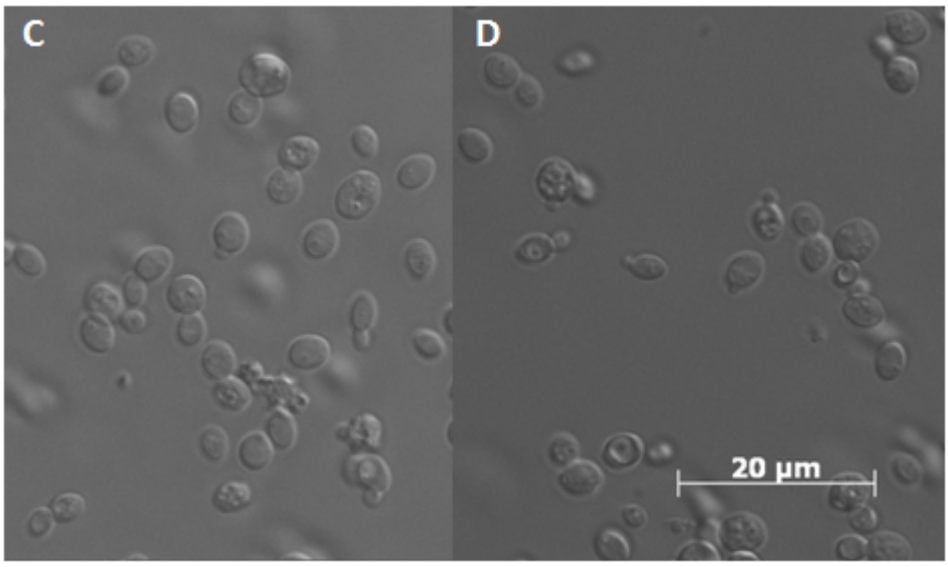

Figure 14: P. pastoris wildtype strain; C: after growth phase on glycerol; D: after fed-batch on methanol after 72 h. No change in cell size occurs during the bioprocess.

5.2 Bioprocess development for a *P. pastoris och1* k.o. strain

5.2.1 Batch cultivations with MeOH pulses

Two batch cultivation at different temperatures (30 and 25 °C) were performed to analyze the maximal specific substrate uptake rate for methanol $q_{Smax,MeOH}$ at these temperatures. During the second batch fermentation at 25 °C, the temperature was decreased to 20 °C and held constant for min. 3 pulses. Furthermore, the correlation (α-factor) between DCW and OD_{600} was determined in order to establish a constant methanol feeding profile in the following fed-batch bioprocesses. Therefore, a sample of the induction phase was taken to analyze this correlation.

The specific substrate uptake rate was determined by doing methanol pulses following a dynamic feeding strategy [45]. These temperatures were chosen due to literature values which are common for *P. pastoris* cultivations [14]. As it is visible in Table 4 $q_{Smax,MeOH}$ shows higher values the lower the temperature is. Thus, this *P. pastoris och1* k.o. strain can take up more methanol at lower temperatures, which also explains the higher volumetric [$U \cdot mL^{-1}$] as well as specific activities [$U \cdot mg^{-1}$] of rHRP A2A. This aspect means that also the specific productivity of this strain is higher the higher the specific substrate uptake rate is.

However, that was shown for the used strain, but there exist other studies were the contrary is shown; the highest specific productivity occurred at a low specific substrate uptake rate [50-52].

30 °C is a common used temperature for *P. pastoris* cultivations, whereat 25 and 20 °C show a slow but still acceptable growth [14]. Due to this and the fact that an increase of the enzymatic activities at lower temperatures exist (Table 4), 20, 25 and 30 °C were chosen as boarders in the continuing DoE experiments.

Table 4: Determined $q_{Smax.,MeOH}$ at different temperatures in batch cultivations and volumetric and specific activities of HRP A2A at these temperatures.

T [°C]	$q_{Smax.,MeOH}$ [mmol·g^{-1}·h^{-1}]	Volumetric activity [U·mL^{-1}]	Specific activity [U·mg^{-1}]
30	0.43	0.34	1.58
25	0.77	8.69	8.10
20	0.80	15.02	12.96

The α-factor was determined by plotting DCW values against OD_{600} values when the strain grows on methanol. Table 5 shows the correlation factors as well as the R^2 values and the respective equations. The analysis of the correlation was done for the *P. pastoris och1* k.o. strain and a *P. pastoris* wildtype strain and was needed to initiate the fed-batch on methanol, according to Eq. 18. Figure 15 shows the correlations between DCW and OD_{600} of the modified *P. pastoris* strain and the wildtype strain. It is visible that both strains have an acceptable correlation.

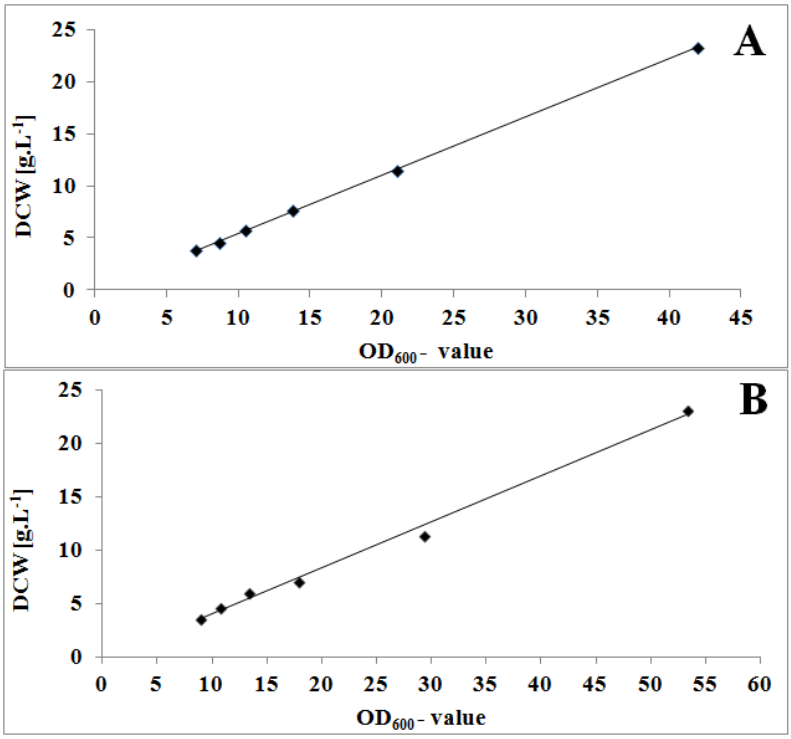

Figure 15: Correlation between DCW [g·L^{-1}]and OD_{600}. A = *P. pastoris och1* k.o. strain; B = wildtype strain

Similar DCW but different OD_{600}-values resulted in diverse correlation-factors. Differences in the correlation between the *P. pastoris* wildtype strain and the *P. pastoris och1* k.o. strain are visible (Table 5). Although the DCW of both strains are comparable, the OD_{600}-values are different, which could be the fact of the cell sizes or morphology (Supplementary table 1). However, the difference of the correlation factor between these two strains is not significant. These factors were used for calculating the biomass after the adaptation pulse and estimating the feeding rate for the constant methanol fed-batch in the DoE experiments.

Table 5: Correlation between DCW and OD_{600} of a sample taken during the induction phase on methanol

	***P. pastoris och1* k.o. strain**	***P. pastoris* wildtype strain**
α - factor	0.5592	0.4303
R^2	0.9999	0.9934
equation	y = 0.5592x - 0,1471	y = 0.4303x - 0,2653

5.2.2 Design of Experiments

In this Design of Experiments (DoE) screening a parameter area for high production of rHRP A2A with the *P. pastoris och1* k.o. strain was determined by varying the parameters temperature, pH and pO_2 concentration during the induction phase. A linear interaction model was created and tested for its validity by using the MODDE 10.0 software (Umetrics). The responses were split into **physiology-related** and **product-related** results. Correlations between strain characteristics, like the yields ($Y_{CO2/S}$, $Y_{X/S}$), methanol accumulation or $q_{S,adapt}$, and the varied process parameters (Table 1) during the induction phase were investigated.

Table 6: Physiology of the *P. pastoris och1* k.o. strain and product characteristics analyzed in the Design of Experiments screening

	Temp.: 20 °C				**Temp.: 25 °C**	**Temp.: 30 °C**			
	pH: 5.0		**pH: 7.0**		**pH: 6.0**	**pH: 5.0**		**pH: 7.0**	
Physiology-related characteristics	**pO_2: 10%**	**pO_2: 30%**	**pO_2: 10%**	**pO_2: 30%**	**pO_2: 20%**	**pO_2: 10%**	**pO_2: 30%**	**pO_2: 10%**	**pO_2: 30%**
$q_{MeOH,adapt}$ [mmol·g^{-1}·h^{-1}]	**0.26**	**0.23**	**0.16**	**0.18**	**0.17**	**0.16**	**0.08**	**0.16**	**0.09**
$\mu_{max,Gly}$ - batch [h^{-1}]	0.20	0.20	0.19	0.19	0.18	0.19	0.19	0.18	0.19
q_{MeOH} set [mmol·g^{-1}·h^{-1}]	0.20	0.20	0.20	0.20	0.20	0.20	0.20	0.20	0.20
q_{MeOH}, real [mmol·g^{-1}·h^{-1}]	**0.28**	**0.20**	**0.20**	**0.24**	**0.20**	**0.21**	**0.18**	**0.21**	**0.17**
$Y_{x/MeOH}$ [C-mol·C-mol^{-1}]	0.20	0.21	0.29	0.33	0.28	0.31	0.18	0.26	0.36
$Y_{CO2/MeOH}$ [C-mol·C-mol^{-1}]	0.80	0.75	0.81	0.69	0.75	0.82	0.85	0.83	0.75
C-Balance [-]	**0.97**	**1.01**	**1.11**	**0.96**	**1.02**	**1.16**	**0.96**	**1.09**	**1.05**
MeOH accumulation [g·L^{-1}]	-	-	-	-	-	0.20	0.90	-	1.34
Product-related characteristics									
q_p [U·g^{-1}·h^{-1}]	**4.43**	**4.29**	**4.27**	**5.58**	**0.76**	**0.07**	**0.03**	**0.06**	**0.01**
η[U·mmol^{-1}]	**12.3**	**16.8**	**17.4**	**23.7**	**3.85**	**0.33**	**0.15**	**0.28**	**0.04**
Vol. productivity [U·L^{-1}·h^{-1}]	**153**	**151**	**137**	**194**	**35.5**	**0.98**	**0.46**	**1.35**	**1.19**
Spec. activity [U·mg^{-1}]	**44.8**	**48.9**	**47.2**	**41.4**	**9.96**	**0.43**	**0.21**	**0.32**	**0.20**

Table 6 shows all relevant data of the DoE experiments, in which a constant feeding strategy with the $q_{S,MeOH}$ real close to the certain $q_{S,MeOH}$ set of 0.2 mmol·g^{-1}·h^{-1} can be recognized. Except experiment 1 (Temp.: 20 °C, pH: 5.0, pO_2 = 10 %) showed a higher $q_{S,MeOH}$ real due to problems with the feeding pump. Hence, this values prove that the applied feeding strategy with the correlation factor between DCW and OD_{600} was successful. The growth phases were executed always under the same conditions and the batch phase run always in the same way. This is also shown in similar specific growth rates between 0.18 - 0.2 h^{-1}. Also the C-balances are all close to 1.0, meaning that no C-atoms were inexplicably lost and that the calculated values are correct (Table 6).

Physiology-related responses:

a) $q_{S,adapt}$:

The physiology characteristic $q_{S,adapt}$ describes how fast the expression system is adapted to the new substrate methanol. Interestingly, an essential influence of the temperature was observed, but also the pH and pO_2 concentration affected $q_{S,adapt}$ (Figure 16). Thus, an interaction between those parameters and this response could be determined and is visualized in a contour-plot designed by MODDE (Figure 16). Higher $q_{S,adapt}$ values are represented at lower temperatures, lower pH and lower pO_2 concentrations. In contrast to that, low $q_{S,adapt}$ values were observed at 30 °C, which means that the expression system needed more time after the growth phase to adapt to methanol at 30 °C. As it is visible in Figure 16, the $q_{S,adapt}$ was around 0.1 $mmol \cdot g^{-1} \cdot h^{-1}$ at 30 °C and 30 % pO_2 concentration but increased at this temperature when pO_2 concentration was lower.

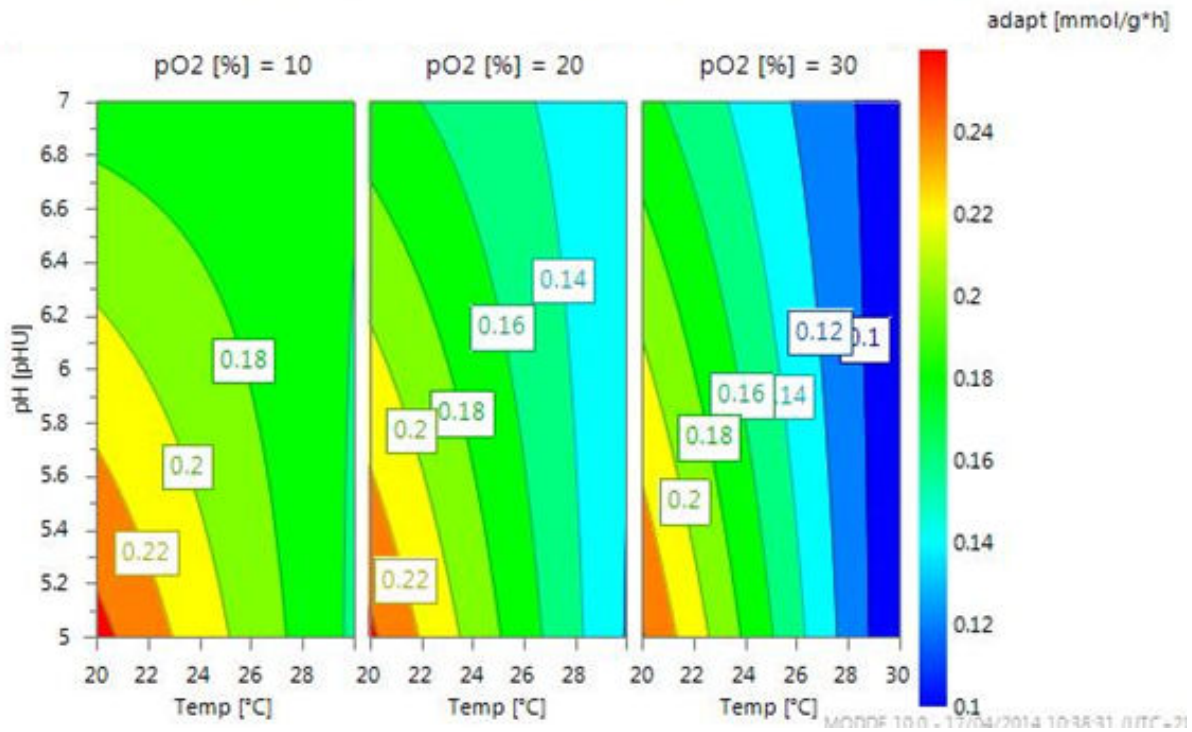

Figure 16: Contour-plot of determined $q_{S,adapt}$ of the DoE experiments. The lower the temperature and the pH, the higher the $q_{S,adapt}$. Also pO_2 concentration influences $q_{S,adapt}$, whereas higher values are achieved at lower concentration.

However, according to the p-values determined by MODDE only the temperature showed a significant influence on this response, as the p-value was below 0.05 (Table 7). Although the contour-plot showed an influence of pH and pO_2, no significant interaction between those two parameters and $q_{S,adapt}$ occurred because the respective p-values were > 0.05.

b) Yields:

As visible in Table 6, the calculated yields, $Y_{CO2/S}$- as well as $Y_{X/S}$ - values are close together showing only a slight deviation. Thus, the influence of the parameters on these responses was not significant. This was also underlined by the p-values, which were all higher than 0.05 meaning that no significant interaction between the responses $Y_{CO2/S}$ and $Y_{X/S}$ and the parameters temperature, pH and pO_2 concentration occurred (Table 7).

c) MeOH accumulation:

Focused on the substrate uptake, it is believed that even the low $q_{S,MeOH}$,set overburdens the metabolism of this modified strain at 30 °C, which resulted in methanol accumulation in all processes with an induction phase at 30 °C, except DoE experiment 5. Methanol accumulation means that the $q_{Smax,MeOH}$ at 30 °C is lower than 0.2 $mmol \cdot g^{-1} \cdot h^{-1}$. It was shown that this modified strain needed more time at 30 °C to adapt to methanol. Methanol accumulation occurred prevalent at 30 °C and 30 % pO_2 concentration, which correlated with the low $q_{S,adapt}$ values at these parameters (Figure 16). However, no significant interactions between the response and the varied parameters could be determined because the p-values were above 0.05.

However, it seems that the temperature has an influence on the methanol accumulation, but no significant interaction between this parameter and the response “MeOH accumulation” could be determined.

To summarize, the *P. pastoris och1* k.o. strain cannot exploit this substrate as effective and fast at higher temperatures and higher pO_2 concentrations as at lower temperatures and pO_2 concentrations, which might be due to more cellular stress.

Table 7: p-values of the physiology-related responses of the DoE experiments

Responses	p-value		
	Temperature	**pH**	**pO2 %**
$Y_{CO2/S}$	0.109	0.237	0.084
$Y_{X/S}$	0.689	0.075	0.951
MeOH acc.	0.0567	0.776	0.098
$q_{S,adapt}$	**0.0139**	0.383	0.098

Product-related responses:

The product-related results are separated into strain characteristics, including specific productivity, volumetric productivity and the efficiency factor, and the product characteristic which means product quality (specific activity).

a) Strain characteristics – specific and volumetric productivity and efficiency factor:

Here, an extensive influence of the temperature on specific productivity as well as on the volumetric activity and the efficiency factor was observed. The following contour-plots (Figure 17-19) represent a parameter area for high recombinant protein production, especially for high rHRP A2A production in the *P. pastoris och1* k.o. strain, which was determined within this DoE screening. All three figures show the same trend with the region for the high rHRP production at the edge of the design space at 20 °C.

In addition to the significant influence of the temperature on the specific productivity, also a slight influence of pH and pO_2 seems to be present (Figure 17). The analysis of the p-values

using MODDE delivered that only the temperature represented a significant interaction with the specific productivity, whereas pH and pO_2 concentration had no significant influence (Table 8).

This is also presented in Figure 18 and 19, where the contour-plot shows not only an influence of the temperature on the volumetric productivity and the efficiency factor, but also a potential effect of pH and pO_2 concentration. However, the analysis of the p-values delivered again that only temperature was the significant influencing parameter. Thus, pH and pO_2 concentration did not affect the volumetric productivity and the efficiency factor significantly (Table 8).

The specific productivity was 50-60 times higher at 20 °C than at 30 °C. The volumetric productivity was even 100-150 times higher values at 20 °C than at 30 °C. The efficiency factor η had 50-fold higher values in the processes with an induction phase at 20 °C compared to 30 °C (Table 6). This means that the substrate was converted more efficiently into product. Hence, the efficiency factor is equivalent to the product yield.

On the basis of Table 6, the temperature must have a significant influence on the responses due to the major differences of the determined values. According to the p-values, temperature significantly influenced the here discussed responses, but also a non-significant effect of pH and pO_2 concentration on these responses could be shown (Table 8).

Table 8: p-values of the product-related responses of the DoE experiments

	Responses	p-value		
		Temperature	**pH**	**pO2 %**
Strain characteristics	Specific productivity	0,000145	0,583	0,298
	Efficiency factor	0,000137	0,725	0,375
	Volumetric productivity	0.0000246	0.499	0.834
Product characteristic	Specific activity	0,000147	0,941	0,355

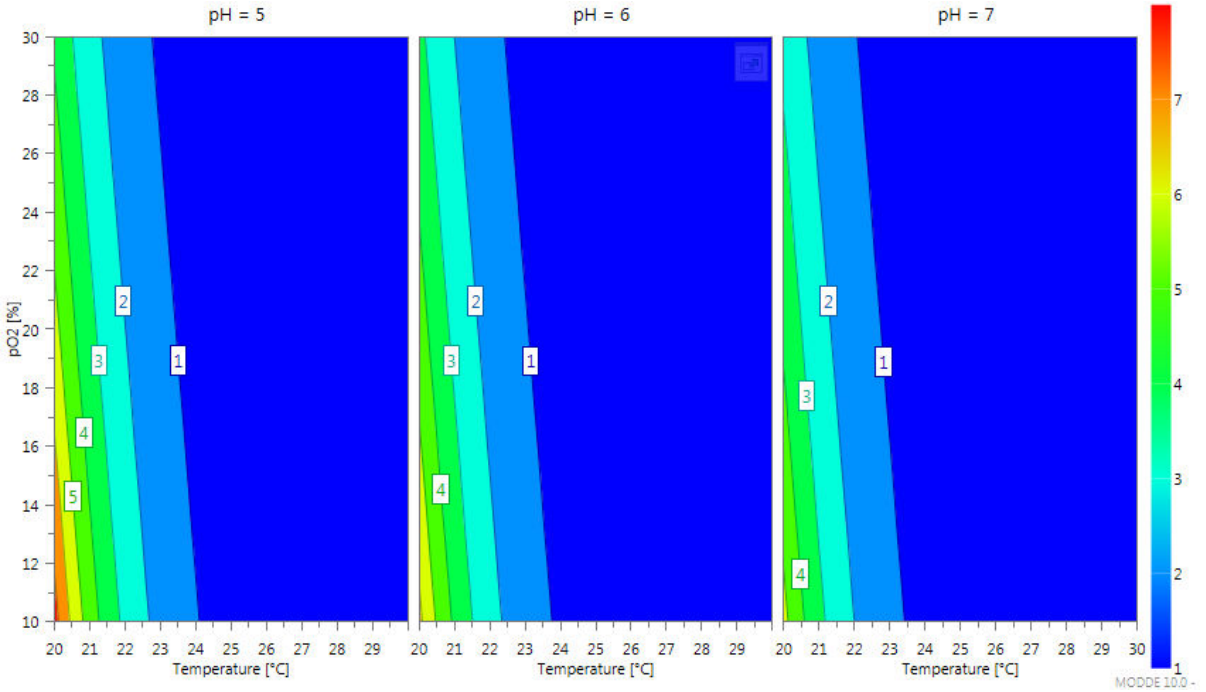

Figure 17: Contour-plot of the specific productivity of the *P. pastoris och1* k.o. strain. No influence of the pH is observed, but an extensive influence of the temperature. Also pO_2 concentration affects the specific productivity. High productivity is achieved at a temperature of 20 °C and 10 % pO_2, delivering values up to 5.5 $U \cdot g^{-1} \cdot h^{-1}$.

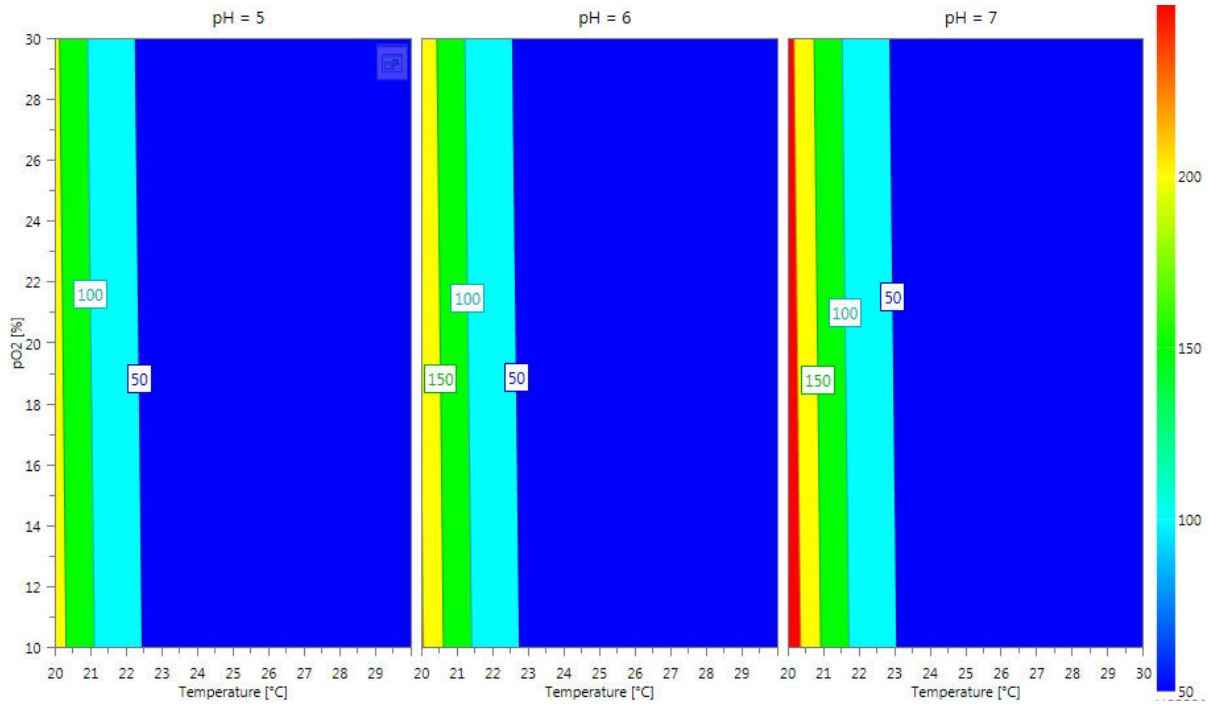

Figure 18: Contour-plot of the volumetric productivity of the *P. pastoris och1* k.o. strain. Temperature has the highest influence, but also pH and pO_2 seems to have a slightly effect on the volumetric productivity.

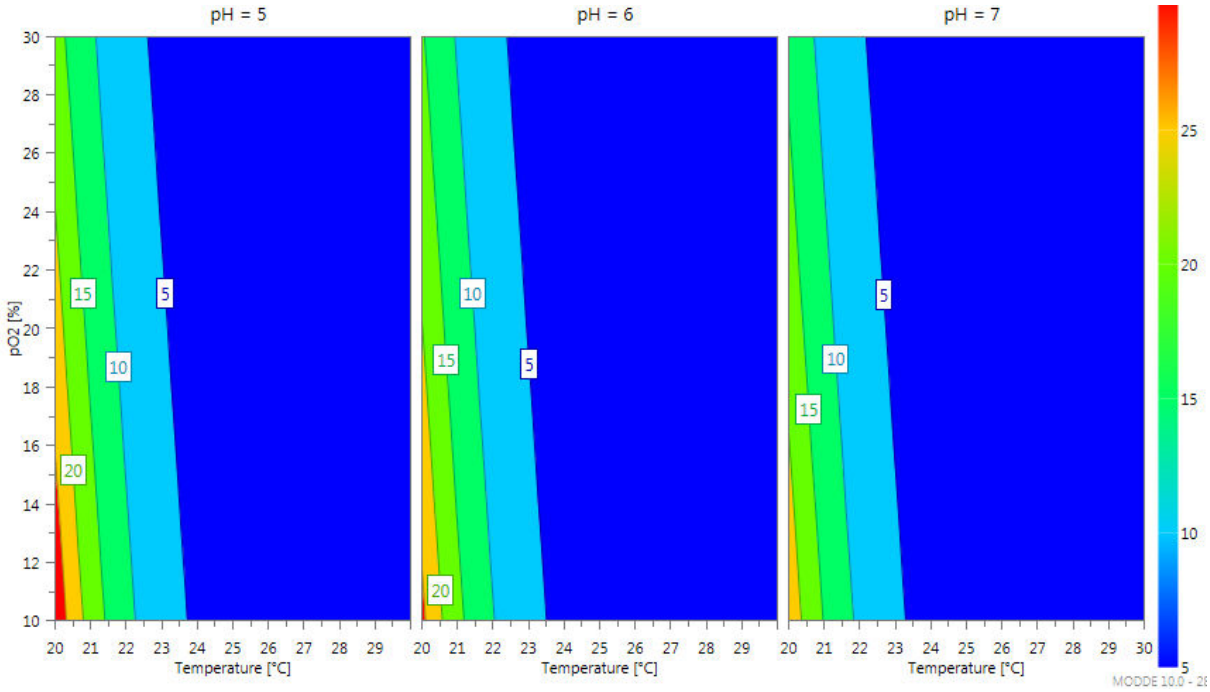

Figure 19: Contour-plot of the efficiency factor of the *P. pastoris och1* k.o. strain. pH does not influence η, whereas temperature illustrates the most-influencing parameter. pO_2 concentration also affects the efficiency factor.

b) Product characteristic – specific activity:

Due to the pH stability of the product between 5.0-10.0 [27], no significant influence of the pH on the specific activity (product quality) could be recognized. Thus, the contour-plot of the product qualities showed the same trend and values at the different pH values (Figure 20). The area for a high product quality of rHRP A2A expressed in the *P. pastoris och1* k.o. strain is at the edge of the design space, at 20 °C and a pO_2 concentration of 10 % (Figure 20). A reason for this is a more effective exploitation of methanol at lower temperatures compared to higher ones, as mentioned before and therefore either the expression of rHRP A2A is higher or the expressed rHRP A2A is more active. 20 °C and 10% pO_2 during the induction phase deliver 100-fold higher product quality values compared to the 30 °C bioprocesses (Table 6). Again, it was shown that the temperature influenced the product quality of rHRP A2A

significantly (p-value < 0.05), whereas no significant interaction between pH or pO_2 concentration and the product quality could be determined (Table 8).

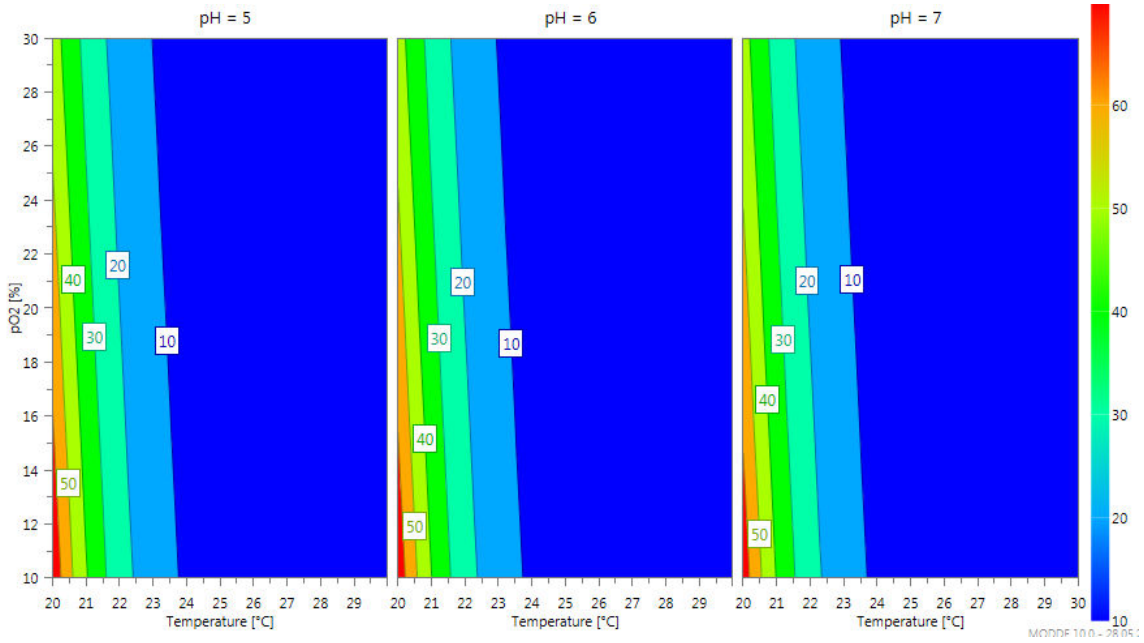

Figure 20: Contour-plot of the specific activity of rHRP A2A. Temperature shows the most influence on specific activity, but also pO_2 concentration affects the spec. activity of the expressed enzyme. pH has no effect due to the boarders in the pH stability range of the protein.

Summarizing, all four analyzed responses are significantly influenced by the temperature, but no significant influence of pH or dissolved oxygen concentration on these responses could be discovered because of the p-values (Table 8).

All contour-plots (Figure 16-20) delivered a parameter area at 20 °C, a pH of 5.0 and a pO_2 concentration of 10 %, in which $q_{S,adapt}$, specific productivity, volumetric productivity, the efficiency factor and the product quality represented higher values compared to higher temperatures. It was shown that temperature is the only significant influencing parameter, but due to the determined areas shown in the contour-plot, pH and pO_2 concentration seem to have a minor influence. Therefore, the parameter area for high rHRP A2A production is located at 20 °C, pH of 5.0 and pO_2 concentration of 10 %.

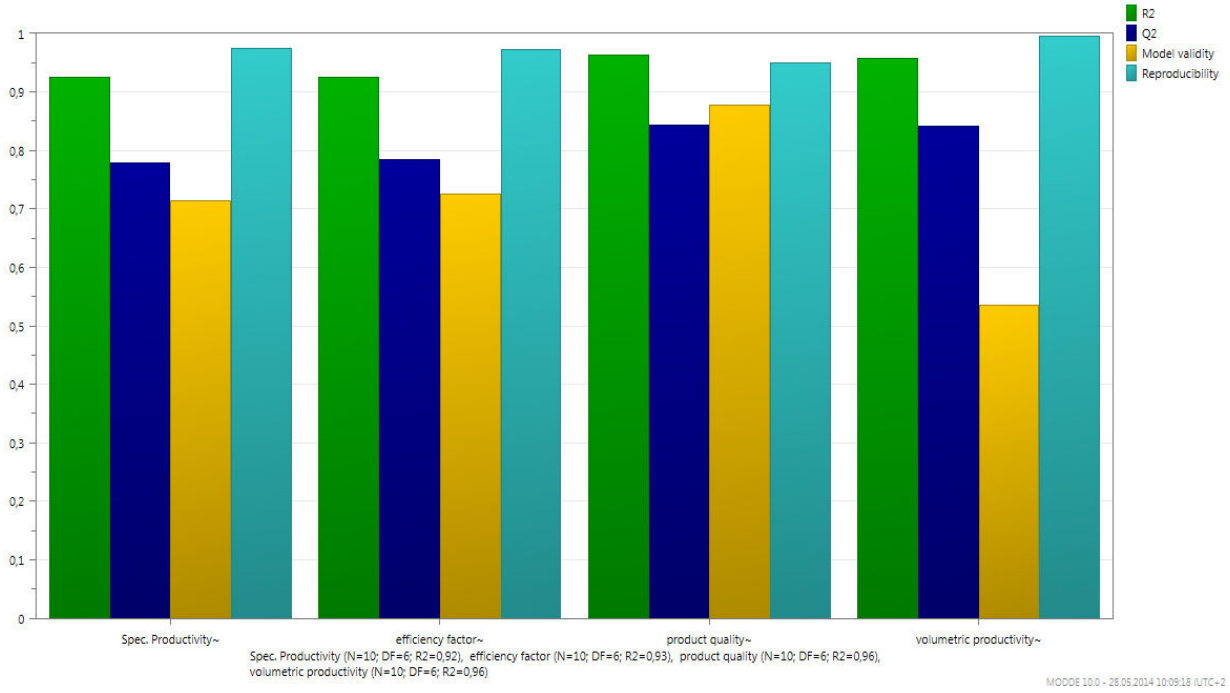

Figure 21: Summary of fit plot of specific productivity, the efficiency factor, product quality and volumetric productivity showing an acceptable validity

Figure 21 shows the regression, the significance, the model validity and the reproducibility. This figure describes that the investigated model for the influence of the three parameters (Temp., pH and pO_2) on the responses (specific productivity, the efficiency factor, product quality and volumetric productivity) is valid.

R^2 describes the goodness of fit and measures how well current runs can be reproduced. In our case, the regression is between 0.9 and 1.0, consequently the goodness of fit is high.

Q^2 describes the goodness or prediction and how well new experiments can be predicted. Figure 21 shows values between 0.75-0.85, thus a good prediction is represented.

The model validity describes a good model if it is higher than 0.25 and indicates significant a "lack of fit" (model imperfections) if it is below 0.25. Due to represented values above 0.4 of all responses in Figure 21, the investigated model is valid.

The shown reproducibility for all responses is between 0.95 and 1.0, which describes that the error is very low. Vice versa, if the reproducibility would be below 0.5 a large error would exist.

Verification runs:

Two verification runs (at 15 and 20 °C, pH of 5.0 and pO_2 of 10%) were done to prove the above described results. Due to the fact that the parameter area for high rHRP A2A production is completely in the edge of the design space, it is unknown if the production of this enzyme would be even higher at temperatures below 20 °C. Moreover, a bioprocess with these parameters was also done with a *P. pastoris* wildtype strain to compare both strains in terms of specific productivity, volumetric productivity, efficiency factor, product quality and $q_{S,adapt}$.

Table 9: Physiology and product characteristics of both verification runs and the bioprocess with the *P. pastoris* wildtype strain. V1 = verification run 1; V2 = verification run 2

	V1	**V2**	***P. pastoris* wt**
	Temp.: 15 °C	**Temp.: 20 °C**	
	pH: 5.0	**pH: 5.0**	
Physiology-related characteristics	**pO_2: 10%**	**pO_2: 10%**	
$q_{S,adapt}$ [mmol·g^{-1}·h^{-1}]	0.21	0.17	0.15
$\mu_{max,Gly}$ [h^{-1}] - batch	0.19	0.21	0.28
q_{MeOH} [mmol·g^{-1}·h^{-1}] set	0.20	0.20	0.20
q_{MeOH} [mmol.g^{-1}.h^{-1}] real	0.17	0.19	0.17
$Y_{x/MeOH}$ [C-mol·C-mol^{-1}]	0.37	0.31	0.24
$Y_{CO2/MeOH}$ [C-mol·C-mol^{-1}]	0.68	0.70	0.77
C-Balance [-]	1.06	0.97	1.06
MeOH accumulation [g·L^{-1}]	-	-	-
Product-related characteristics			
q_p [U·g^{-1}·h^{-1}]	1.44	5.53	7.34
volumetric productivity [U·L^{-1}·h^{-1}]	56.2	158	349
efficiency factor [U·mmol^{-1}]	8.62	29.09	39.10
product quality [U·mg^{-1}]	19.82	50.39	105.47

Table 9 shows the physiology-related and product-related characteristics of both verification runs and the bioprocess with the *P. pastoris* wildtype strain. The *P. pastoris och1* k.o. strain has a similar $q_{S,adapt}$ at 15 °C compared to the processes at 20 °C (Figure 16). Furthermore, both verification runs exhibit similar values for $q_{S,MeOH}$ real, which was closed to the set value, and also for $Y_{X/S}$ and $Y_{CO2/S}$. The C-balance was approximately at 1.0. Both verification runs did not show any methanol accumulation because of a more efficient consumption of the substrate at lower temperatures, which was also mentioned before.

Due to the described area for high rHRP A2A production, which was present in the edge of the design space (Figure 17-20), the verification run 1 was executed also at 15 °C to analyze if this strain had even a higher productivity compared to the processes at 20 °C. However, the results showed an approx. 3-time lower specific productivity, volumetric productivity as well as efficiency factor. Even the product quality was decreased more than 50 % compared to the process at 20 °C (Table 9). The specific productivity and the efficiency factor were even 3-times lower. Thus, an optimal region for recombinant protein production, especially for HRP production, with this *P. pastoris och1* k.o. strains, might be in the range of 16-20 °C.

Verification run 2 proved the results which were determined in the DoE screening, because the specific and volumetric productivity and the efficiency factor as well as the product quality were comparable. Also the physiology-related characteristics were similar to the DoE results.

The *P. pas*toris wildtype strain showed also high rHRP A2A production at the same parameters (T.: 20 °C, pH: 5.0 and pO_2: 10 %) as the *P. pastoris och1* k.o. strain. In regard of $q_{S,adapt}$, the wildtype strain delivered a lower adaptation time to the substrate methanol compared to the modified strain and also a lower biomass yield. The specific growth rate during the batch phase was higher which means a faster growth of this strain compared to the *P. pastoris och1* k.o. strain. This difference in the velocity of the growth was also reported in various studies, not only for *P. pastoris* but also for other yeasts like *S. cerevisiae* where the

och1 gene was knocked-out [4, 5, 43, 44]. No methanol accumulation occurred during the process and the C-balance was close to 1.0.

With respect to the strain characteristics of these two strains, some differences were observed. Whereas the *P. pastoris och1* k.o. strain exhibited a specific productivity of 4.2 - 5.5 $U \cdot g^{-1} \cdot h^{-1}$, the wildtype strain had a higher specific productivity of 7.34 $U \cdot g^{-1} \cdot h^{-1}$. Also the volumetric productivity was approx. 50 % higher in the wildtype strain compared to the *P. pastoris och1* k.o. strain (Table 9). Moreover, the substrate was more efficiently converted to product, which could be recognized in a higher efficiency factor of the wildtype strain.

With regard to the product characteristic, the product quality of rHRP A2A expressed in the *P. pastoris* wildtype strain was 50 % higher compared to the *P. pastoris och1* k.o. strain. The modified strain apparently exported more endogenous proteins, which decreased the purity of the product. This aspect could be also seen in the measurements of the protein contents, where the modified strain had a higher extracellular protein concentrations compared to the wildtype strain, which may be also a consequence of the gene knock-out. Another possibility of a lower product quality might result in a lower enzymatic activity due to the less-glycosylation, but this can be excluded because the cultivations were performed in the same way.

However, the *P. pastoris* wildtype strain has the ability to grow faster and to produce more pure rHRP A2A in slightly higher amounts, but the product is hyperglycosylated, which is not the case with *P. pastoris och1* k.o. strain [2].

It was discovered that the parameter area for high rHRP A2A production with the *P. pastoris och1* k.o. strain is at 20 °C, pH of 5.0 and a pO_2 concentration of 10 %, which could be proved by the two verification runs. Due to the results of the verification run 1, the optimal region for the highest rHRP production may lie between 16-20 °C, but therefore further optimization studies have to be done which was beyond the scope of this Thesis.

5.2.3 Additional experiments

Precursor experiments:

As described before, a parameter area for high rHRP A2A production with both, the modified and the wildtype *P. pastoris* strain was determined. In addition to that, different heme-precursors were tested for a potential enhancement of rHRP production in the *P. pastoris och1* k.o. strain and the *P. pastoris* wildtype strain.

In shake flasks experiments, three different precursors $FeSO_4$, δ-Ala and hemin as well as the HRP production without a precursor were investigated at 20 °C. As it is visible in Figure 22, enzymatic activities are more or less 4-fold higher with the precursor hemin used during the cultivation of the *P. pastoris och1* k.o. strain and for the wildtype strain even higher.

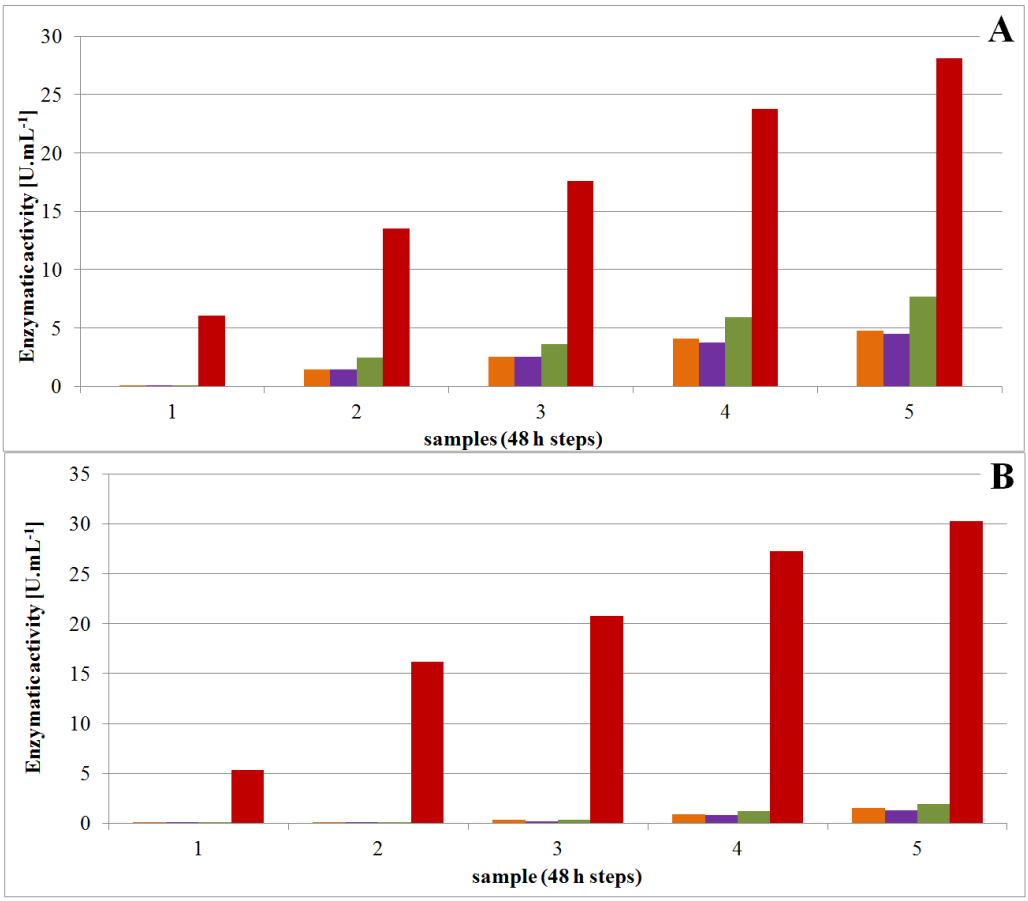

Figure 22: Investigation of no precursor and three different precursors on the enzymatic activities of HRP A2A. A: *P. pastoris och1* k.o. strain; **B**: *P. pastoris* wildtype strain; orange: without precursor; violet: δ-Ala [1mM]; green: $FeSO_4$ [1 mM]; red: hemin [30 µM]

Due to these high activities, the background of the hemin precursor was determined resulting in a value of 0.5 $U.mL^{-1}$ by measuring the hemin-solution with the $CuBiAn^{XC}$ enzymatic robot. No utilization of a precursor delivers similar results as δ-Ala, whereas $FeSO_4$ shows higher enzymatic activities. Nevertheless, the precursor hemin seems to be the best option for the support of the HRP production in the *P. pastoris och1* k.o. strain. The concentration of hemin was lower compared to the other precursors, because of precipitation concentrations above 100 µM.

The activity of rHRP A2A in the *P. pastoris* wildtype strain was even 10-fold higher adding the precursor hemin. There were no huge differences in the enzymatic activity using the other precursors or no precursor. Hence, hemin is also for the rHRP production in the wildtype strain the best of those studied precursors.

Protease inhibitor:

The specific productivity at 30 °C was very low in the bioreactor experiments and also the specific activity was low, which might be the effect of the expression of a lot of other proteins. Another reason could be the presence of proteases produced by the host strain and transferred into the fermentation broth during the process. These endogenous proteases may degrade the target protein rHRP and thus, may be responsible for the low activity values. Hence, the influence of a protease inhibitor on rHRP production at this temperature in the *P. pastoris och1* k.o. strain and the *P. pastoris* wildtype strain was studied.

Due to the low specific activities at 30 °C, shake flask experiments at this temperature were done by expressing rHRP A2A in the *P. pastoris och1* k.o. and the *P. pastoris* wildtype strain. These experiments were done in double preparation, whereas a protease inhibitor was added to half of the shake flasks. Sampling was done every 24 hours and enzymatic activity was measured. After 8 days induction time, no differences between the samples with the protease inhibitor and the samples without the inhibitor were observed. After 96 hours induction time

with 0.5 % (v/v) methanol pulses, no extracellular enzymatic activity could be measured, which might be the reason of the cultivation conditions. Thus, those experiments may be repeated at 25 °C to analyze if an effect of proteases on the enzymatic activity is present. However, a reason for the very low enzymatic activities at 30 °C can be the expression proteases but also misfolding of the enzyme itself.

However, the protein concentrations were similar (Supplementary table 2). An explanation thatfore could be higher cellular stress on the one hand but also incorrect folding due to the enzyme's difficult structure with 4 disulfide bridges on the other hand. For sure, shake flasks are not optimal incubation systems for *P. pastoris*, as aeration is a very important aspect for this yeast and thus, oxygen may not be sufficiently provided.

Nevertheless, the cells were harvested and digested by high pressure homogenization followed by intracellular activity measurement. However, no enzymatic activity could be detected from the cell lysate, but a protein band at 35 kDa could be seen on a SDS-PAGE which describes the molecular weight of the unglycosylated polypeptide chain of HRP (Figure 23). HRP extract from plant is visible with a molecular weight of 46 kDa and intracellular rHRP is present at 35 kDa. Due to the fact that the intracellular proteins did not go through the secretion pathway where the *N*-glycosylation occurs, the presented results are reasonable.

Although no enzymatic activity could be measured in the intracellular space, the SDS-PAGE showed that rHRP A2A was produced, but was not exported into extracellular space. As mentioned before, less enzymatic activity can be the effect of proteases but also of higher cellular stress or misfolding at this temperature.

Therefore, these protease inhibitor experiments should be repeated either in the bioreactor at 30 °C or in shake flasks at 25 or 20 °C in order to determine, if proteases are present and influence the enzymatic activity.

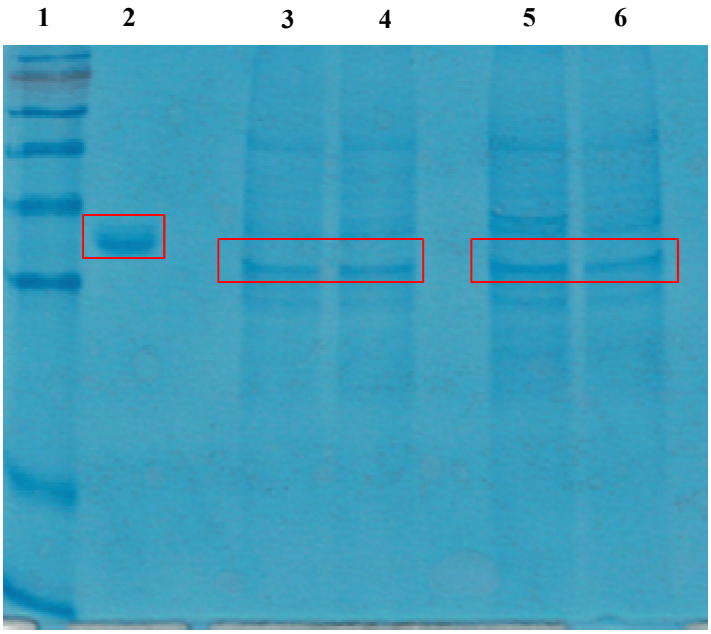

Figure 23: SDS-PAGE showing intracellular rHRP A2A expressed in *P. pastoris och1* k.o. or in the wildtype strain. Lane 1 = SeeBlue®Plus2 Pre-stained standard; lane 2 = HRP plant; lanes 3 and 4 = HRP A2A in wildtype (wt) without protease inhibitor (p.i.) and with p.i.; lanes 5 and 6 = HRP A2A in *och1* k.o. strain without p.i. and with p.i.; Red frame indicates the HRP band.

5.3 Enzyme purification

All fermentation broths with an enzymatic activity above 3 $U \cdot mL^{-1}$ at the end of the bioprocess were harvested, centrifuged, the supernatant was concentrated and the buffer changed by UF/DF. During the first step of the DSP, namely microfiltration, approximately 20-30 % of the total units of the product were lost, because the target enzyme could not be recovered from the membrane surface. Furthermore, biomass stuck together and was surrounded by a liquid film, in which the enzyme might be enclosed. The loss during the UF/DF step was between 5-20 % of the total units, using only one membrane module.

Moreover, the product was concentrated 10-15-fold and the buffer was changed to prepare the enzyme for subsequent purification.

Furthermore, potential effects of the varied process parameters during the induction phase on the purification of HRP A2A were studied by doing a 2-step purification [27]. The 2-step chromatography consisting of HCIC and AEX with a CIM-DEAE monolithic column was done for rHRP A2A not only expressed in the *P. pastoris och1* k.o. strain under different conditions, but also expressed in the *P. pastoris* wildtype strain under the determined parameters for high productivity. The analyzed purification factors describing the efficiency of the purification/ chromatography step are shown in Table 10.

One can see that the resulting purification factors of the HCIC chromatography of the first experiments were 3-times higher than at DoE experiment 7 and 8. A reason for that might be the used resin, which was new at the beginning of these purifications. After the purifications of the DoE experiments, the resin was changed and the HCIC step was done with rHRP A2A expressed in the *P. pastoris* wildtype strain. The resulting PF was higher again, which supports the theory that the resin was fouling during the purifications of the DoE experiments. Also the verification run 2 was purified with this 2-step chromatography strategy, which delivered similar results. This purification was also done after the resin of the HCIC was changed, and therefore higher PFs were scored. Thus, differences of purification factors cannot be assigned to upstream changes but probably result from the change of the resin. Hence, whenever influences of changes in the bioprocess on the downstream process are investigated, exactly the same settings must be used in order to correlate these two process stages.

Thus, a suggestion for an efficient purification would be the change of the resin after the HCIC chromatography.

However, the AEX chromatography using the monolithic column worked better for the DoE experiments 7 and 8 (compare Table 2). After HCIC the PFs were lower, that means more

other proteins were still present. Thus, all proteins which could not be separated from the target protein during the HCIC, could be bound to the stationary phase in the AEX, and therefore the PFs of DoE experiment 7 and 8 in the AEX were higher compared to first purification step. The conclusion of this is, impurities that cannot be separated from the product in the HCIC, will be separated in the next step, resulting in a product's higher purity.

Table 10. Purification factors of the 2-step chromatography purification of the DoE experiments and rHRP A2A expressed in the wildtype strain

DoE experiment	PF - HCIC	PF - AEX	PF total
1	4.83	1.59	7.68
2	3.31	1.13	3.74
7	1.54	3.10	4.77
8	1.92	4.62	8.88
centre points (average)	2.80	1.95	5.46
DoE verification run 2	4.42	1.23	5.44
rHRP A2A expressed in wt	4.19	1.07	4.48

In summary, the total purification factors of these 2 steps were in a range of 3.7 to 8.8, except DoE experiment 1 and 8 showed a higher total PF. Both, experiment 1 and 8 had the settings 20°C and pO_2 of 30%, indicating that the cultivation temperature and dissolved oxygen may affect the product's properties in a way that impurities can be more effectively removed by this 2-step purification protocol.

For rHRP expressed in the wildtype strain, the HCIC worked better whereat the PF in the AEX chromatography was lower as in the DoE experiments. This means, that a lot of impurities could be separated in the first purification step.

In total, there might be an influence on the purification because all products produced at a pO_2 concentration of 10 % showed lower total PFs compared to those produced at 30 % pO_2. However, we could not create a model with these results.

As mentioned before, the product could be found in the flowthrough, which seems to be a reason of the glycosylation of the product. Because of the surrounding of sugar chains, the hydrophobic regions of the product are covered by the extensive glycosylation and could not interact with the stationary phase. A similar effect appeared in the AEX chromatography, because of the neutrality of the mannose sugar chains no interaction between the stationary phase and the product occurred. Hence, the product could be found in the flowthrough, but impurities bound to the column and were thereby removed. Although rHRP A2A expressed in the *P. pastoris och1* k.o. strain is less-glycosylated, this purification strategy works anyways. This supports the theory, that not only N-glycosylation is present on the product, but also O-glycosylation.

The following figure shows a typical example for the chromatography steps showing the UV-signal at 280 nm for proteins and at 404 nm for the heme group indicative for heme-proteins (Figure 24).

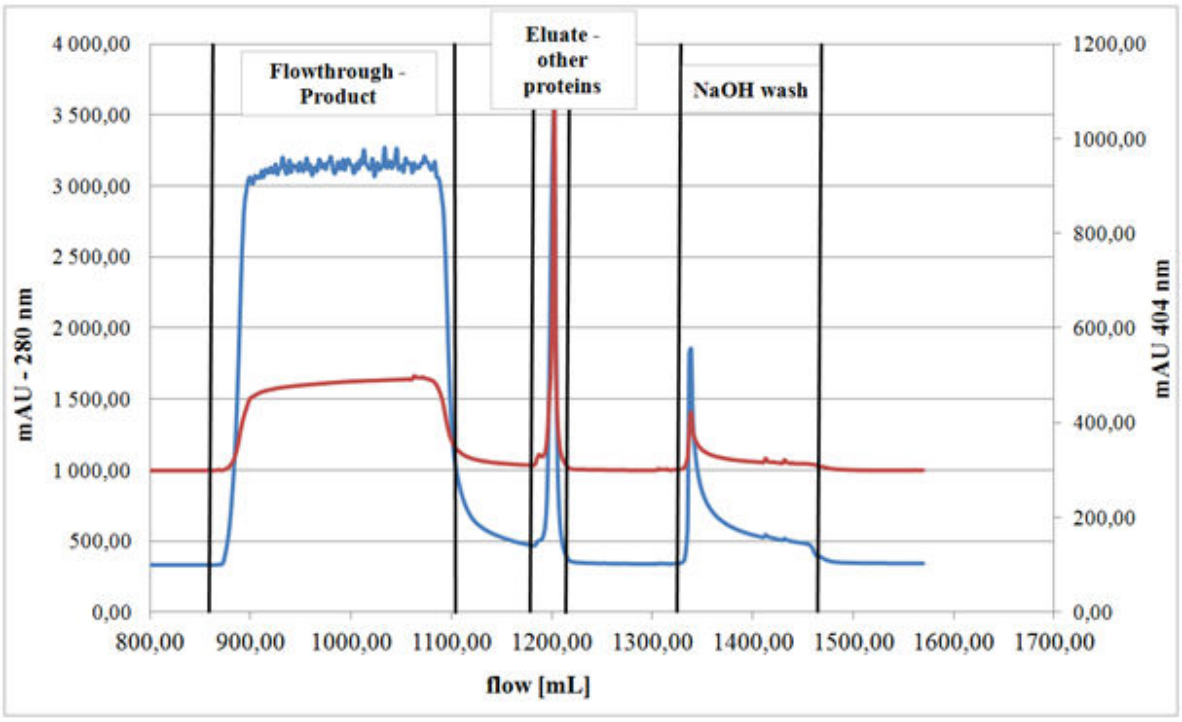

Figure 24: HCIC of the DoE experiment 8. The first peak describes the flowthrough, the second peak eluted proteins and the third peak shows the remaining proteins, which could only be eluted using NaOH.

5.4 Enzyme characterization

Biochemical characterization:

All purified products were analyzed for their kinetic constants, using the substrate ABTS and H_2O_2 as a saturating substrate. The analysis were performed by measuring the increase of absorbance at 420 nm within 60 seconds. K_M, $v_{max.}$ as well as $k_{cat.}$ were determined for the purified enzyme solutions from the DoE experiments, for rHRP A2A expressed in the *P. pastoris* wildtype, for the plant HRP and also for hyperglycosylated rHRP isoenzyme C1A (Table 11).

Table 11: Biochemical characterization of the DoE experiments in comparison to other HRP samples.

Sample	K_M [mmol·L^{-1}]	$v_{max.}$ [mmol·L^{-1}·s^{-1}]	$k_{cat.}$ [s^{-1}]	$K_M/k_{cat.}$ [mM·s^{-1}]	Spec. activity [U·mg^{-1}]
DoE experiment 1	2.56	93.7	54.6	21.4	743
DoE experiment 2	2.44	99.3	57.9	23.7	717
DoE experiment 7	1.03	98.4	57.4	56.0	613
DoE experiment 8	2.07	71.8	41.9	20.3	554
DoE centre points ave.	1.73	11.0	6.39	3.7	113
DoE verification run 2 (20 °C)	2.46	97.0	55.57	23.0	752
rHRP A2A (wt)	6.18	447	267	42.1	445
rHRP C1A (wt)	5.03	256	149	29.7	715
plant HRP	0.06	552	322	5059	1000

All rHRP A2A products expressed in the *P. pastoris och1* k.o. strain showed similar K_M values, which describes an equal affinity of the products to the substrate ABTS. Only the samples produced with the centre point parameters showed a very decreased $v_{max.}$ and K_M/k_{cat} ratio, which may be the effect of an unsuccessful purification because of the low specific activity (Table 11). On the other hand hyperglycosylated rHRP A2A as well as C1A had a little bit lower affinity to the substrate because of higher Michaelis-Menten constants. The HRP extract from plant showed a very low K_M value and therefore the highest affinity to ABTS of all analyzed samples. These results show that the presence of less sugar chains on the product, increases the affinity to the substrate (lower K_M value).

Focused on the maximal reaction rate $v_{max.}$, a difference in the recombinant proteins produced in the *P. pastoris och1* k.o. strain were observed. Here, a temperature difference during the induction phase was present. $V_{max.}$, k_{cat} and therefore K_M/k_{cat} of the purified products produced with the centre point parameters were 8 times lower compared to the other DoE experiments, including the verification run 2. An exception was DoE experiment 8, which showed a higher $K_M/k_{cat.}$ value due to the lower K_M constant.

Hyperglycosylated rHRP A2A and C1A convert the substrate faster, although their affinity is lower to ABTS compared to rHRP A2A expressed in the *och1* k.o. strain. Also the turnover of ABTS for rHRP C1A, which describes the efficiency of the reaction, was higher compared to rHRP A2A expressed in the *P. pastoris och1* k.o. strain. The max. reaction rate for both hyperglycosylated isoenzymes C1A and A2A is higher and their substrate affinity is lower compared to the less-glycosylated rHRP A2A, which resulted in comparable $K_M/k_{cat.}$ values.

However, plant HRP showed very low K_M values and therefore the highest substrate affinity in relation to the other samples. This enzyme had also the highest maximal reaction rate and the highest efficiency of all measured samples. Figure 25 represents an a typical Michaelis-Menten-plot.

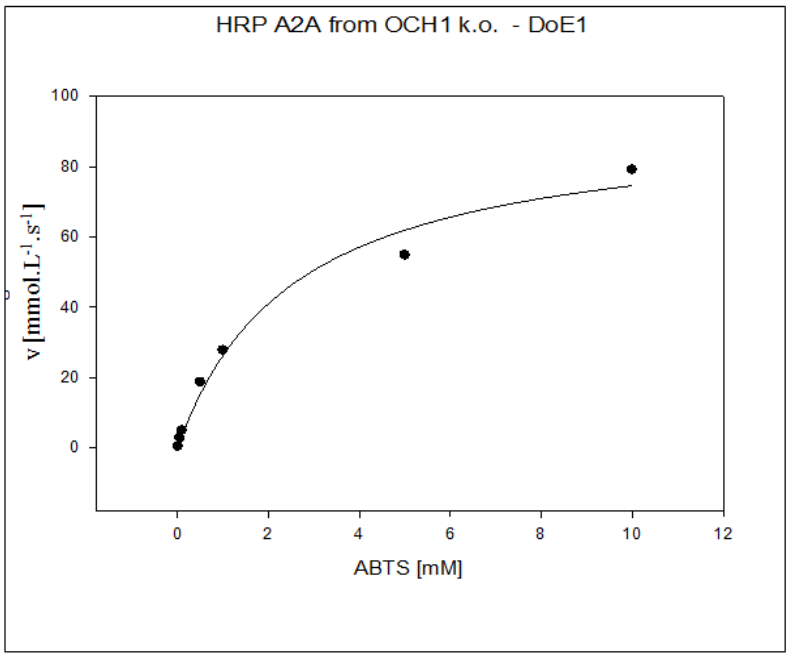

Figure 25: Kinetic model of the DoE experiment 1. x-axis shows the ABTS concentration and y-axis the reaction rate.

Thermal stability:

The thermal stability of the proteins was determined by incubating the enzyme solutions at 60 °C. At certain timepoints, samples were taken and protein content as well as enzymatic activity were determined.

Table 12 lists the analyzed half-life times of the corresponding samples. It can be seen that rHRP A2A expressed in the *P. pastoris och1* k.o. strain showed a half-life time which is approximately 50 % lower as the half-life time of the hyperglycosylated rHRP A2A from the wildtype strain. Thus, the reduced glycosylation on the product decreased the thermal stability. The potential influence of glycosylation of recombinant proteins on the thermal stability is known [28]. However, the variation of the process parameters did not have an influence on the enzyme's stability.

Interestingly, hyperglycosylated rHRP C1A showed a stability for approx. 50 minutes, a value that was reported before [12], and is therefore 8-10 times more stable than rHRP A2A.

Furthermore, plant HRP is less stable than purified and concentrated rHRP C1A, because it consists of 19 different isoenzymes [12]. Some of these 19 isoenzymes might have a thermal stability which is very low in comparison to C1A, which might result in a reduced total thermal stability of the plant HRP compared to the pure single isoenzyme C1A.

Table 12: Analyzed half-life times of the characterized HRP samples

Sample	$\tau_{1/2}$ [min]
DoE experiment 1	3.88
DoE experiment 2	2.85
DoE experiment 7	3.19
DoE experiment 8	5.03
DoE centre points ave.	3.27
DoE verification run 2	3.76
rHRP A2A (wt)	6.11
rHRP C1A (wt)	48.81
plant HRP	10.10

Summing up the enzyme characterization, rHRP A2A is stable at 60 °C for a shortened time compared to rHRP C1A, but it showed a slightly higher affinity to ABTS, thus a lower $v_{max.}$ rate and k_{cat}. A HRP isoenzyme mixture from plant had the highest affinity to the substrate, the highest maximal reaction rate and also the highest efficiency, but the stability of this enzyme at 60 °C is 4-5 times lower than of the recombinant isoenzyme C1A.

Interestingly, the sugars on the surface of the product influence the thermal stability of the product which can be seen on the basis of rHRP A2A expressed in the *P. pastoris och1* k.o. strain compared to hyperglycosylated rHRP A2A (Table 12).

SDS-PAGE:

To visualize the produced recombinant proteins, a SDS-PAGE was performed. As expected, rHRP A2A and rHRP C1A could be found at a molecular weight of 66 kDa (Figure 26). The band of the plant HRP can be seen at 45 kDa. The reduced glycosylation of rHRP A2A expressed in the *P. pastoris och1* k.o. strain could be proved earlier [2] and the molecular weight is decreased accordingly. The concrete size of this enzyme is not determined yet, but it is obvious in Figure 26 that the band is between 50 - 60 kDa. The reduced molecular weight of recombinant proteins due to the expression in a *och1* defective *P. pastoris* strain was reported in literature before. When an influenza neuraminidase was expressed in a *P. pastoris* strain and the the hyperglycosylation was reduced as a consequence of *och1*-deletion, the molecular weight shifted from 59-97 kDa to 52-57 kDa [3].

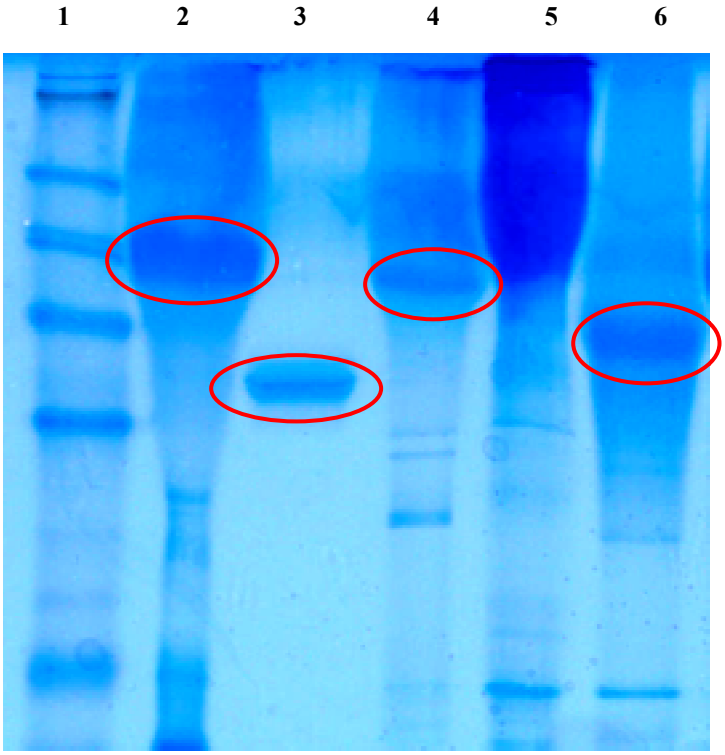

Figure 26: SDS-PAGE of the produced HRP samples. Lane 1 = SeeBlue®Plus2 Pre-stained standard; lane 2 = rHRP C1A hyperglycosylated; lane 3 = plant HRP A2A, lane 4= HRP A2A hyperglycosylated.; lane 5 = rHRP A2A in the *och1* k.o. strain; lane 6 = rHRP A2A in the *och1* k.o. strain; red circle indicates the HRP band.

5.5 Enzyme/prodrug combination for potential targeted cancer treatment

5.5.1 Reaction rate between HRP and IAA

The potential application of the produced, purified, characterized and concentrated rHRP A2A samples for targeted cancer treatment was investigated by analyzing the reaction rate between the iron-peroxidase and the plant hormone IAA. The reaction rate of less-glycosylated rHRP A2A produced at 20 °C and of the hyperglycosylated rHRP A2A and C1A as well as of the plant HRP were determined. All samples were normalized to the protein content of the plant HRP of 0.1 $mg \cdot mL^{-1}$.

Figure 27 shows an example for the stopped-flow-measurements. The fitted reaction rates determined at the different IAA concentrations were plotted against the IAA concentrations. The gradient of the slope represents the reaction rate between the plant HRP and IAA. The so-called K-value describes how fast the reaction between HRP and IAA runs.

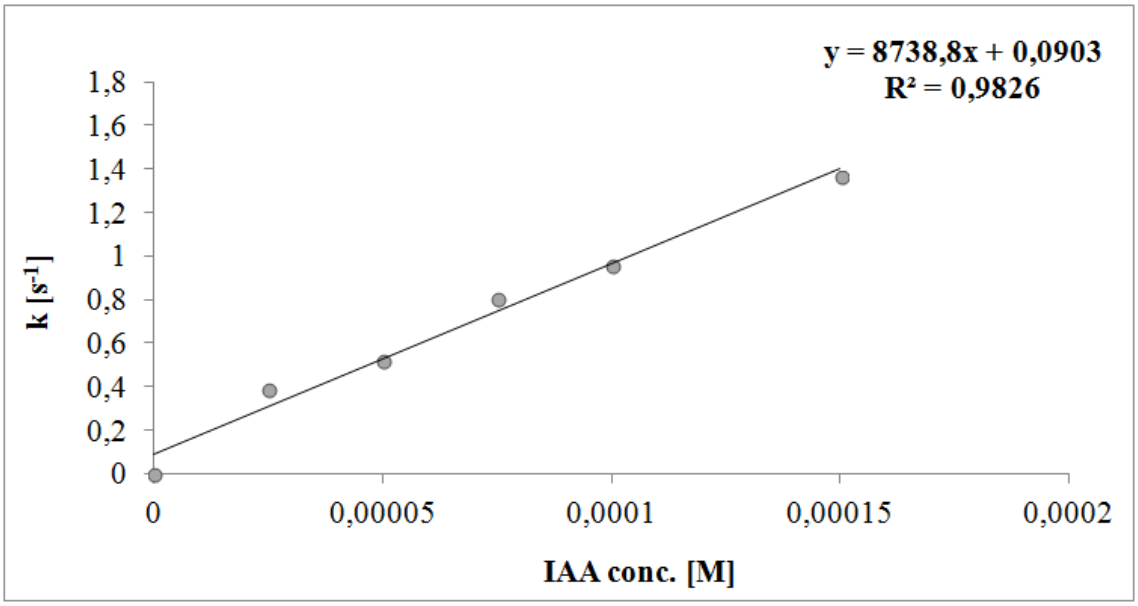

Figure 27: Fitted reaction rates of the plant HRP plotted against their the different IAA concentrations.

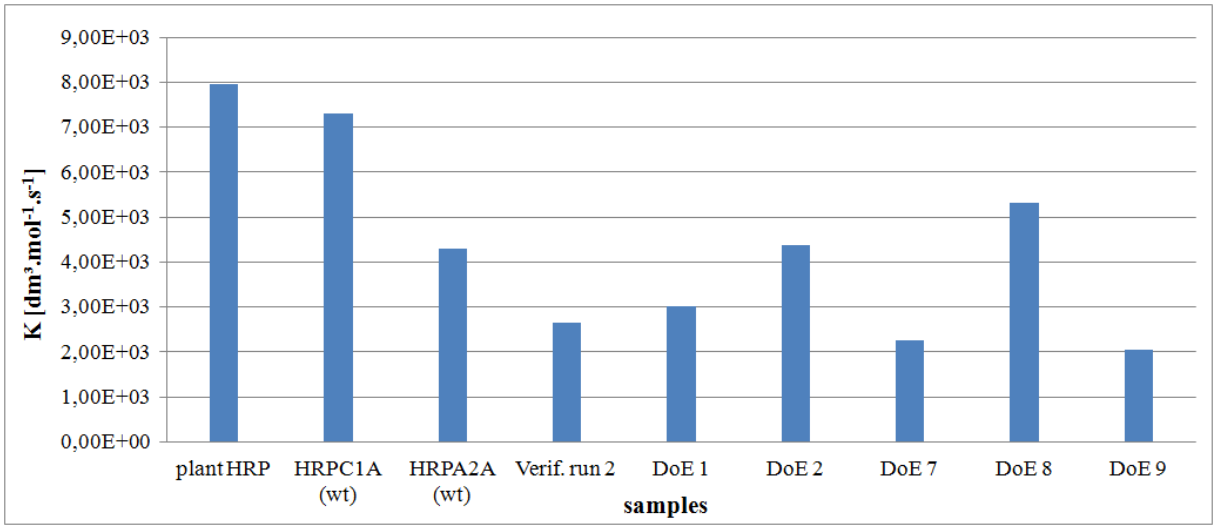

Figure 28: Reaction rates of all HRP samples.

It is visible that all recombinant HRP samples reacted slower than plant HRP (Figure 28). Hyperglycosylated rHRP C1A reacted a little bit slower with IAA than the plant HRP, but faster than all rHRP A2A samples. The DoE experiments showed deviated K-values, but all of them are slower compared to the plant HRP. Due to this deviation an influence of the different process condition at the 20 °C processes cannot be excluded. However, rHRP A2A reacts slower with IAA compared to rHRP C1A. All samples were normalized to the protein content of plant HRP (0.1 mg·mL^{-1}] and therefore the purity of the several samples might be an issue in this measurement. In addition to the reaction rates of HRP and IAA, it is also important to determine the efficiency of the reaction, especially when these substances should be used for targeted cancer treatment.

5.5.2 Measurement of the IAA turnover

With this analysis the IAA turnover was studied, which was done by performing a RP-HPLC with a defined IAA concentration of 100 µM. These studies were done at 25 and 37 °C for the hyperglycosylated rHRP C1A, A2A, the plant HRP and less-glycosylated rHRP A2A

(Verification run 2). All samples were measured in the presence and absence of H_2O_2, but the results without the utilization of 10 µM H_2O_2 are more interesting for targeted cancer treatment studies with mammalian cells.

As shown in Figure 29, intermediates of IAA were detected during the reaction with HRP by using the RP-HPLC. On the basis of this HPLC chromatogram, the success of the reaction between HRP and IAA can be recorded because of the production of MOI, a substance that delivers cytotoxins and triggers apoptosis of mammalian cancer cells and is therefore important for targeted cancer treatment [7-10].

When HRP was absent, only the IAA peak and no intermediates were detected as a fact of no oxidation of the plant hormone and no formation of intermediates (Figure 28; dotted line).

The efficiency of the reaction between HRP and IAA describes how much IAA was oxidized by HRP during a certain time at 25 and 37 °C, which results in the end product MOI. The more IAA is oxidized the higher are the amounts of the intermediates and as a consequence, more MOI is produced.

The following figures (Figure 30 and 30) show the IAA turnover of several HRP samples. It is visible that rHRP A2A was not active without H_2O_2 at both temperatures, regardless if the enzyme was expressed in the *P. pastoris och1* k.o. or in the wildtype strain.

When H_2O_2 was present (10 µM), rHRP A2A could oxidize IAA, but with a still lower efficiency compared to the plant HRP or rHRP C1A without H_2O_2. This fact was observed at both temperatures. On the contrary, rHRP C1A, also expressed in the wildtype strain, oxidized the plant hormone nearly as efficient as the plant HRP at 25 as well as at 37 °C. No significant differences between the reactions with or without H_2O_2 were detected.

The oxidation of IAA by rHRP C1A at 37 °C was more efficient as at 25 °C. After 250 hours, rHRP C1A showed a reduction of the IAA concentration of approximately 40 %, whereas at 37 °C a reduction of nearly 52 % was achieved.

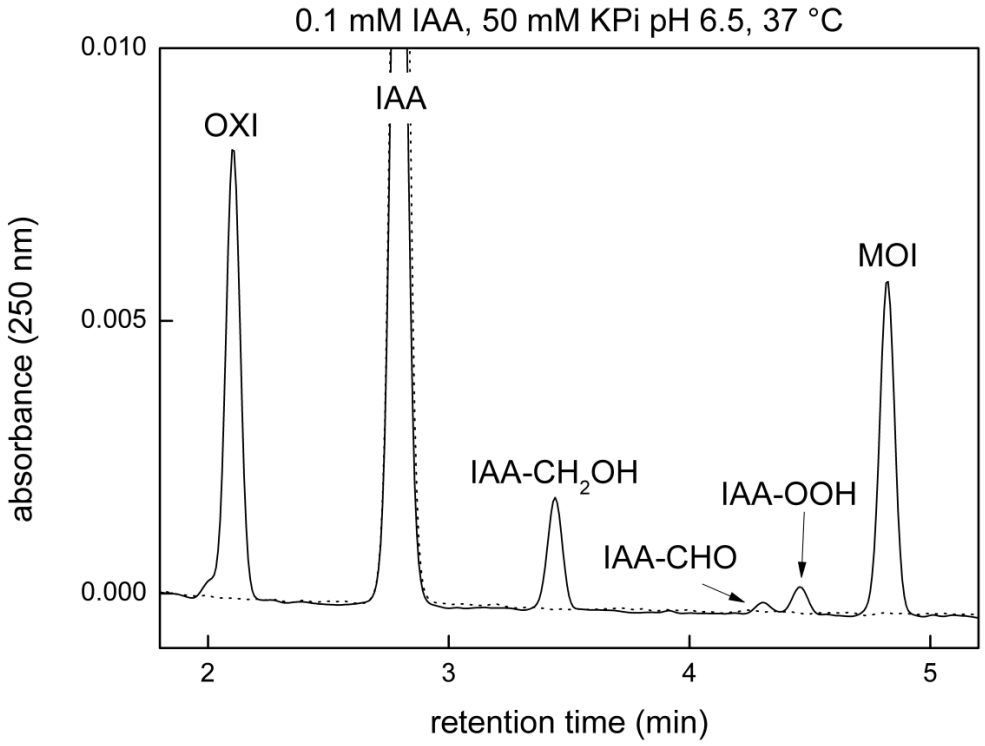

Figure 29: Intermediates of the IAA turnover measured by RP-HPLC at 37 °C for 66 min. Black solid line = + 97 µg/mL HRP; black dotted line = no HRP. Solid line shows the chromatogram when HRP was present and peaks of the intermediates of IAA. The dotted line represents the detectable peaks without HRP.

Interestingly, rHRP C1A oxidized IAA slightly more efficient as the plant HRP, which might be the fact of the enzyme preparations. Whereas rHRP C1A is one single isoenzyme, the plant HRP consists of 19 different isoenzymes with a percentage of approximately 70 % of isoenzyme C1A [12]. Thus, the total efficiency of the plant HRP could be decreased due to the presence of other isoenzymes which may have a lower IAA turnover.

Interestingly, no negative effect of the hyperglycosylation on the efficiency of the product rHRP C1A was observed. Moreover, no negative effect of the modification (gene knock-out) of the *P. pastoris* could be seen because both rHRP A2A products reacted in the same way. Because of this, the *P. pastoris och1* k.o. strain can be used to produce less-glycosylated rHRP for potential utilization for targeted cancer treatment.

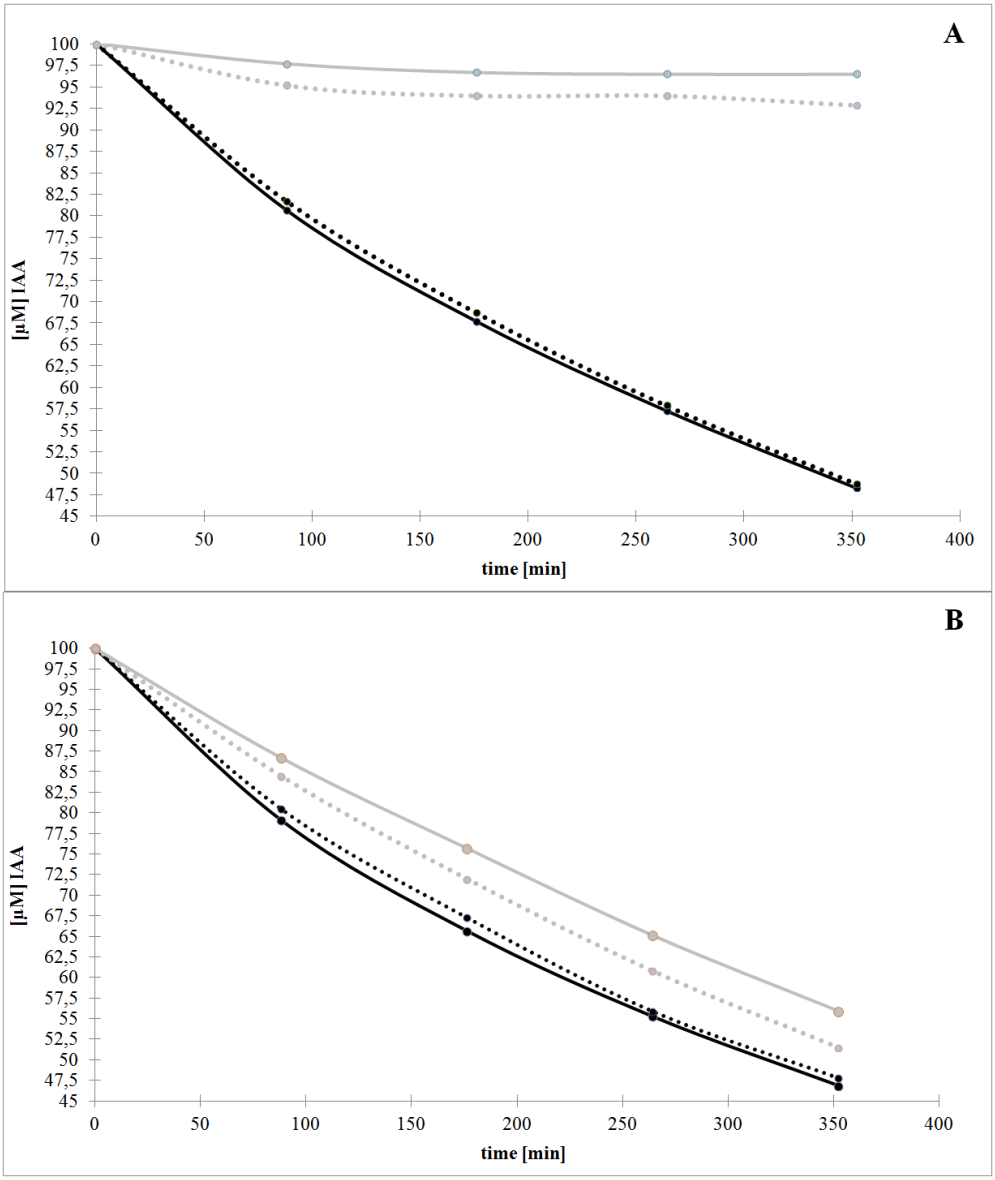

Figure 30: IAA turnover of different HRP samples at 25 °C with an IAA concentration of 100 µM; A = without H_2O_2; B = with H_2O_2. Black solid line = plant HRP; black dotted line = rHRP C1A in wt strain (hyperglycosylated); grey solid line = rHRP A2A in wt strain (hyperglycosylated); grey dotted line = rHRP A2A in the *och1* k.o. strain (verification run 2).

As mentioned before, a potential candidate for targeted cancer treatment studies with mammalian cells should be active without H_2O_2 because of possible toxic effects of this substrate on human cells. Therefore, rHRP A2A is no potential candidate due to its dependency on H_2O_2 during the oxidation of IAA. Although H_2O_2 is produced within the cell during respiration and common metabolism - which could react with HRP -, it is removed by a set of distinct enzymes such as catalases, for example. However, the application of the

isoenzyme A2A is still no option for targeted cancer therapies because of its lower efficiency compared to rHRP C1A or plant HRP even in presence of H_2O_2.

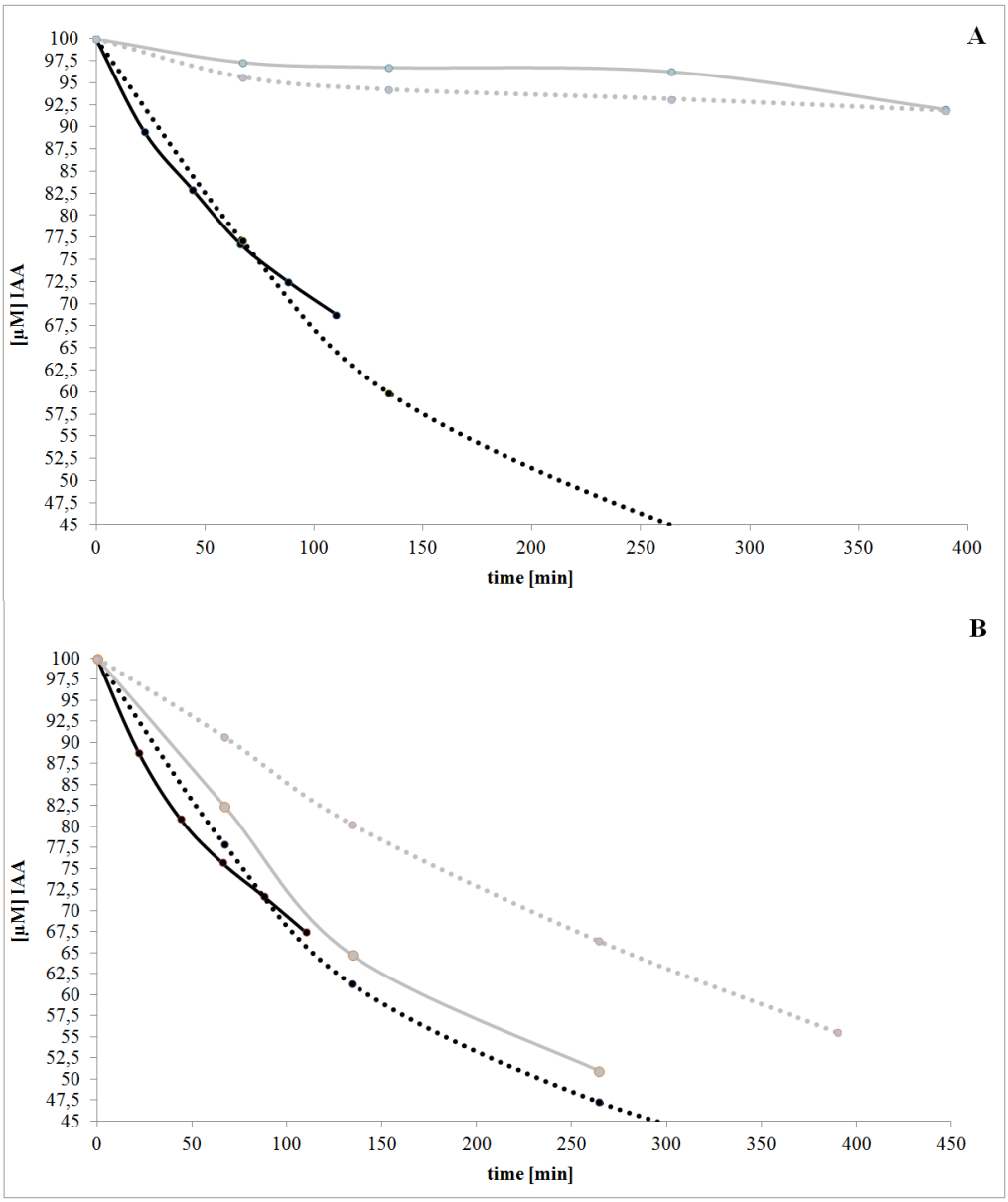

Figure 31: IAA turnover of different HRP samples at 37 °C with an IAA concentration of 100 µM; A = without H_2O_2; B = with H_2O_2. Black solid line = plant HRP; black dotted line = rHRP C1A in wt strain (hyperglycosylated); grey solid line = rHRP A2A in wt strain (hyperglycosylated); grey dotted line = rHRP A2A in the *och1* k.o. strain (verification run 2).

To summarize the enzyme/prodrug investigations, no negative effect of the *P. pastoris och1* k.o. strain compared to the wildtype strain could be detected during the velocity and efficiency studies. First we analyzed the velocity of the reaction between HRP and IAA for

several HRP samples, where no differences due to the glycosylation could be recognized. This study showed that rHRP A2A reacted slower than rHRP C1A and the plant HRP, whereas rHRP C1A and plant HRP were comparable. Moreover, hyperglycosylated rHRP C1A showed a similar efficiency to the plant HRP at 25 °C and even a slightly higher IAA turnover at 37 °C, whereas hyper- and less-glycosylated rHRP A2A was just active with hydrogen peroxide. Thus, a negative effect of the hyperglycosylation neither on the velocity nor on the efficiency of the reaction between HRP and IAA was observed.

The produced rHRP A2A is no option for a targeted cancer treatment due to its limited potential to oxidize IAA without H_2O_2. The HRP isoenzyme C1A seems to be a superior candidate for further targeted cancer treatment studies, but is hyperglycosylated. Therefore, the expression of this enzyme in the *P. pastoris och1* k.o. strain would be interesting.

6 Conclusions

The host organism *P. pastoris* is frequently used for recombinant protein production due to high cell densities and the ability to perform all post-translational modifications of higher eukaryotes. Due to the hyperglycosylation of secreted proteins, these products cannot be used as pharmaceuticals in medicine because of an immunogenic reaction when they are injected into the human body. One strategy to solve this problem is strain engineering in order to change or modify the glycosylation pathway of this yeast. Here, a *P. pastoris* strain with a knocked out *och1* gene, which initiates the hyperglycosylation, was cultivated in order to produce less-glycosylated recombinant proteins in a controlled bioprocess.

In a multivariate Design of Experiments screening, a still missing controllable bioprocess for a *P. pastoris och1* k.o. strain was developed. Expression of the used model protein HRP isoenzyme A2A happened during the induction phase running a constant methanol fed-batch under controlled conditions. The fed-batch was initiated by a simple feeding strategy, in which a correlation factor between DCW and OD_{600} of cells during the induction phase was determined before. In this DoE experiments, the influence of three process parameters (temperature, pH and pO_2) on the specific and volumetric productivity, on the efficiency factor of this modified strain as well as on the specific activity of the expressed enzyme were investigated. The evaluation of the DoE delivered a parameter area for high rHRP A2A production at 20 °C, pH of 5.0 and a pO_2 concentration of 10 %, where the temperature was the only significant influencing parameter. It could be shown that this *P. pastoris och1* k.o. strain could take up more methanol at lower temperatures, therefore the production at 20 °C was the highest compared to the other used temperatures. In comparison to a *P. pastoris*

wildtype strain, the *och1* k.o. strain delivered not as much product as the wildtype strain, but the product is less-glycosylated. Thus, the *P. pastoris och1* k.o. strain could be interesting for the production of pharmaceuticals and proteins for medical purposes because the glycosylation is reduced and hence less adverse reactions can be expected.

Higher pO_2 concentrations during the process resulted in higher total PFs of the DoE experiments. For analyzing a concrete influence of the chosen dissolved oxygen concentrations in USP to the 2-step purification in the DSP, further experiments should be performed.

Biochemical characterization was done with several HRP samples. Here, rHRP A2A expressed in the *P. pastoris och1* k.o. strain showed a slightly higher affinity to ABTS as the hyperglycosylated rHRP A2A and C1A, but the maximal reaction rates and turnover values were lower. However, plant HRP delivered the highest values in all characterization parameters. Focused on the thermal stability, hyper- and less-glycosylated rHRP A2A had similar half-life times, but lower than HRP plant, whereas hyperglycosylated rHRP C1A had the highest stability at 60 °C. Thus, it seems that hyperglycosylation may increase temperature stability, which was also observed in another study [28]. Investigations of a potential utilization for targeted cancer treatment of the produced enzyme were done at the Department of Oncology at the University of Oxford. Not only the less-glycosylated rHRP A2A, but also hyperglycosylated rHRP C1A and A2A and the plant HRP were studied. Here, it was concluded that rHRP A2A is no potential candidate for targeted cancer treatment, because it could not oxidize IAA without the presence of H_2O_2. Besides the efficiency, also the velocity of the reaction between this enzyme and IAA was lower compared to the plant HRP or rHRP C1A. The latter one delivered comparable efficiency values to the plant HRP at 25 °C but even higher values at 37 °C. Also the velocity of the reaction of rHRP C1A with IAA was similar to plant HRP, which leads to conclusion that rHRP C1A is a potential candidate for further targeted cancer treatment studies with mammalian cells.

7 Outlook

This Thesis presents a developed bioprocess, in which a DoE a parameter area for high production of less-glycosylated recombinant proteins with the *P. pastoris och1* k.o. strain could be determined at 20 °C, pH of 5.0 and a pO_2 concentration of 10 %. Due to the results of the verification run at 15 °C, the optimal parameter area for high production of recombinant proteins, especially for high rHRP A2A production, is expected to be between 16-20 °C. The optimal region for the highest productivity has to be determined by doing optimization studies with this modified strain. A variation of the temperature in this narrowed range will deliver the optimal region, underlined by the fact that the temperature is the only productivity-influencing parameter.

Furthermore, this modified strain has a higher $q_{Smax,MeOH}$ at 20 °C than at 30 °C and so it is possible to rise the feeding rate using a $q_{S,MeOH}$ above 0.2 $mmol \cdot g^{-1} \cdot h^{-1}$, but only for process temperatures below 30 °C. In this Thesis, a constant $q_{S,MeOH}$ was used to compare the influence of temperature, pH and pO_2 concentration on the productivity.

An optimal case would describe the analysis of a $q_{S,MeOH}$ where specific productivity as well as product quality is as high as possible. To determine such a $q_{S,MeOH}$ dynamic feeding strategy studies should be done. Due to a time-effect on the specific productivity, repetitive fed-batch processes with a different $q_{S,MeOH}$, rising stepwise from lower to higher, and from higher to lower values seems to be the method of choice to find the optimal $q_{S,MeOH}$ for the recombinant protein production with this *P. pastoris och1* k.o. strain.

In consideration of the potential utilization of HRP isoenzyme C1A for targeted cancer treatment studies, this enzyme should be expressed in the *P. pastoris och1* k.o. strain to produce this enzyme with less heterogeneous glycosylation and analyze the reaction between the new produced enzyme and the plant hormone IAA again.

8 References

1. Greco, O., et al., *Development of a novel enzyme/prodrug combination for gene therapy of cancer: horseradish peroxidase/indole-3-acetic acid.* Cancer Gene Therapy, 2000. **7**(11): p. 1414-1420.
2. Krainer, F.W., et al., *Knockout of an endogenous mannosyltransferase increases the homogeneity of glycoproteins produced in Pichia pastoris.* Sci Rep, 2013. **3**: p. 3279.
3. Yang, Y.L., et al., *Expression, purification and characterization of low-glycosylation influenza neuraminidase in alpha-1,6-mannosyltransferase defective Pichia pastoris.* Mol Biol Rep, 2012. **39**(2): p. 857-64.
4. Zhang, D., et al., *[Pichia pastoris X-33 with OCH1 gene deletion and its expression of glycoprotein GM-CSF]*. Wei Sheng Wu Xue Bao, 2011. **51**(5): p. 622-9.
5. Wang, Y., et al., *[A Pichia pastoris with alpha-1, 6-mannosyltransferases deletion and its use in expression of HSA/GM-CSF chimera]*. Sheng Wu Gong Cheng Xue Bao, 2007. **23**(5): p. 907-14.
6. Chen, Z., et al., *Enhancement of the gene targeting efficiency of non-conventional yeasts by increasing genetic redundancy.* PLoS One, 2013. **8**(3): p. e57952.
7. Folkes, L.K., L.P. Candeias, and P. Wardman, *Toward targeted "oxidation therapy" of cancer: Peroxidase-catalysed cytotoxicity of indole-3-acetic acids.* International Journal of Radiation Oncology Biology Physics, 1998. **42**(4): p. 917-920.
8. Folkes, L.K., et al., *5-Fluoroindole-3-acetic acid: a prodrug activated by a peroxidase with potential for use in targeted cancer therapy.* Biochemical Pharmacology, 2002. **63**(2): p. 265-272.
9. Folkes, L.K., S. Rossiter, and P. Wardman, *Reactivity toward thiols and cytotoxicity of 3-methylene-2-oxindoles, cytotoxins from indole-3-acetic acids, on activation by peroxidases.* Chemical Research in Toxicology, 2002. **15**(6): p. 877-882.
10. Folkes, L.K. and P. Wardman, *Oxidative activation of indole-3-acetic acids to cytotoxic species - a potential new role for plant auxins in cancer therapy.* Biochemical Pharmacology, 2001. **61**(2): p. 129-136.
11. Folkes, L.K. and P. Wardman, *Kinetics of the reaction between nitric oxide and glutathione: implications for thiol depletion in cells.* Free Radic Biol Med, 2004. **37**(4): p. 549-56.
12. Krainer, F.W., et al., *Purification and basic biochemical characterization of 19 recombinant plant peroxidase isoenzymes produced in Pichia pastoris.* Protein Expr Purif, 2014. **95**: p. 104-12.
13. Cereghino, J.L. and J.M. Cregg, *Heterologous protein expression in the methylotrophic yeast Pichia pastoris.* Fems Microbiology Reviews, 2000. **24**(1): p. 45-66.
14. Macauley-Patrick, S., et al., *Heterologous protein production using the Pichia pastoris expression system.* Yeast, 2005. **22**(4): p. 249-270.
15. Krainer, F.W., et al., *Recombinant protein expression in Pichia pastoris strains with an engineered methanol utilization pathway.* Microbial Cell Factories, 2012. **11**: p. 22.
16. Cregg, J.M., et al., *Functional-Characterization of the 2 Alcohol Oxidase Genes from the Yeast Pichia-Pastoris.* Molecular and Cellular Biology, 1989. **9**(3): p. 1316-1323.
17. Romanos, M.A., C.A. Scorer, and J.J. Clare, *Foreign Gene-Expression in Yeast - a Review.* Yeast, 1992. **8**(6): p. 423-488.
18. Orman, M.A., P. Calik, and T.H. Ozdamar, *The influence of carbon sources on recombinant-human-growth-hormone production by Pichia pastoris is dependent on*

phenotype: a comparison of Mut(s) and Mut(+) strains. Biotechnology and Applied Biochemistry, 2009. **52**: p. 245-255.
19. Ascacio-Martinez, J.A. and H.A. Barrera-Saldana, *Production and secretion of biologically active recombinant canine growth hormone by Pichia pastoris.* Gene, 2004. **340**(2): p. 261-266.
20. Pla, I.A., et al., *Evaluation of Mut(+) and Mut(S) Pichia pastoris phenotypes for high level extracellular scFv expression under feedback control of the methanol concentration.* Biotechnology Progress, 2006. **22**(3): p. 881-888.
21. Hamilton, S.R. and T.U. Gerngross, *Glycosylation engineering in yeast: the advent of fully humanized yeast.* Current Opinion in Biotechnology, 2007. **18**(5): p. 387-92.
22. Wildt, S. and T.U. Gerngross, *The humanization of N-glycosylation pathways in yeast.* Nat Rev Microbiol, 2005. **3**(2): p. 119-28.
23. De Pourcq, K., K. De Schutter, and N. Callewaert, *Engineering of glycosylation in yeast and other fungi: current state and perspectives.* Appl Microbiol Biotechnol, 2010. **87**(5): p. 1617-31.
24. Vervecken, W., et al., *In vivo synthesis of mammalian-like, hybrid-type N-glycans in Pichia pastoris.* Applied and Environmental Microbiology, 2004. **70**(5): p. 2639-46.
25. Nagasu, T., et al., *Isolation of new temperature-sensitive mutants of Saccharomyces cerevisiae deficient in mannose outer chain elongation.* Yeast, 1992. **8**(7): p. 535-47.
26. Nakayama, K., et al., *OCH1 encodes a novel membrane bound mannosyltransferase: outer chain elongation of asparagine-linked oligosaccharides.* Embo j, 1992. **11**(7): p. 2511-9.
27. Spadiut, O., et al., *Purification of a recombinant plant peroxidase produced in Pichia pastoris by a simple 2-step strategy.* Protein Expr Purif, 2012. **86**(2): p. 89-97.
28. Li, P., et al., *Expression of recombinant proteins in Pichia pastoris.* Appl Biochem Biotechnol, 2007. **142**(2): p. 105-24.
29. Hamilton, S.R., et al., *Humanization of yeast to produce complex terminally sialylated glycoproteins.* Science, 2006. **313**(5792): p. 1441-3.
30. Veitch, N.C., *Horseradish peroxidase: a modern view of a classic enzyme.* Phytochemistry, 2004. **65**(3): p. 249-259.
31. Veitch, N.C. and A.T. Smith, *Horseradish peroxidase.* Advances in Inorganic Chemistry, Vol 51, 2001. **51**: p. 107-162.
32. Smith, A.T., et al., *Expression of a Synthetic Gene for Horseradish Peroxidase-C in Escherichia-Coli and Folding and Activation of the Recombinant Enzyme with Ca-2+ and Heme.* Journal of Biological Chemistry, 1990. **265**(22): p. 13335-13343.
33. Dunford, H.B., *Heme peroxidases.* Wiley-VCH, New York, 1999.
34. Lavery, C.B., et al., *Purification of Peroxidase from Horseradish (Armoracia rusticana) Roots.* Journal of Agricultural and Food Chemistry, 2010. **58**(15): p. 8471-8476.
35. Passardi, F., et al., *Peroxidases have more functions than a Swiss army knife.* Plant Cell Reports, 2005. **24**(5): p. 255-265.
36. Hartmann, C. and P.R.O. Demontellano, *Baculovirus Expression and Characterization of Catalytically Active Horseradish-Peroxidase.* Archives of Biochemistry and Biophysics, 1992. **297**(1): p. 61-72.
37. Segura, M.D., et al., *High-level expression and purification of recombinant horseradish peroxidase isozyme C in SF-9 insect cell culture.* Process Biochemistry, 2005. **40**(2): p. 795-800.
38. Morawski, B., et al., *Expression of horseradish peroxidase (HRP) in S-cerevisiae and P-pastoris.* Abstracts of Papers of the American Chemical Society, 2000. **219**: p. U165-U165.

39. Morawski, B., et al., *Functional expression of horseradish peroxidase in Saccharomyces cerevisiae and Pichia pastoris.* Protein Engineering, 2000. **13**(5): p. 377-384.
40. Ryan, B.J., N. Carolan, and C. O'Fagain, *Horseradish and soybean peroxidases: comparable tools for alternative niches?* Trends Biotechnol, 2006. **24**(8): p. 355-63.
41. El-Said, S.M., *Detoxification of pesticides aqueous solution using horseradish peroxidase.* Pak J Biol Sci, 2013. **16**(6): p. 287-90.
42. Rossiter, S., L.K. Folkes, and P. Wardman, *Halogenated indole-3-acetic acids as oxidatively activated prodrugs with potential for targeted cancer therapy.* Bioorganic & Medicinal Chemistry Letters, 2002. **12**(18): p. 2523-2526.
43. Zhou, J., et al., *Influence of N-glycosylation on Saccharomyces cerevisiae morphology: a golgi glycosylation mutant shows cell division defects.* Curr Microbiol, 2007. **55**(3): p. 198-204.
44. Bates, S., et al., *Outer chain N-glycans are required for cell wall integrity and virulence of Candida albicans.* J Biol Chem, 2006. **281**(1): p. 90-8.
45. Dietzsch, C., O. Spadiut, and C. Herwig, *A dynamic method based on the specific substrate uptake rate to set up a feeding strategy for Pichia pastoris.* Microbial Cell Factories, 2011. **10**: p. 14.
46. Wechselberger, P., P. Sagmeister, and C. Herwig, *Real-time estimation of biomass and specific growth rate in physiologically variable recombinant fed-batch processes.* Bioprocess Biosyst Eng, 2013. **36**(9): p. 1205-18.
47. Salaheddin, C., et al., *Characterisation of recombinant pyranose oxidase from the cultivated mycorrhizal basidiomycete Lyophyllum shimeji (hon-shimeji).* Microbial Cell Factories, 2010. **9**.
48. Gazarian, I.G., et al., *Identification of skatolyl hydroperoxide and its role in the peroxidase-catalysed oxidation of indol-3-yl acetic acid.* Biochemical Journal, 1998. **333**: p. 223-232.
49. Nelson, D.P. and L.A. Kiesow, *Enthalpy of decomposition of hydrogen peroxide by catalase at 25°C (with molar extinction coefficients of H_20_2 solutions in the UV).* Analytical Biochemistry, 1972. **49**: p. 474-478.
50. Hoffmann, K., S. Onodera, and R. Noiva, *Expression of recombinant human protein disulfide isomerase in the yeast Pichia pastoris.* Faseb Journal, 1996. **10**(6): p. 677-677.
51. Khatri, N.K. and F. Hoffmann, *Impact of methanol concentration on secreted protein production in oxygen-limited cultures of recombinant Pichia pastoris.* Biotechnol Bioeng, 2006. **93**(5): p. 871-9.
52. Khatri, N.K. and F. Hoffmann, *Oxygen-limited control of methanol uptake for improved production of a single-chain antibody fragment with recombinant Pichia pastoris.* Appl Microbiol Biotechnol, 2006. **72**(3): p. 492-8.

9 Figures and Tables

10 Abbreviations

ABTS = 2.2' azino bis 3-ethylbenzthiazoline-6-sulphonic acid

AEX = anion exchange chromatography

AOX = Alcohol oxidase

BSA = bovine serum albumin

CER = Carbondioxide Evolution Rate [mmol ・ L^{-1} ・ h^{-1}]

CIM-DEAE = Convective Interactive Media‐Diethylaminoethyl

CV = Column volumes

δ -Ala = δ-Aminolevulinic acid

DAS = Dihydroxyacetone synthase

DF = diafiltration

DoE = Design of Experiments

DolP = dolichol phosphate

Fuc = Fucose

GlcNAc = *N*-acetylglucosamine

H_2O_2 = hydrogen peroxide

HCIC = hydrophobic charge induction chromatography

HRP = horseradish peroxidase

IAA = indole-3-acetic acid

k_{cat} = catalytic constant [s^{-1}]

kDa = Kilodalton

K_M = Michaelis-Menten Constant [mmol · L^{-1}]

Man = mannose

mAU = Milli Absorbance Units

MF = micofiltration

MOI = 3-methylen-2-oxindole

Mut^- = methanol utilization minus

Mut+ = methanol utilization plus

Mut^S = methanol utilization slow

(m)V = (Milli) Volt

MW = Molecular weigth [kDa]

OD_{600} = Optical density at 600 nm

PF = purification factor

PID = proportional-integral-derivative

PP = potassium phosphate

q_P = Specific productivity [U · g^{-1} · h^{-1}] or [g · g^{-1} · h^{-1}]

q_S = Specific substrate uptake rate [mmol · g^{-1} · h^{-1}]

rHRP recombinant horseradish peroxidase

UF = ultrafiltration

v_{max} = maximum reaction velocity or rate

Xyl = Xylose

$Y_{x/s}$ = Yield biomass to substrate [g · g^{-1}]

$Y_{CO2/s}$ = Yield carbon dioxide to substrate [g · g^{-1}]

μ = Specific growth rate [h^{-1}]

η = efficiency factor [U · $mmol^{-1}$]

$\tau_{1/2}$ = half life time [min]

11 Appendix

Supplementary table 1: Correlation between DCW and OD_{600} of a *P. pastoris* wildtype strain and the *och1* k.o. strain.

***P. pastoris och1* k.o. strain**		***P. pastoris* wildtype strain**	
OD_{600}	**DCW [$g.L^{-1}$]**	**OD_{600}**	**DCW [$g.L^{-1}$]**
41.93	23.32	53.21	23.08
21.02	11.53	29.20	11.31
13.74	7.62	17.75	7.05
10.44	5.71	13.23	6.04
8.68	4.61	10.58	4.57
7.00	3.82	8.88	3.53

Supplementary table 2: Protein contents of the protease experiment cultivating the *P. pastoris och1* k.o. and wildtype strain.

	Protein conc. [$mg.mL^{-1}$] after 24 h induction	**Protein conc. [$mg.mL^{-1}$] after 48 h induction**	**Protein conc. [$mg.mL^{-1}$] after 72 h induction**	**Protein conc. [$mg.mL^{-1}$] after 96 h induction**
wildtype with p.i.	0.080	0.157	0.165	0.153
wildtype without p.i.	0.090	0.160	0.167	0.153
och1 k.o. with p.i.	0.096	0.162	0.170	0.179
och1 k.o. without p.i.	0.103	0.163	0.169	0.171

Supplementary table 3: MF and UF/DF of the DoE experiment 1

	sample	Absorbance 1	Absorbance 2	average	protein conc. [mg.mL^{-1}]	Loss of protein [%]	vol. activity [U.mL^{-1}]	ca. Vol. bottles [ml]	Total Units	Loss of total units [%]	spec. activity [U.mg^{-1}]
DoE experiment 1	Crude extract	0.24	0.21	0.22	0.22		6.28	2300	14433		28.74
						53.83				31.70	
	MF	0.22	0.22	0.22	0.10		4.59	2150	9858		45.49
										9.39	
	UF - Product	0.66	0.63	0.65	0.60		41.90	180	7542		69.91

Supplementary table 4: MF and UF/DF of the DoE experiment 2

	sample	Absorbance 1	Absorbance 2	average	protein conc. [mg.mL^{-1}]	Loss of protein [%]	vol. activity [U.mL^{-1}]	ca. Vol. bottles [ml]	Total Units	Loss of total units [%]	spec. activity [U.mg^{-1}]
DoE experiment 2	Crude extract	0,22	0,24	0,23	0,23		6,76	2200	14861		29,96
						74,35				54,34	
	MF	0,12	0,13	0,13	0,06		3,31	2050	6786		57,24
										25,53	
	UF - Product	0,60	0,63	0,61	0,57		46,73	195	9111		82,05

Supplementary table 5: MF and UF/DF of the DoE experiment 7

	sample	Absorbance 1	Absorbance 2	average	protein conc. [mg.mL^{-1}]	Loss of protein [%]	vol. activity [U.mL^{-1}]	ca. Vol. bottles [ml]	Total Units	Loss of total units [%]	spec. activity [U.mg^{-1}]
DoE experiment 7	Crude extract	0.33	0.33	0.33	0.31		17.14	1980	33937		54.85
						32.55				21.12	
	MF	0.21	0.21	0.21	0.21		13.52	1980	26770		64.15
										18.95	
	UF - Product	0.87	0.87	0.86	0.79		117.9	150	17685		149.01

Supplementary table 6: MF and UF/DF of the DoE experiment 8

	sample	Absorbance 1	Absorbance 2	average	protein conc. [mg.mL^{-1}]	Loss of protein [%]	vol. activity [U.mL^{-1}]	ca. Vol. bottles [ml]	Total Units	Loss of total units [%]	spec. activity [U.mg^{-1}]
DoE experiment 8	Crude extract	0.55	0.55	0.55	0.512		24.16	2100	50736		47.15
						62.87				53.89	
	MF	0.189	0.189	0.189	0.190		11.14	2100	23394		58.56
										24.20	
	UF - Product	0.629	0.628	0.6285	0.582		58.9	230	13547		101.13

Supplementary table 7: MF and UF/DF of DoE experiment 9

	sample	Absorbance 1	Absorbance 2	average	protein conc. [mg.mL^{-1}]	Loss of protein [%]	vol. activity [U.mL^{-1}]	ca. Vol. bottles [ml]	Total Units	Loss of total units [%]	spec. activity [U.mg^{-1}]
DoE experiment 9	Crude extract	0.27	0.264	0.267	0.260		4.07	2240	9116.8		15.66
						36.06				28.09	
	MF	0.151	0.173	0.162	0.166		2.98	2200	6556		17.94
										5.67	
	UF - Product	0.832	0.817	0.8245	0.757		26.3	180	4734		34.73

Knockout of an endogenous mannosyltransferase increases the homogeneity of glycoproteins produced in *Pichia pastoris*

Florian W. Krainer[1], Christoph Gmeiner[2], Lukas Neutsch[3], Robert Pletzenauer[2], Anton Glieder[4] and Oliver Spadiut[2*]

[1] Graz University of Technology, Institute of Molecular Biotechnology, Graz, Austria

[2] Vienna University of Technology, Institute of Chemical Engineering, Research Area Biochemical Engineering, Vienna, Austria

[3] University of Vienna, Department of Pharmaceutical Technology and Biopharmaceutics, Vienna, Austria

[4] Austrian Centre of Industrial Biotechnology (ACIB GmbH), Graz, Austria

[*]Corresponding Author: Oliver Spadiut, Vienna University of Technology, Institute of Chemical Engineering, Research Area Biochemical Engineering, Gumpendorfer Strasse 1a, A-1060 Vienna, Austria. Tel: +43 1 58801 166473, Fax: +43 1 58801 166980; e-mail: oliver.spadiut@tuwien.ac.at

Abstract

The methylotrophic yeast *Pichia pastoris* is a common host for the recombinant production of biocatalysts and biopharmaceuticals. It is capable of performing posttranslational modifications such as the glycosylation of secreted proteins. However, the activity of the *OCH1* encoded α-1,6-mannosyltransferase triggers subsequent hypermannosylation of secreted proteins at great heterogeneity, which is typical for yeast derived proteins and considerably hampers downstream processing and reproducibility. Horseradish peroxidases are versatile enzymes with applications in diagnostics, bioremediation and cancer treatment. Despite the importance of these enzymes, they are still isolated from the roots of the horseradish plant at low yields as a mixture of different isoenzymes with different biochemical properties.

Here we show the production of homogeneous glycoprotein species of recombinant horseradish peroxidases by use of a *P. pastoris* platform strain in which *OCH1* was irreversibly deleted. This *och1* knockout strain had a growth impaired phenotype and showed significant rearrangements of cell wall components, but nevertheless secreted homogeneously glycosylated protein at a volumetric productivity of 70% of a wildtype based strain. Recombinant protein production in this strain not only abides by Quality by Design principles, but also greatly facilitates the reproducibility of production processes, downstream processing and the development of specific applications.

Keywords

Pichia pastoris, glycoprotein, glycosylation, glycoengineering, *OCH1*, mannosyltransferase, horseradish peroxidase, plant peroxidase, bioreactor cultivation, recombinant protein production

Introduction

The methylotrophic yeast *Pichia pastoris* has long been used for the production of recombinant proteins at high titers. Up to 22g.L^{-1} have been reported for intracellularly produced recombinant hydroxynitrile lyase (1) and approximately 15g.L^{-1} for secreted recombinant gelatin (2), demonstrating the high production capacity of this microbial host while being able to grow on comparatively simple and inexpensive media. Not only can *P. pastoris* be grown to cell densities as high as 160g.L^{-1} cell dry weight (3), it is also capable of performing posttranslational modifications, including the formation of correct disulfide bridges and the glycosylation of secretory proteins, rendering *P. pastoris* specifically suitable for the production of complex eukaryotic proteins (4).

Glycosylation has long been known to affect various protein properties such as solubility, stability and enzymatic activity (*e.g.* (5, 6)), which need to be evaluated on a case-by-case basis. Whereas only little is known about O-linked glycosylation, the biosynthesis of N-glycans is well understood. N-glycans are linked to the amino groups of asparagine residues that are recognized by glycotransferases in the sequence motif N-X-S/T, where X is any amino acid but proline. Initially, the biosynthesis steps of N-glycans in yeast and mammals are identical. Dolichol phosphate-linked N-acetylglucosamine (DolP-GlcNAc) is synthesized by the transfer of GlcNAc from uridine diphosphate (UDP) onto DolP on the cytoplasmatic side of the ER. After extension to DolP-linked $Man_5GlcNAc_2$, this structure is enzymatically flipped to the ER lumen, where further glucose (Glc) and Man residues are added to form a core glycan, $Glc_3Man_9GlcNAc_2$, which is transferred to an asparagine within the N-X-S/T sequence motif of a nascent protein chain. Subsequently, the three terminal Glc residues and one Man residue are trimmed by glucosidases I and II and an ER-residing α-1,2-mannosidase to form $Man_8GlcNAc_2$. At this point, the newly formed glycoprotein is transported to the Golgi apparatus, which is where the yeast and mammalian N-glycosylation pathways diverge

(7–9). In the mammalian Golgi apparatus, α-1,2-mannosidases trim the core glycan further to form $Man_5GlcNAc_2$. Ultimately, addition of GlcNAc by a β-N-acetylglucosaminyltransferase I (GnTI), trimming of two further Man residues by a mannosidase II and yet further addition of GlcNAc, galactose (Gal) and sialic acid (Sia) residues by the respective transferases result in the complex N-glycan structures of mammalian proteins (10).

In the yeast Golgi, on the other hand, the $Man_8GlcNAc_2$ glycan is not subjected to further trimming reactions but is substantially extended. In *Saccharomyces cerevisiae*, more than 100 Man residues may account for hypermannosyl N-glycans on secretory proteins. However, the extent of hypermannosylation varies considerably and seems to depend on so far unknown influences, causing vast heterogeneity in the N-glycan pattern of secreted glycoproteins. In *S. cerevisiae* as well as in *P. pastoris* and other yeasts, the first reaction in hypermannosylation is catalyzed by an α-1,6-mannosyltransferase (Och1p) that is encoded by the gene Outer Chain elongation 1 (*OCH1*), which was first discovered and characterized in *S. cerevisiae* (11, 12). Och1p uses Man from guanosin diphosphate and links it to the core glycan by an α-1,6-glycosidic bond, forming a substrate that triggers additional mannosylation (Figure 32). Whereas *S. cerevisiae* holds a repertoire of Golgi-resident α-1,2-, α-1,3 and α-1,6-mannosyl and mannosylphosphate transferases, *P. pastoris* seems to lack the Golgi-resident α-1,3-mannosyltransferase, but to possess four additional β-mannosyltransferases instead (7, 13, 14).

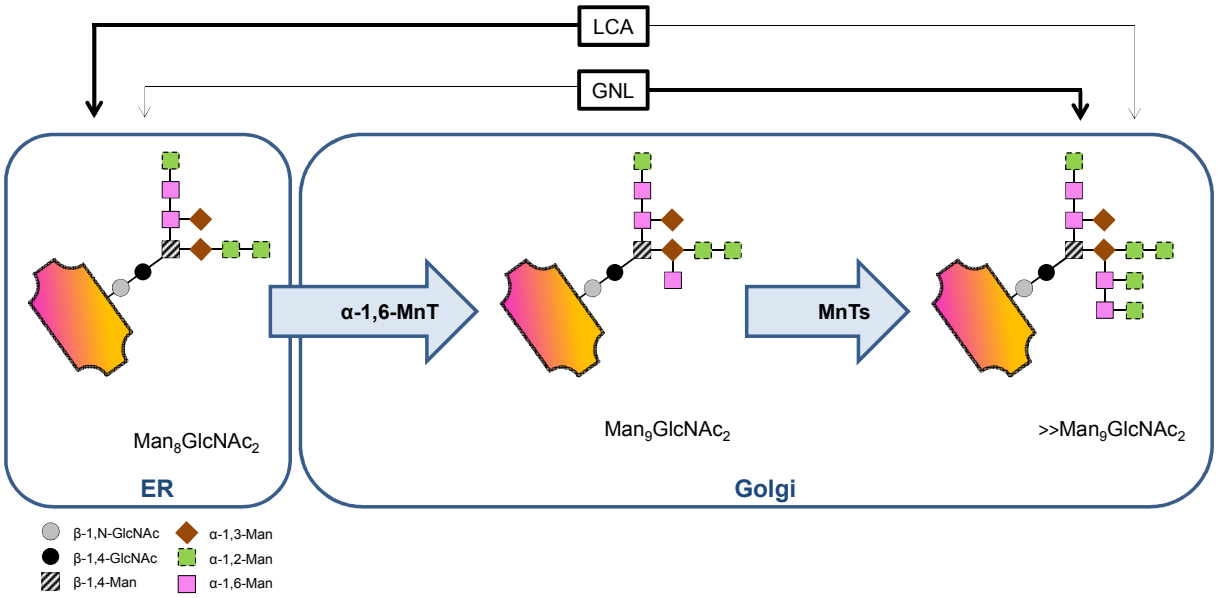

Figure 32: Och1p in N-glycan biosynthesis. In the Golgi, the N-linked $Man_8GlcNAc_2$ core glycan is extended by the α-1,6-mannosyltransferase activity (α-1,6-MnT) of Och1p, which is further heterogeneously hyperglycosylated by several additional mannosyltransferases (MnTs). *Galanthus nivalis* lectin (GNL) and *Lens culinaris* lectin (LCA) bind to the different glycan structures either with high (thick arrow) or low (thin arrow) specificity.

Although not as extensive as those of *S. cerevisiae*, the N-glycans of *P. pastoris* are also of the high mannose type and the humanization of the N-glycosylation machinery of *P. pastoris* has been the subject of several studies (Table 13).

Table 13: Humanization of N-glycans in *P. pastoris*. Selected studies focusing on the humanization of the N-glyans on *P. pastoris* derived glycoproteins. Mns, mannosidase; GnT, β-N-acetylglucosaminyltransferase; UDP-GlcNAc, uridine diphosphate-N-acetylglucosamine; *OCH1*, outer chain elongation gene.

content	references
introduction of α-1,2-Mns, GnTI and an UDP-GlcNAc transporter via a combinatorial genetic library approach in a *Δoch1*::*URA3* strain	(13, 15)
introduction of an UDP-GlcNAc transporter, α-1,2-MnsIA, MnsII, GntI, GntII in a *Δoch1*::*URA3* strain	(16)
introduction of α-1,2-Mns and GnTI, *OCH1* inactivation via a knockin plasmid	(10)
GlycoSwitch plasmids for *OCH1* inactivation and introduction of glycosidase and glycosyltransferase activities to produce complex terminally galactosylated glycoproteins	(17)
introduction of sialic acid biosynthesis pathway and corresponding transporter and transferase activities to produce complex terminally sialylated glycoproteins	(18)

Here, we report the deletion of the *OCH1* gene from the *P. pastoris* genome in an irreversible and straight forward approach. Hereby, we generated a new *P. pastoris* platform strain that allows the production of recombinant proteins with glycan structures of significantly increased homogeneity compared to proteins produced in a wildtype strain. In contrast to previous glycoengineering studies, which required several time- and labor-intensive steps of strain engineering, we achieved more homogeneously glycosylated protein with a single gene knockout step. Horseradish peroxidase (HRP) is a versatile enzyme with applications in diagnostics and histochemistry, bioremediation and cancer treatment. However, due to the lack of an appropriate recombinant production process, HRP preparations are still derived from horseradish roots as mixtures of different isoenzymes (19). We produced recombinant HRP in an *och1* knockout strain in the controlled environment of a bioreactor, purified and

characterized the enzyme, hereby demonstrating the general applicability of this new platform strain by the example of this industrially and medically relevant enzyme.

Materials and Methods

Chemicals

Enzymes and deoxynucleotide triphosphates were obtained from Thermo Scientific (formerly Fermentas, Germany). Phusion™ High-Fidelity DNA-polymerase was from Finnzymes (Finland). 2,2'-azino-bis(3-ethylbenzthiazoline-6-sulfonic acid) diammonium salt (ABTS) was purchased from Sigma-Aldrich (Austria). Difco™ yeast nitrogen base w/o amino acids (YNB), Difco™ yeast nitrogen base w/o amino acids and ammonia sulfate (YNB2), Bacto™ tryptone and Bacto™ yeast extract were purchased from Becton Dickinson (Austria). Zeocin™ was purchased from InvivoGen (France) via Eubio (Austria). Fluorescein isothiocyanate (FITC) labeled lectins for microscopic analysis were obtained from Vector Laboratories (USA), comprising wheat germ agglutinin (WGA) from *Triticum vulgaris*, *Lens culinaris* agglutinin (LCA), *Galanthus nivalis* lectin (GNL) and *Solanum tuberosum* lectin (STL). FM® 4-64 membrane stain and Hoechst 33342 or 4',6-diamidino-2-phenylindole (DAPI) nucleic acid stains were purchased from Life Technologies (USA). Other chemicals were obtained from Carl Roth (Germany).

Microorganisms

DNA manipulations were performed in accordance to standard protocols (20) in *E. coli* Top10F' (Life Technologies, formerly Invitrogen, Austria). All *P. pastoris* strains in this study were based on the wildtype strain CBS 7435 (identical to NRRL Y-11430 or ATCC 76273).

Initial *OCH1* knockout studies were performed in a *ku70* deletion strain, previously described by Näätsaari *et al.* (21), hereafter called *Pp*ku70-. Since *P. pastoris* strains with Mut^S phenotype have been repeatedly shown to be superior over strains with Mut^+ phenotype for the production of recombinant proteins (*e.g.* (22)), the ultimate *och1* knockout strain was based on a Mut^S strain described in (21), hereafter called *Pp*MutS.

Deletion of the *OCH1* gene

Based on the genome sequence of the *P. pastoris* wildtype strain CBS 7435 (23), the primers OCH1-5int-fw1 and OCH1-5int-rv1 were designed to amplify a DNA fragment upstream the *OCH1* open reading frame (ORF) from genomic DNA isolated according to (24). Primers OCH1-3int-fw1b and OCH1-3int-rv1b were designed to amplify a fragment downstream of the *OCH1* ORF. OCH1-5int-rv1 and OCH1-3int-fw1b were designed to add sequences that overlap with the *FRT* flanked inner part of a flipper cassette. All primer sequences are listed in Table 14.

Table 14: Oligonucleotide primer list. Primers used for the amplification of upstream and downstream sequences of the *OCH1* locus from genomic DNA, for amplification of the whole *OCH1* locus for Sanger sequencing, for amplification of fragments to assemble pPpT4_BamHI_OCH1rescue and to amplify the *OCH1* ORF.

primer name	sequence (5' - 3')
OCH1-5int-fw1	GAACTGTGTAACCTTTTAAATGACGGGATCTAAATACGTCATG
OCH1-5int-rv1	CTATTCTCTAGAAAGTATAGGAACTTCGGCTGATGATATTTGCTACGAACACTG

OCH1-3int-fw1b	GTTCCTATACTTTCTAGAGAATAGGAACTTCGCGAGATTAGAGAATGAATACCTTCTTCTAAGCGATCG
OCH1-3int-rv1b	GAAGTATTAGGAGCTGAAGAAGCAGAGGCAGAG
OCH1check-fw1	CACACATATAAAGGCAATCTACG
OCH1check-rv2	CAATAACTTCTGCAATAGACTGC
OCH1rescue-fw1	TTCATAGGCTTGGGGTAATAG
OCH1rescue-rv1	CTTGAGCGGCCGCTTAGTCCTTCCAACTTCCTTC
OCH1rescue_T4fw	GCATACATTTGAAGGAAGTTGGAAGGACTAAGCGGCCGCTCAAGAGGAT
OCH1rescue_T4rv	CTATTTCTCTGTCATCTATCTATTACCCCAAGCCTATGAAGGATCTGGGTACCGCAGG
OCH1-ORF-fw	ATGGCGAAGGCAGATGGC
OCH1-ORF-rv	TTAGTCCTTCCAACTTCCTTCAAATG

The two *OCH1* targeting fragments of approximately 1.5kb each were used to assemble a flipper cassette via overlap extension PCR (21). Transformation of 100ng of the assembled flipper cassette into either *Pp*ku70- or *Pp*MutS was performed as described by Lin-Cereghino *et al.* (25). Transformants were identified on yeast extract-peptone-dextrose (YPD) agar plates containing 100mg.L^{-1} Zeocin™. Double homologous recombination of the flipper cassette in the *OCH1* locus was verified by PCR using the primers OCH1check-fw1 and OCH1check-rv2 (Table 14) and Sanger sequencing, using isolated genomic DNA as template. Expression of the FLP recombinase gene was induced by growing positive transformants on minimal methanol agar plates. The FLP recombinase mediated excision of the *FRT* flanked inner part of the flipper cassette was shown by restored sensitivity of the cells towards Zeocin™ and again by PCR and Sanger sequencing. The cassette construct and the knockout workflow are

schematically shown in Figure 33. The resulting *Pp*ku70- *och1* knockout strain was designated *Pp*FWK1, the *Pp*MutS *och1* knockout strain was designated *Pp*FWK3.

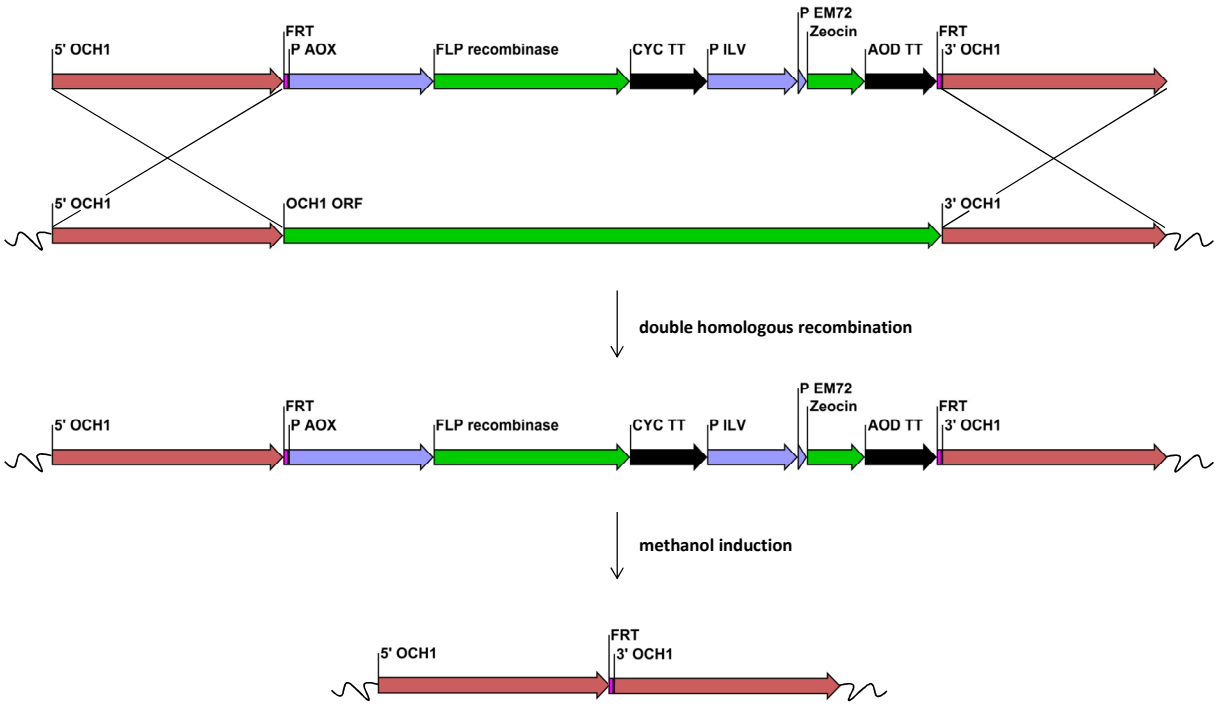

Figure 33: Schematic workflow of the knockout of *OCH1* using a flipper cassette. The regions 5' OCH1 and 3' OCH1 represent sequences upstream and downstream, respectively, of the *OCH1* ORF. The 34bp flipper recombinase target (FRT) sequences flank the *AOX1* promoter (P AOX1), the FLP recombinase ORF, the *CYC1* transcription terminator (CYC TT), a constitutive eukaryotic and a prokaryotic promotor (P ILV and P EM72, respectively), a *ble* ORF mediating Zeocin™ resistance and an *AOD* transcription terminator (AOD TT). A double homologous recombination event replaced the *OCH1* ORF in the genome with the flipper cassette. Growth of recombinant cells on methanol induced the production of the FLP recombinase which recognized the two *FRT* sites and excised the inner sequence, leaving only one *FRT* site in the genome. Single fragments are not drawn to scale.

Complementation of the observed phenotype of the *Pp*FWK3 strain was performed by transforming a plasmid that was constructed by assembly (26) of two fragments, which were generated by PCR using the primers OCH1rescue-fw1 and OCH1rescue-rv1 using genomic DNA from *Pp*MutS as template, and OCH1rescue_T4fw and OCH1rescue_T4rv using the plasmid pPpT4_S (21) as template (Table 14). The resulting plasmid contained the wildtype *OCH1* ORF plus 698bp of upstream sequence, putatively harboring the natural *OCH1* promoter, and was designated pPpT4_BamHI_OCH1rescue. Approximately 500ng of *BamHI* linearized plasmid were transformed to *Pp*FWK3, aliquots were plated on YPD Zeocin™ agar plates and incubated at 28°C for two days. PCR with the primers OCH1check-fw1 and OCH1check-rv2 from isolated genomic DNA of transformant strains was performed to confirm the unaltered replacement of the former *OCH1* ORF by a single *FRT* site. A second PCR with the primers OCH1-ORF-fw and OCH1-ORF-rv from the same genomic DNA was performed to confirm the presence of a plasmid transmitted *OCH1* ORF somewhere else in the genome. A resulting strain with restored wildtype phenotype was designated *Pp*FWK3^{R}.

Production of the reporter enzyme horseradish peroxidase in shake flask experiments

Aliquots of approximately 2µg of *SmiI* linearized plasmid pPpT4_S (21) harboring either of two horseradish peroxidase (HRP) isoenzyme genes, HRP1 and HRP2, each containing nine potential N-glycosylation sites (Näätsaari *et al.*, manuscript in preparation) were transformed into either *Pp*MutS or *Pp*FWK3. HRP1 encodes for the well studied HRP isoenzyme C1A, whereas HRP2 encodes for a new acidic HRP isoenzyme. Transformations were performed according to (25) with the following modification: Whereas an overnight culture of *Pp*MutS was diluted to an OD_{600} of 0.2 to grow to an OD_{600} of 0.8-1.0 in approximately 5h prior to

preparation of the cells for electroporation, an overnight culture of *Pp*FWK3 was diluted to a starting OD_{600} of 0.7 to account for its decreased growth rate. Transformants were grown on YPD Zeocin™ agar plates and randomly chosen for screening in micro scale cultivations in 96-deep well plates, similarly to (27). The cells were cultivated in 250µL iron-supplemented BMD1% (11g.L^{-1} α-D(+)-glucose monohydrate, 13.4g.L^{-1} YNB, 0.4mg.L^{-1} D(+)-biotin, 278mg.L^{-1} $FeSO_4$ $7H_2O$, 0.1M potassium phosphate buffer, pH6.0) for approximately 60h, then induced once with 250µL BMM2 (1% (v/v) methanol, 13.4g.L^{-1} YNB, 0.4mg.L^{-1} D(+)-biotin, 0.1M potassium phosphate buffer, pH6.0) and three times with 50µL BMM10 (5% (v/v) methanol, 13.4g.L^{-1} YNB, 0.4mg.L^{-1} D(+)-biotin, 0.1M potassium phosphate buffer, pH6.0) per well 12h, 24h and 36h after the first addition of BMM2. Induction with the methanol containing media BMM2 and BMM10 induced the production of HRP which was under control of the *AOX1* promoter. Efficient secretion of HRP to the supernatant was facilitated by fusion of the prepro signal sequence of the *S. cerevisiae* mating factor alpha to the N-terminus of the mature HRP. The respective HRP production strains were designated *Pp*MutS^{HRP1} and *Pp*MutS^{HRP2}, *Pp*FWK3^{HRP1} and *Pp*FWK3^{HRP2}.

Small scale cultivations were performed in 0.5L Ultra Yield Flasks (BioSilta, Finland) in 45mL iron-supplemented BMD1%. After approximately 60h, 5mL BMM10 were added, 12h and 36h, and 24h and 48h after the first induction pulse, 0.5mL pure methanol, and 0.25mL pure methanol, respectively, were added. HRP activity in the supernatant was determined by mixing 15µL of culture supernatant with 140µL of assay solution (1mM ABTS, 0.8mM H_2O_2, 50mM NaOAc buffer, pH4.5) and following the increase in absorbance at 405nm in a Spectramax Plus 384 platereader (Molecular Devices, Germany) at room temperature for 3min. Promising clones were streaked to single colonies and cultivated again in quadruplicates for rescreening. The HRP isoenzyme C1A has been extensively studied previously (*e.g.* (28)), whereas HRP2 represents a new acidic HRP isoenzyme (Näätsaari *et*

al., manuscript in preparation). In this study, we therefore focused on the new isoenzyme, HRP2. The copy number of the HRP2 gene in selected *Pp*MutS and *Pp*FWK3 transformant strains was determined via quantitiative real-time PCR according to a protocol of Abad *et al.* (29) and as described previously in (22).

Bioreactor cultivations

Four different *P. pastoris* strains (Table 15) were characterized in terms of physiology, biomass growth and productivity by a novel, dynamic strategy of conducting methanol pulses during batch cultivations in the controlled environment of a bioreactor, which we have described recently (22, 30, 31).

Table 15: *P. pastoris* strains used for biotechnological characterisation during bioreactor cultivations.

strain	name
P. pastoris Mut^S	*Pp*MutS
P. pastoris Mut^S HRP2	*Pp*$MutS^{HRP2}$
P. pastoris Mut^S *och1*	*Pp*FWK3
P. pastoris Mut^S *och1* HRP2	*Pp*$FWK3^{HRP2}$

Culture Media

Yeast nitrogen base medium (YNBM): 20g.L^{-1} α-D(+)-glucose monohydrate, 3.4g.L^{-1} YNB2, 10g.L^{-1} $(NH_4)_2SO_4$, 0.4g.L^{-1} D(+)-biotin, 0.1M potassium phosphate buffer, pH6.0.

Trace element solution (PTM1): 6g.L^{-1} $CuSO_4.5H_2O$, 0.08g.L^{-1} NaI, 3g.L^{-1} $MnSO_4.H_2O$, 0.2g.L^{-1} $Na_2MoO_4.2H_2O$, 0.02.L^{-1} H_3BO_3, 0.5g.L^{-1} $CoCl_2$, 20g.L^{-1} $ZnCl_2$, 65g.L^{-1} $FeSO_4.7H_2O$, 0.2g.L^{-1} D(+)-biotin, 5mL.L^{-1} 95-98% H_2SO_4.

Basal salt medium (BSM): 44g.L^{-1} α-D(+)-glucose monohydrate, 1.17g.L^{-1} $CaSO_4.2H_2O$, 18.2g.L^{-1} K_2SO_4, 14.9g.L^{-1} $MgSO_4.7H_2O$, 4.13g.L^{-1} KOH, 26.7mL.L^{-1} 85% (v/v) o-phosphoric acid, 0.2mL.L^{-1} Antifoam Struktol J650, 4.35mL.L^{-1} PTM1, NH_4OH as N-source (see experimental procedure).

Base: NH_4OH, concentration was determined by titration with 0.25 M potassium hydrogen phthalate.

Preculture

Frozen stocks (-80°C) of either *Pp*MutS^{HRP2} and *Pp*FWK3^{HRP2} were precultivated in 100mL of YNBM in 1L shake flasks at 30°C and 230rpm for max. 24h. The preculture was transferred aseptically to the respective culture vessel. The inoculation volume was 10% of the final starting volume.

Batch cultivation

Batch cultivations were carried out in a 3L working volume Labfors glass bioreactor (Infors, Switzerland). BSM was sterilized in the bioreactor and pH was adjusted to pH5.0 by using concentrated ammonia solution after autoclaving. Sterile filtered PTM1 was transferred to the reactor aseptically. Dissolved oxygen (dO_2) was measured with a sterilizable polarographic dissolved oxygen electrode (Mettler Toledo, Switzerland). The pH was measured with a sterilizable electrode (Mettler Toledo, Switzerland) and maintained constant with a step controller using 2.5M ammonia solution. Base consumption was determined gravimetrically. Cultivation temperature was set to 30°C and agitation was fixed to 1495rpm. The culture was aerated with 2.0vvm dried air and offgas of the culture was measured by using an infrared cell

for CO_2 and a paramagnetic cell for O_2 concentration (Servomax, Switzerland). Temperature, pH, dO_2, agitation as well as CO_2 and O_2 in the offgas were measured online and logged in a process information management system (PIMS Lucullus; Biospectra, Switzerland).

After the complete consumption of the substrate glucose, which was indicated by an increase of dO_2 and a drop in offgas activity, the first methanol pulse (adaptation pulse) of a final concentration of 0.5% (v/v) was conducted with methanol supplemented with PTM1 (12mL PTM1 per 1L of methanol). Subsequently, between five and seven pulses were performed with 1% or 2% (v/v) methanol for each strain. For each pulse, at least two samples were taken to determine the concentrations of substrate and product as well as dry cell weight and OD_{600} to calculate the strain specific parameters. The induction period for *Pp*MutS^{HRP2} and *Pp*FWK3^{HRP2} was carried out in 1mM presence of the heme precursor δ-aminolevulinic acid.

Analysis of growth- and expression-parameters

Dry cell weight (DCW) was determined by centrifugation of 5mL culture broth (4,000xg, 10min, 4°C), washing the pellet with 5mL deionized water and subsequent drying at 105°C to a constant weight in an oven. OD_{600} of the culture broth was measured using a spectrophotometer (Genesys 20; Thermo Scientific, Austria).

The activity of HRP was determined using a CuBiAn XC enzymatic robot (Innovatis, Germany). Cell free samples (10µL) were added to 140µL of 1mM ABTS in 50mM potassium phosphate buffer, pH6.5. The reaction mixture was incubated at 37°C and was started by the addition of 20µL of 0.075% H_2O_2. Changes of absorbance at 415nm were measured for 80s and rates were calculated. Calibration was done using commercially available horseradish peroxidase (Type VI-A, Sigma-Aldrich, Austria, P6782, Lot# 118K76734) as standard at six different concentrations (0.02; 0.05; 0.1; 0.25; 0.5 and 1.0U.mL^{-1}). Protein concentrations were determined at 595nm using the Bradford Protein Assay Kit (Bio-Rad Laboratories GmbH, Austria) with bovine serum albumin as standard.

Substrate concentrations

Concentration of methanol was determined in cell free samples by HPLC (Agilent Technologies, USA) equipped with a Supelcoguard column, a Supelcogel C-610H ion-exchange column (Sigma-Aldrich, Austria) and a refractive index detector (Agilent Technologies, USA). The mobile phase was 0.1% H_3PO_4 with a constant flow rate of 0.5mL.min^{-1} and the system was run isocratically. Calibration was done by measuring standard points in the range of 0.1 to 10g.L^{-1} methanol.

Data analysis

Strain characteristic parameters were determined at a carbon dioxide evolution rate (CER) above 2.5mmol.g^{-}1.h^{-1} during each methanol pulse. Measurements of biomass, product and substrate concentration were executed in duplicates. Along the observed standard deviation for the single measurement, the error was propagated to the specific rates q_s and q_p as well as to the yield coefficients. The error of determination of the specific rates and the yields was therefore set to 10% and 5%, respectively (30, 31).

Phenotypic strain characterization

Lectin based glycoprofiling via fluorescence microscopy

Qualitative analysis of lectin binding was performed by incubating 500µL of *Pp*MutS or *Pp*FWK3 cell suspensions in 20mM HEPES buffer, pH7.4, at an OD_{600} of 0.3 with 500µL of the respective lectin solution (250pmol.mL^{-1} in 20mM HEPES, pH7.4) for 30min at 4°C. If appropriate, 5µg.mL^{-}1 HOECHST 33342 nucleic acid stain or 0.5µg.mL^{-}1 FM® 4-64 membrane stain were included in the incubation mix. After thorough washing by repeated centrifugation (1700xg, 5min) and resuspension, cells were diluted into 1.0mL of particle free

phosphate buffered saline (PBS; 50mM, pH7.4) and mounted in FlexiPERM® coverslip 12-well plates for microscopic analysis. Images were acquired on a Zeiss Epifluorescence Axio Observer.Z1 deconvolution microscopy system (Carl Zeiss, Germany) equipped with LD Plan-Neofluar objectives and the LED illumination system Colibri®. Exposure wavelengths and filter sets of the individual channels were chosen according to the respective fluorophore(s) (DAPI/Hoechst 33342: ex/em 365/450nm; FITC: ex/em 485/525nm; FM® 4-64 ex/em 485/>620nm), and combined with differential interference contrast (DIC) images for ease of orientation. Exposure time and illumination parameters were adjusted individually for optimal visibility. For bud scar visualization, Z-stack image series of representative spots were recorded and processed via moderate iterative deconvolution. Lectin cytoadhesion was quantified by incubating the cells with the respective lectin solutions and FM® 4-64 as described above (4°C, 30min), followed by extensive washing. Cells were then lysed by treatment with Triton X-100/SDS (1.0/1.0 %) for 24h under vivid agitation. The FITC fluorescence intensity in the lysis buffer was assessed in a microplate reader (TECAN, Austria) at ex/em 485/525nm and normalized to the content of FM® 4-64 for direct comparison between the individual samples. Lectin solutions without cells were subjected to the same treatment and analyzed in order to exclude potential degradation of the fluorophore. Control experiments via fluorescence-activated cell sorting (FACS) were performed to verify similar uptake of the membrane stain in both strains.

Membrane permeabilization experiments

To gain information on the steric accessibility of cell wall-embedded chitin and other carbohydrates, cell permeability was enhanced by treatment with concentrated methanol at -20°C for 20min, followed by lectin staining. The cells contained in 1.0mL of precooled suspension (OD_{600} of 0.3) were harvested by centrifugation, resuspended in 100µL PBS buffer and added dropwise to 1.0mL of icecold methanol under vivid agitation. After 20min,

cells were pelleted again and excessive solvent was removed via repeated washing and centrifugation with fresh PBS buffer. After rehydration in 1.0mL of 20mM HEPES buffer, pH7.4, cells were subjected to the same lectin staining protocol as described above and analyzed via fluorescence microscopy. Efficient membrane permeabilization was verified via successful counterstaining of the nuclear DNA with a normally non-membrane permeable DAPI dye.

Enzyme purification

Size exclusion chromatography

The supernatants from *Pp*MutS^{HRP1}, *Pp*MutS^{HRP2}, *Pp*FWK3^{HRP1} and *Pp*FWK3^{HRP2} produced in small scale cultures in 0.5L Ultra Yield Flasks were concentrated to approximately 500µL each using Vivaspin 20 tubes (Sartorius Stedim Biotech, Germany) with 10kDa MWCO, prior to size exclusion chromatography (SEC) on a HiLoad™ 16/60 Superdex 200 prep grade column (GE Healthcare Europe, Austria). SEC was performed at a flow rate of approximately 9cm.h^{-1}, fractions of 1.2mL were collected and assayed for HRP activity using ABTS as substrate.

Hydrophobic charge induction chromatography

To purify the secreted HRP2 isoenzyme produced in bioreactor cultivations, the fermentation broth was harvested and centrifuged (4,000xg, 20min) and the cell free supernatant was subjected to diafiltration with buffer (500mM NaCl, 20mM NaOAc, pH6.0) for a subsequent purification step via a mixed mode resin (hydrophobic charge induction chromatography, HCIC). We have recently described this flowthrough based strategy for the HRP isoenzyme C1A (32). The used resin was a MEP HyperCel™ resin (Pall, Austria), the flowrate was set to

100cm.h^{-1} and fractions of 10mL were collected. The catalytic activity and the protein content in all fractions were determined, active fractions were pooled and concentrated via ultrafiltration to approximately 3mg.mL^{-1} for HRP2 produced in *Pp*Muts^{HRP2} and 0.3mg.mL^{-1} for HRP2 produced in *Pp*FWK3^{HRP2} for subsequent enzyme characterization.

Enzyme characterization

The two HRP2 isoenzyme preparations produced in either *Pp*Muts^{HRP2} or in *Pp*FWK3^{HRP2} were characterized to determine differences between the hypermannosylated HRP2 isoenzyme and its glycovariant produced in the *Pp*FWK3^{HRP2}.

Kinetic constants with ABTS

The kinetic constants for ABTS and H_2O_2 were determined for both HRP2 glycovariants. The reaction was started by adding 10µL concentrated enzyme solution (3mg.mL^{-1} HRP2 from *Pp*MutS^{HRP2} and 0.3mg.mL^{-1} HRP2 from *Pp*FWK3^{HRP2}) to 990µL reaction buffer containing ABTS in varying concentrations (0.01–10mM), 1mM H_2O_2 and 50mM potassium phosphate, pH6.5. The change in absorbance at 420nm was recorded in a spectrophotometer UV-1601 (Shimadzu, Japan) at 30°C controlled with a temperature controller (CPS controller 240 A; Shimadzu, Japan). Absorption curves were recorded with a software program (UVPC Optional Kinetics; Shimadzu, Japan).

Thermal stability

Both enzyme solutions were incubated at 60°C for 1h. At different time points, aliquots were withdrawn, the solutions were centrifuged (20,000xg, 15min) to pellet precipitated proteins and the remaining catalytic activity in the supernatants was measured (33).

Results

Knockout of *OCH1* from *Pp*ku70- and *Pp*MutS

In yeast, the *OCH1* gene encodes an α-1,6-mannosyltransferase whose activity triggers the subsequent transfer of further mannose residues onto the N-glycans of secreted proteins, resulting in heterogeneously hyperglycosylated protein species that appear as a smear on SDS gels, *e.g.* (28, 30). This hyperglycosylation not only limits the use of yeast derived proteins as biopharmaceuticals but also impedes traditional downstream processing significantly. Hence, a *P. pastoris* strain that allows the production of less heterogeneously glycosylated proteins would considerably relieve protein production processes with *P. pastoris*.

Transformation of a flipper cassette targeting to the *OCH1* locus in the genome of the *Pp*ku70- strain resulted in only few Zeocin™ resistant clones. However, Sanger sequencing of a PCR amplified fragment of the *OCH1* locus from genomic DNA showed that the majority of the tested transformants had correct integration of the transformed cassette. The transformants grew slowly and formed colonies of abnormal shape (Figure 34).

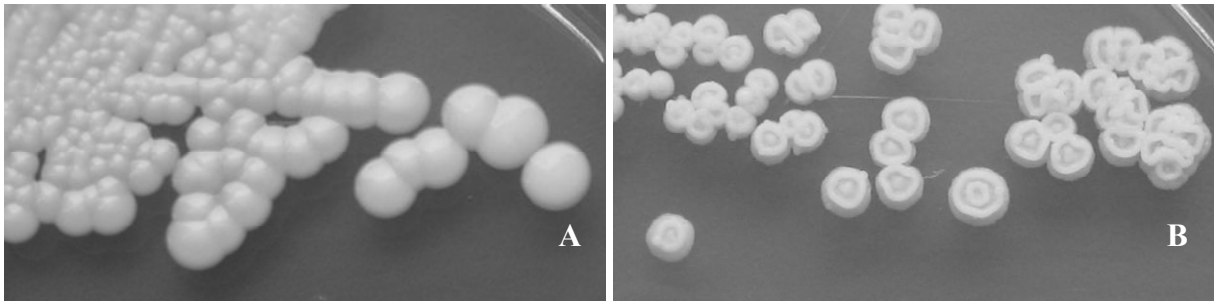

Figure 34: Colony phenotypes. A, *Pp*MutS; B, *Pp*FWK3. Both strains were grown on YPD agar.

This phenotype was preserved when these strains were grown on minimal methanol agar plates to induce the production of the FLP recombinase and subsequent excision of the inner part of the flipper cassette containing the expression cassettes for the FLP recombinase and the Zeocin™ resistance enzyme. Reconstituted sensitivity to Zeocin™, PCR and Sanger sequencing of the former *OCH1* locus confirmed the successful excision of the inner part of the flipper cassette, and efficient replacement of the former *OCH1* ORF with a single *FRT* site of 34bp.

Transformation of the same *OCH1* flipper cassette to *Pp*MutS resulted in hundreds of clones resistant to Zeocin™. Initial PCR based screenings of over 100 randomly chosen clones did not give any positive hits, analogously to what has been described by Vervecken *et al.* (10). However, after having identified the corresponding phenotype of positive transformants in the *Pp*ku70- based *och1* knockout strain *Pp*FWK1, also *Pp*MutS based transformants with correct integration of the flipper cassette could be spottet easily on the agar plates. Increasing the incubation time of the transformed cells on the agar plates to at least four days allowed growth of the *och1* knockout colonies to a size at which their abnormal shape was an obvious hint to their genotype (Figure 34). Again, Zeocin™ sensitivity was reconstituted by induction of the FLP recombinase on minimal methanol agar plates and the replacement of the *OCH1* ORF by a single *FRT* site was shown by PCR and Sanger sequencing. The observable phenotype of the generated *och1* knockout strain *Pp*FWK3 included slow growth, abnormal colony shape and temperature sensitivity at 37°C (data not shown). Upon transformation of the wildtype *OCH1* promoter and *OCH1* ORF to *Pp*FWK3, the detrimental phenotype was found to be complemented. PCR analyses confirmed the unaltered replacement of the former *OCH1* ORF by a *FRT* site, but the presence of the complementing *OCH1* ORF somewhere else in the genome due to ectopic integration of the transformed plasmid pPpT4_BamHI_OCH1rescue.

Production of HRP isoenzymes in the strains *Pp*MutS^{HRP} and *Pp*FWK3^{HRP}

To show the applicability of the generated *och1* knockout strain for the production of recombinant proteins, vectors harboring genes coding for HRP isoenzymes (Näätsaari *et al.*, manuscript in preparation) were transformed to either *Pp*MutS or *Pp*FWK3. Transformation of the linearized constructs to *Pp*FWK3 resulted in fewer Zeocin™ resistant clones than in the case of transformation to *Pp*MutS, but sufficient to allow screening for HRP activity after cultivation in a 96-deep well plate in minimal media. Despite the apparent growth defect of *Pp*FWK3, the volumetric yields in HRP activity were comparable to those of *Pp*MutS based transformants from micro scale cultivations.

Prior to cultivation of *Pp*MutS^{HRP2} or *Pp*FWK3^{HRP2} in the bioreactor, both strains were analyzed in terms of copy number of the transformed HRP2 gene to ensure comparability on this level. Both strains were found to have a single copy integration of the HRP2 encoding gene and were thus considered suitable for comparative bioreactor cultivations.

Strain characterization in bioreactors

We characterized four *P. pastoris* strains (Table 2) with a recently published method of conducting dynamic experiments during batch cultivations in the controlled environment of a bioreactor (30, 31, 34). After depletion of glucose, a first methanol adaption pulse with a final concentration of 0.5% (v/v) was applied. The adaptation times to the new substrate methanol ($\Delta time_{adapt}$), defined as the maximum in offgas activity, were determined for all four *P. pastoris* strains and are shown in Table 16.

The calculated carbon dioxide evolution rate (CER), illustrating the metabolic activity of the different strains, the specific substrate uptake rate (q_s) and, where appropriate, the specific productivity (q_p) during the methanol pulses are shown in Supplementary Figures 1-4. As shown in Supplementary Figures 1 and 2, the CER profiles for the strains *Pp*MutS and *Pp*MutS^{HRP2} showed a similar pattern during the consecutive methanol pulses and q_s values stayed constant over time. In contrast, the CER profiles for the strains *Pp*FWK3 and *Pp*FWK3^{HRP2} changed significantly over time (Supplementary Figures 3 and 4). After each methanol pulse, less CO_2 was produced per time and volume, indicating that the *P. pastoris* cells became metabolically less active. Thus, the consumption of 1% (v/v) methanol took longer after each consecutive pulse (compare Supplementary Figures 1 and 2 with Supplementary Figures 3 and 4). The altered metabolic activity of the *och1* knockout strains was also depicted in the calculated yields ($Y_{X/S}$ and $Y_{CO2/S}$), which are shown in Figure 35.

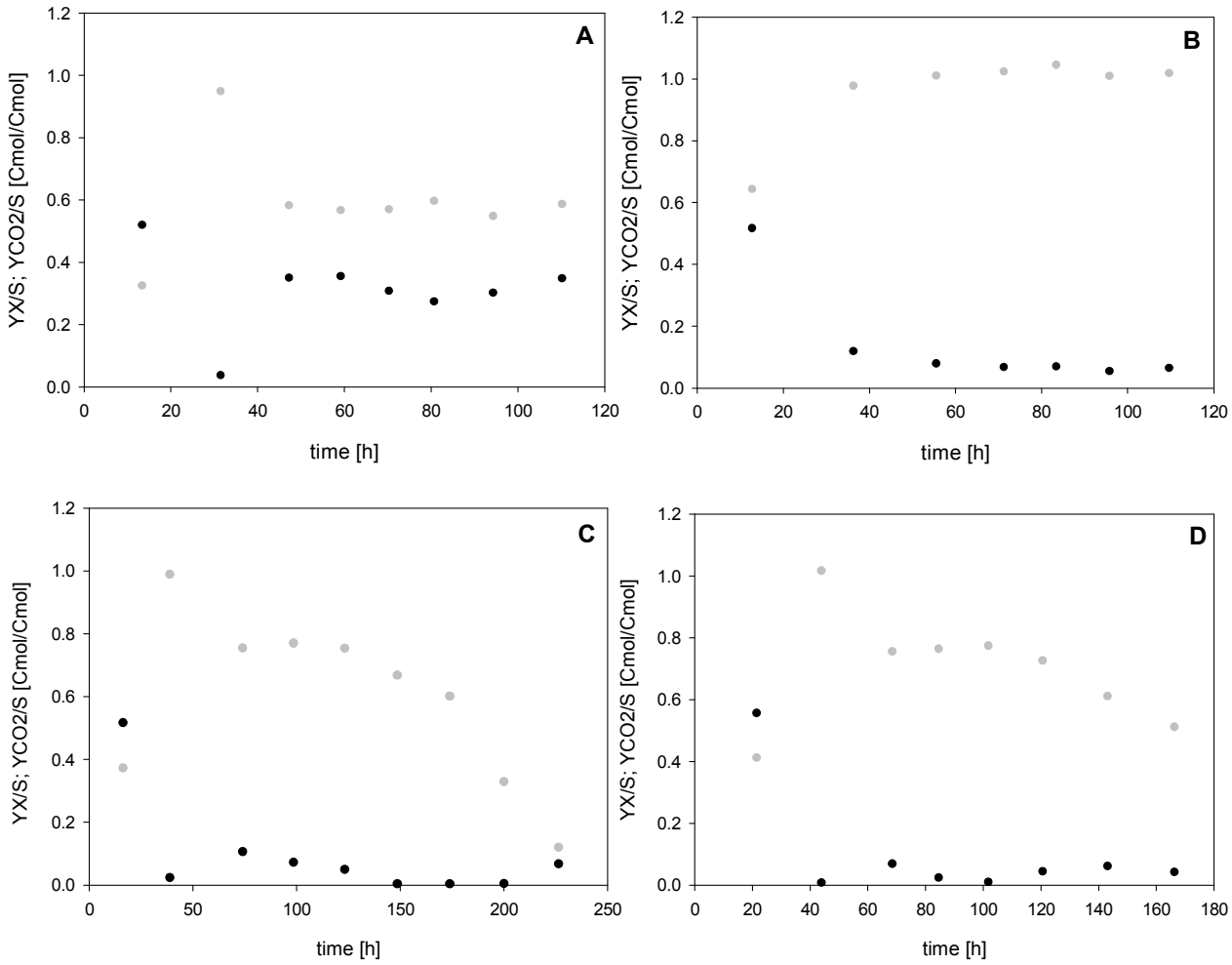

Figure 35: Calculated yields for the different *P. pastoris* strains during batch cultivations with methanol pulses. A, *Pp*MutS; B, *Pp*MutS^{HRP2}; C, *Pp*FWK3; D, *Pp*FWK3^{HRP2}. grey dot, carbon dioxide yield ($Y_{CO2/S}$); black dot, biomass yield ($Y_{X/S}$).

For the strains *Pp*MutS and *Pp*MutS^{HRP2} both the carbon dioxide yield ($Y_{CO2/S}$) and the biomass yield ($Y_{X/S}$) stayed constant during the six conducted methanol pulses (Figure 35**Fehler! Verweisquelle konnte nicht gefunden werden.**A and B). Evidently, the insertion

of the HRP2 gene into strain *Pp*MutS affected its physiology as $Y_{X/S}$ decreased significantly, whereas $Y_{CO2/S}$ increased (compare Figure 35A and B). Hence, *Pp*MutS^{HRP2} mainly used the substrate methanol for protein production and dissimilation than for biomass growth.

Interestingly, the calculated yields for *Pp*FWK3 and *Pp*FWK3^{HRP2} strains showed a very different behaviour. Although $Y_{X/S}$ was again rather constant, $Y_{CO2/S}$ decreased dramatically in the course of the six to seven consecutive methanol pulses (Figure 35C and D), indicating that these two strains became more and more metabolically inactive. Since HPLC analysis revealed that no undesired metabolites were produced in significant amounts during any of the four cultivations, the C-balances for strains *Pp*FWK3 and *Pp*FWK3^{HRP} only closed at the beginning of cultivation but rapidly decreased over time, whereas the C-balances for strains *Pp*MutS and *Pp*MutS^{HRP} were always determined close to 1.0 (Supplementary Figure 5).

A summary of the determined strain specific parameters of the four different *P. pastoris* strains is given in Table 16.

Table 16: Strain specific parameters of the different *P. pastoris* Mut^S strains

	***Pp*MutS**	***Pp*MutS^{HRP2}**	***Pp*FWK3**	***Pp*FWK3^{HRP2}**
$\Delta time_{adapt}$ (h)	15.7	19.9	6.6	8.9
max. μ_{Gly} (h^{-1})	0.30	0.31	0.20	0.20
q_{Gly}($mmol.g^{-1}.h^{-1}$)	2.9	3.1	1.9	1.9
$Y_{X/Gly}$ ($Cmol.Cmol^{-1}$)	0.63	0.41	0.61	0.54
$Y_{CO2/Gly}$ ($Cmol.Cmol^{-1}$)	0.33	0.64	0.37	0.44
q_{MeOH} ($mmol.g^{-1}.h^{-1}$)	0.62	0.70	0.52	0.43
$q_{MeOH\ max}$ ($mmol.g^{-1}.h^{-1}$)	0.67	0.78	0.69	0.53

$Y_{X/MeOH}$ (Cmol.Cmol^{-1})	0.39	0.07	0.05	0.04
$Y_{CO2/MeOH}$ (Cmol.Cmol^{-1})	0.57	1.02	constantly decreasing	constantly decreasing
C-balance	0.97	1.04	constantly decreasing	constantly decreasing
q_p (U.g^{-1}.h^{-1})	-	0.77	-	0.50
vol. productivity (U.L^{-1}.h^{-1})	-	2.6	-	1.8
efficiency factor (η) (U.mmol^{-1}; (22))	-	1.1	-	1.2

As shown in Table 16, both *Pp*FWK3 strains needed less than half of the adaptation time ($\Delta time_{adapt}$) compared to the *Pp*MutS strains. The altered glycosylation machinery in the *Pp*FWK3 strains seems to allow a faster adaption to methanol, which could be of great significance for industrial applications where fast and efficient bioprocesses are required. As expected, the adaptation times of the strains hosting the recombinant enzyme were longer compared to the strains not carrying this additional gene. Regarding the maximum specific growth rate (μ) on glycerol *Pp*FWK3 strains grew approximately 1.5-fold slower than *Pp*MutS strains. The yields on glycerol showed a similar pattern for *Pp*MutS and *Pp*FWK3 strains, as the yields were shifted towards production of carbon dioxide rather than biomass, when the strains were hosting the gene for recombinant HRP. The average specific substrate uptake rates for both substrates glycerol and methanol were lower for the *Pp*FWK3 strains than for *Pp*MutS strains. In respect to the maximum specific uptake rate for methanol ($q_{MeOH\ max}$) the values for the different strains were quite similar. However, these values were determined during the 3rd and the 5th methanol pulse for *Pp*MutS and *Pp*MutS^{HRP2},

respectively. The values during the other pulses were alike. For *Pp*FWK3 strains on the other hand, these maxima could only be determined during the first methanol pulse. After that the values for q_s decreased constantly, indicating a progressional reduction of the metabolic activity of the *Pp*FWK3 strains during the consecutive methanol pulses. This was also underlined by constantly decreasing $Y_{CO2/S}$ and C-balances. However, despite this seemingly negative impact, *Pp*FWK3^{HRP2} produced the HRP isoenzyme at specific and volumetric productivities which were only reduced by 35% and 30%, respectively, compared to *Pp*MutS^{HRP2}. In a previous study, we introduced the efficiency factor η, which puts the productivity of the strains in direct relation to the consumed substrate (22). In this respect, the *och1* knockout strain *Pp*FWK3^{HRP2} even showed a higher ratio than *Pp*MutS^{HRP2} and thus proved to be of justifiable interest for the production of recombinant proteins.

Strain morphology

Cell morphology and cell division of an och1 knockout strain

Consistent with previous reports on Och1p deficient *S. cerevisiae* strains (35, 36), we found the N-glycosylation mutant to be characterized by a significantly altered phenotype and growth profile (Table 16). In contrast to the wildtype based strain *Pp*MutS, the *och1* knockout strain *Pp*FWK3 grew in the form of large cell clusters with clumpy appearance and multibudded cells (Figure 36). Daughter cells within these clusters displayed clearly segregated vacuoles, but remained stably attached to the wall of mother cells (**Fehler! Verweisquelle konnte nicht gefunden werden.**).

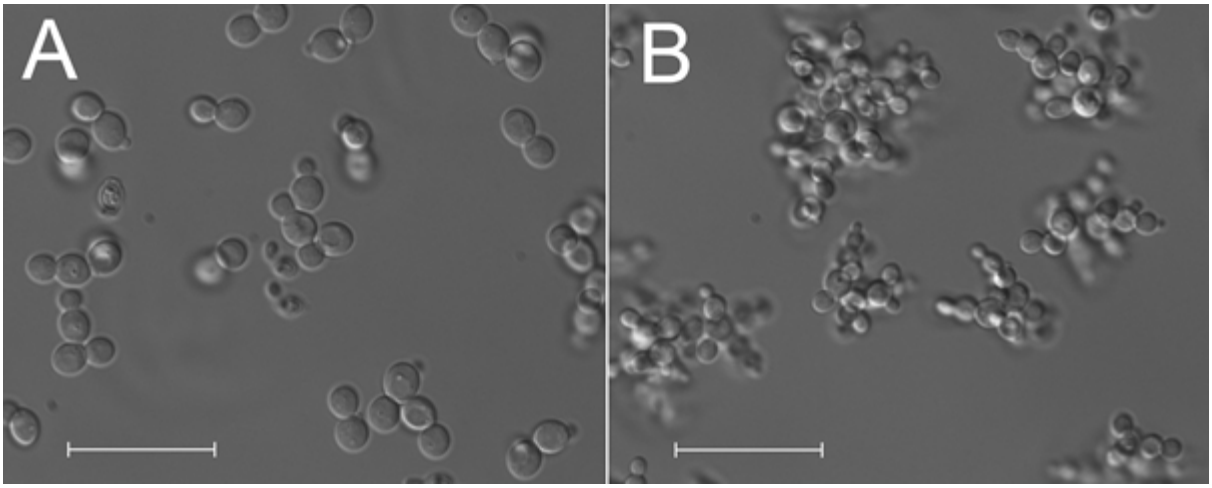

Figure 36: Phenotypic change in *P. pastoris* upon *och1* knockout. Representative DIC micrographs of *Pp*Muts and *Pp*FWK3. A, *Pp*MutS cells in batch culture. B, covalently linked clusters of multibudded cells in *Pp*FWK3 during the same cultivation phase. Scale bars represent 25µm.

Knockout induced stress response is reflected by a spatial rearrangement of WGA/STL binding sites

The direct functional implication of the engineered N-glycosylation in *Pp*FWK3 for cell morphology and cytokinesis was further illustrated by a striking difference in the chitin deposition after *och1* knockout (**Fehler! Verweisquelle konnte nicht gefunden werden.**). In lectin based glycoprofiling studies, we observed substantially altered binding patterns for WGA, with the reactive carbohydrate motifs being homogeneously distributed across the entire cell surface in the *och1* knockout strain, instead of remaining confined to the bud scars as in *Pp*MutS (Figure 37 and **Fehler! Verweisquelle konnte nicht gefunden werden.**).

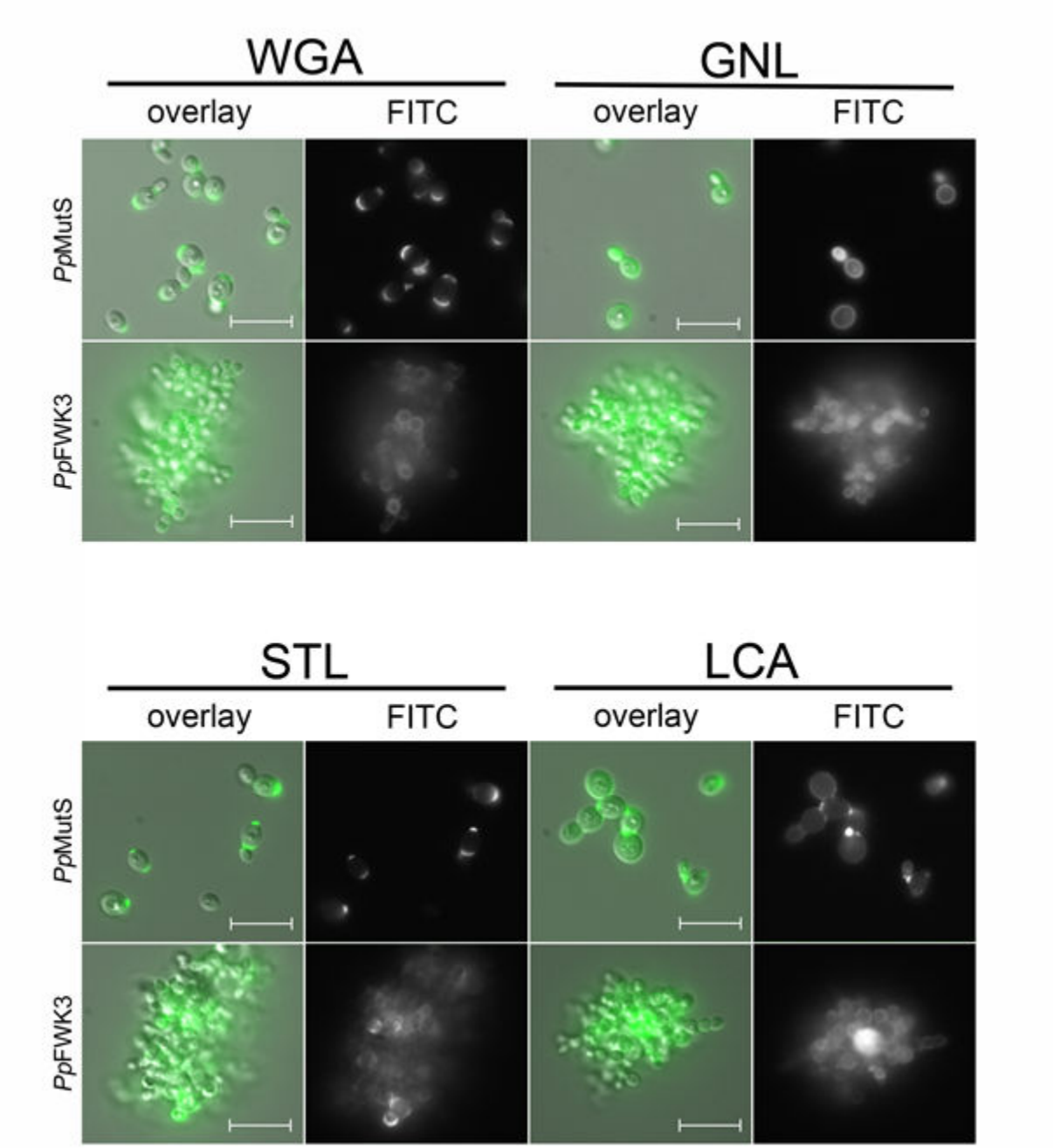

Figure 37: Lectin based glycoprofiling of surface carbohydrate motifs in *Pp*MutS and *Pp*FWK3. Live cells harvested in the exponential growth phase of batch cultivation were incubated with fluorescein labeled. Micrographs show the isolated channel for FITC detection and merged images with DIC (overlay). Scale bars represent 10µm.

In order to assess whether a mere alteration in the steric accessibility of chitin chains in the lateral wall was responsible for the difference in the WGA staining behavior or whether chitin was actually specifically localized at bud scars, *Pp*MutS cells were subjected to the same fluorescence microscopic analysis after treatment with concentrated methanol, leading to denaturation of mannoproteins and a substantial increase in cell wall permeability (37). The efficiency of the cell wall permeabilization protocol was validated by concomitant incubation with a usually non-membrane penetrating DAPI dye, which could readily access the nuclear space after methanol treatment. Still, methanol permeabilized *Pp*MutS cells displayed only the conventional, bud scar selective staining pattern, contrasting to the generalized binding of GNL, which served as a control (**Fehler! Verweisquelle konnte nicht gefunden werden.**).

Quantitatively, comparative overall ratios of WGA/FM® 4-64 were found for *Pp*MutS and the *och1* knockout strain *Pp*FWK3 (Figure 38), indicating that mainly a spatial redistribution of chitin may be induced by altering the glycosylation machinery, but without general enhancement of the total cellular chitin level. In other words, the rather high chitin concentration at the bud scars in *Pp*MutS seemed to be reduced in favor of an increased chitin deposition in the lateral cell walls of *Pp*FWK3. These results were also confirmed via the chitin binding lectin STL, which has a similar carbohydrate specificity profile as WGA but only limited affinity to isolated GlcNAc residues (Figure 38).

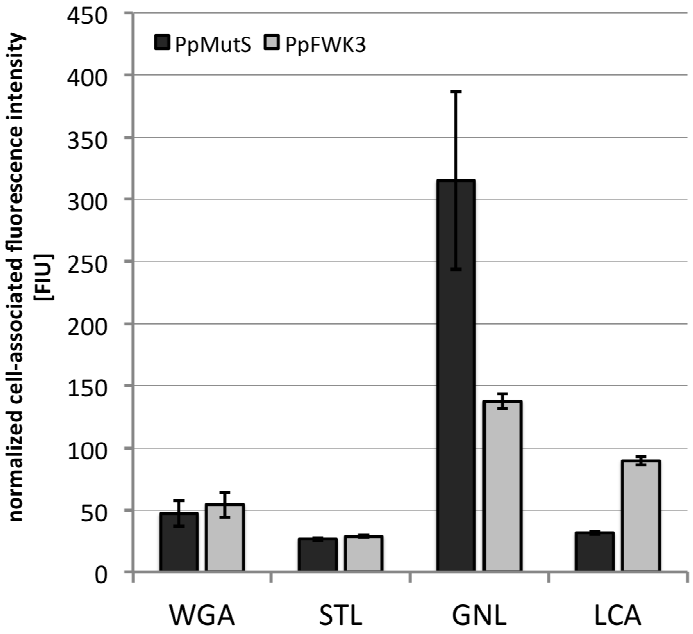

Figure 38: Quantitative determination of lectin binding on *Pp*MutS and *Pp*FWK3 cells. Cell suspensions adjusted to the same concentration level were incubated with FITC labeled lectins. After thorough washing, cells were lysed and the fluorescence intensity of the lysis buffer recorded. Binding data was normalized to the average cellular content of FM® 4-64, which was shown to be similar in both strains via FACS analysis. Values represent mean±SD of three independent experiments.

Inactivation of the Och1p activity shifted the interaction capacity of mannose specific lectins

Corresponding to the expected functional impact of a lack of Och1p activity, the *och1* knockout cells of the *Pp*FWK3 strain displayed a lower binding capacity for GNL than *Pp*MutS cells (Figure 38). GNL interacts with high mannose N-glycans and preferably reacts with α-1,3-Man residues, but also binds to α-1,6 linked Man residues (38, 39). In the current study, the GNL/FM® 4-64 ratio was reduced by 50% in *Pp*FWK3 as compared to *Pp*MutS, but still remained the lectin with highest binding capacity for this strain (Figure 38). In striking contrast, the binding levels of LCA were increased upon *och1* knockout (Figure 38).

Both, GNL and LCA showed an equal distribution across the entire cell wall (Figure 37), corresponding to the established localization of their putative targets.

Enzyme characterization

In order to demonstrate the successful decrease of heterogeneity in the glycosylation of either HRP1 or HRP2 when produced in an *och1* knockout strain, SEC was performed (Figure 39). A SEC elution profile has higher specificity and sensitivity than an image of a sodium dodecyl sulfate polyacrylamide gel and was therefore preferably used for this purpose. HRP1 produced in *Pp*MutS^{HRP1} eluted with higher heterogeneity and at large sizer than HRP1 produced in *Pp*FWK3^{HRP1}. Also, HRP2 showed higher heterogeneity when produced in *Pp*MutS^{HRP2}. However, the major glycol-species of HRP2 produced in *Pp*MutS^{HRP2} eluted at the same size as HRP2 produced in *Pp*FWK3^{HRP2}.

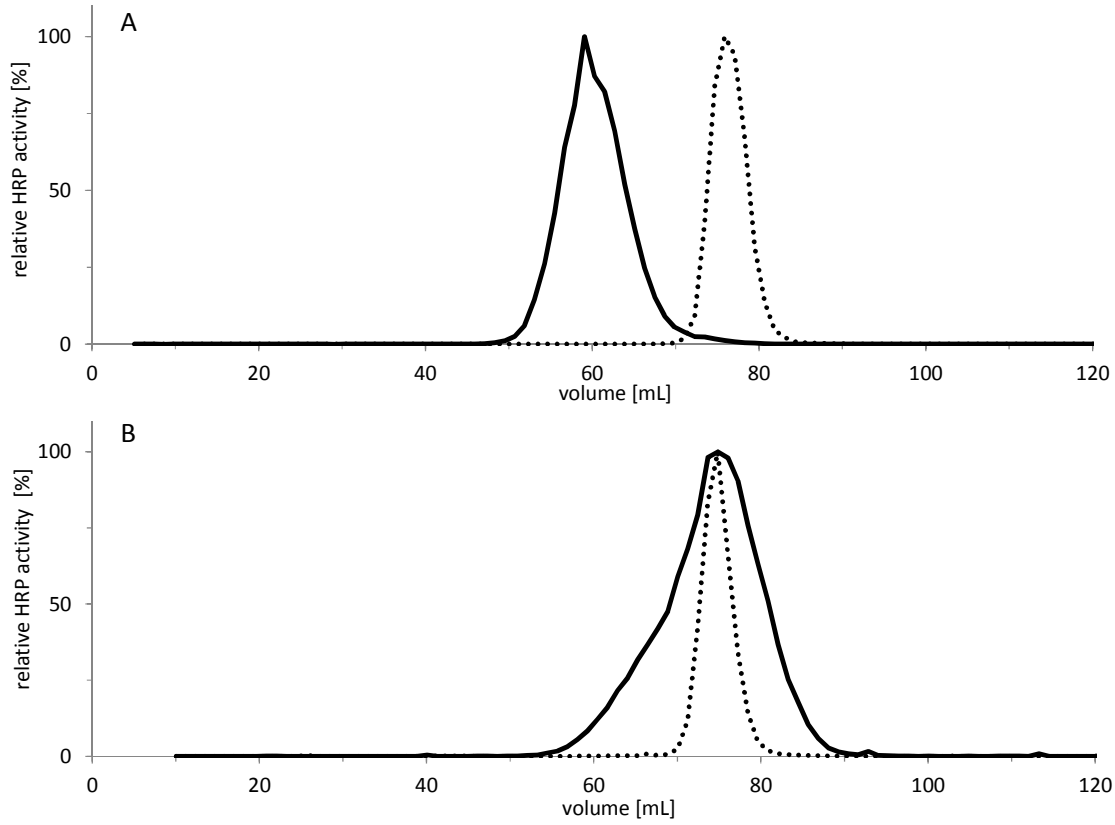

Figure 39: Size exclusion chromatograms of HRP1 and HRP2 glycovariants. A, HRP1; HRP1 produced in *Pp*MutS^{HRP1}, solid line; HRP1 produced in *Pp*FWK3^{HRP1}, dashed line. B, HRP2; HRP2 produced in *Pp*MutS^{HRP2}, solid line; HRP2 produced in *Pp*FWK3^{HRP2}. The measured HRP activities per fraction are shown as relative activities with the respective maximum activities set to 100%.

Judging by the size exclusion chromatograms (Figure 39), HRP produced in a *Pp*MutS^{HRP} strain significantly differed in its surface glysosylation pattern compared to HRP produced in a *Pp*FWK3^{HRP} strain, which showed a much higher homogeneity.

To check whether the kinetic constants or the stability of the enzyme were affected by the altered glycosylation pattern, we exemplarily characterized partially purified preparations of HRP2. HRP2 preparations produced by either *Pp*MutS^{HRP2} or *Pp*FWK3^{HRP2} in bioreactor

cultivations were purified by using a recently described strategy for HRP isoenzyme C1A (32). Both HRP2 preparations did not bind to the mixed mode HCIC resin but were found in the flowthrough, *i.e.* 93% of HRP2 produced in *Pp*MutS^{HRP2} and 87% of HRP2 produced in *Pp*FWK3^{HRP2}. Contaminating proteins were retained on the resin, leading to a partial purification at a factor of approximately two for both enzyme solutions. After purification, the fractions with the highest purification factor were pooled and ultrafiltrated. The enzyme HRP2 produced in *Pp*MutS^{HRP2} was concentrated to around 3.0mg.mL^{-1}, whereas HRP2 produced in *Pp*FWK3^{HRP2} could not be concentrated due to the immediate formation of precipitates during ultrafiltration and the resulting clogging of the membrane, indicating a reduced stability of this enzyme preparation.

We determined the kinetic constants for both enzyme preparations with H_2O_2 as electron donor at saturating concentration and ABTS as electron acceptor in varying concentrations (Table 17; Supplementary Figure 6).

Table 17: Enzymatic characterization of homogeneously glycosylated HRP2. Kinetic constants of HRP2 produced in either *Pp*MutS^{HRP2} or *Pp*FWK3^{HRP2}.

production strain	K_M [mM]	k_{cat} [s^{-1}]	k_{cat}/K_M [$s^{-1}.mM^{-1}$]	$\tau_{1/2}$ [s]
*Pp*MutS^{HRP2}	2.4	0.82	0.34	384
*Pp*FWK3^{HRP2}	2.0	0.67	0.34	198

As shown in Table 17 the kinetic constants of HRP2 were not significantly altered by its homogenized glycosylation pattern.

The stability of the produced HRP2 glycovariants at 60°C was studied by determination of the half life times ($\tau_{1/2}$) (Table 5, Supplementary Figure 7; (33)). Although the missing glycans on the surface of the recombinant enzyme did not affect the catalytic behaviour, the enzyme's thermostability was reduced by around 50%.

Discussion

Despite the numerous advantages of using *P. pastoris* as a host organism for recombinant protein production, its inherent heterogeneous yeast type hyperglycosylation of secreted proteins was usually addressed by extensive and elaborated strain modifications. Here, we present a straight forward approach for the generation of a wildtype based *P. pastoris* platform strain that allowed the production of more homogeneously glycosylated recombinant proteins due to an irreversible deletion of the *OCH1* gene.

Yeast hypermannosylation largely depends on the initial activity of an α-1,6-mannosyltransferase in the Golgi apparatus. Elimination of this activity was achieved by replacement of the *OCH1* ORF with a single 34bp *FRT* site by using a flipper cassette. However, this approach required double homologous recombination at the correct locus in the genome. Unfortunately, homologous integration events only play a minor part in *P. pastoris*, as recently demonstrated by Näätsaari *et al.* (21) and which was found to be especially true for the *OCH1* locus by Vervecken *et al.* (10). A new *P. pastoris* strain with inactivated non-homologous end joining pathway, *Pp*ku70-, proved to be a particularly convenient tool to identify the phenotype of the specific knockout strain in this study. Since homologous integration was the sole possibility for recombination events in the *Pp*ku70- strain, the total number of positive transformants was predominantly made up by transformants with homologous integration. The fact that particularly few colonies were obtained by targeting of

the transformed flipper cassette to the *OCH1* locus when using the *Pp*ku70- strain also supported the hypothesis of increased difficulty of homologous recombination in that locus.

An *och1* knockout strain of *S. cerevisiae* was described to show several defects such as impaired budding and increased temperature sensitivity (11). Choi *et al.* mentioned temperature sensitivity and increased flocculation for their *P. pastoris och1* knockout strain (13), but neither them nor Vervecken *et al.* (10) described any further severe growth defects. Surprisingly, the *och1* knockout strain in this study was found to show not only formation of cell clusters and temperature sensitivity, but also decreased growth which might be due to an impaired cell wall structure and thus complicated bud formation. Explanations for these divergent findings remain speculative, but might be due to single nucleotide polymorphisms and hence different strain backgrounds. Also, a secondary integration event of the transformed flipper cassette cannot be completely excluded. However, considering that as little as 100ng of the cassette were transformed and that all clones that exposed the described phenotype had the correct integration of the cassette in the *OCH1* locus indicates that the observed phenotype can be ascribed rather to the knockout of *OCH1* than to any additional genomic rearrangement. Also, the similarity of the observed phenotype in the present *P. pastoris och1* knockout strain to the phenotype described for a *S. cerevisiae och1* knockout strain (11) very much suggests that the deletion of the *OCH1* gene is actually responsible for the phenotype observed in this study. Most strikingly, reintroduction of the wildtype *OCH1* gene to the *och1* knockout strain *Pp*FWK3 restored its phenotype, thus conclusively linking the observed phenotype of *Pp*FWK3 to the deletion of the *OCH1* gene.

Transformation of the *och1* knockout strain with a linearized vector harboring an expression cassette for the production of HRP isoenzymes via electroporation was found to result in lower transformation efficiency than electroporation of a *P. pastoris* wildtype strain. This

increased sensitivity to electroporation might be another reflection of the altered cell wall composition that could be shown by lectin based glycoprofiling.

The detailed characterization of the different *P. pastoris* strains in the bioreactor revealed that the *och1* knockout strains were physiologically impaired compared to their wildtype equivalents. During the consecutive pulses, the carbon dioxide yield $Y_{CO2/S}$ and the C-balances constantly decreased, indicating a loss in metabolic activity. This was also apparent in the CER signals during the single methanol pulses (Supplementary Figure 3 and 4). At the beginning of the cultivation, methanol was metabolized much faster than during later methanol pulses. We followed the morphology of the *P. pastoris* cells during cultivations via microscopy and identified formation of cell clusters by the *och1* knockout strains. Obviously, the altered surface glycosylation of *och1* knockout cells also affected the budding process. Instead of budding off, the daughter cells stayed attached to the mother cell. The microscopically observed increased tendency for cluster formation may be regarded an effect which is intrinsically linked to the loss of the polymannan layer upon Och1p inactivation. Cell disruption experiments showed that neither treatment with Triton X-100, 0.5% EDTA or 5M urea, nor extensive mechanic shearing via sonication allowed breaking the clusters to single cells. Thus, we concluded that deficiencies in the constitutive cell division machinery upon Och1p inactivation led to a strong, covalent linkage between the cell walls, which remained intact even after the end of the normal budding process. The exact nature of this linkage remains speculative at the current point, but may be associated to aberrant glycosylation steps in the glycan backbone, occurring as a compensatory adaptation to the lack of Och1p activity (36, 40). Due to these very dense and compact formations we hypothesize that the cells in the center of these clusters became limited in oxygen and nutrients and showed no more metabolic activity. Since these cell clusters increased in size over time, the overall metabolic activity of the total amount of cells in the bioreactor decreased, which we observed in

decreasing $Y_{CO2/S}$ and C-balances. However, these cell clusters were still able to produce recombinant proteins. In fact, both the specific productivity and the volumetric productivity, the main focus of industrial bioprocesses, for the HRP isoenzyme were only reduced by 35% and 30%, respectively, compared to the *P. pastoris* strain with an intact *OCH1* gene. However, due to the constant decrease in metabolic activity over time, use of the *och1* knockout strain in industrial processes will require considerable modifications to current standard protocols to optimize recombinant protein production in this strain.

The highly specific interaction of WGA with the exposed chitin ring of bud scars (41) has previously been reported for other yeasts and can be used for the precise determination of the number of cell divisions performed by a mother cell (42, 43). To the best of our knowledge, this is the first confirmation of this structure-related specificity for *P. pastoris*. However, in the *och1* knockout strain, we noticed an almost complete loss of bud scar selectivity. The reasons for the regionally diverse distribution in *Pp*FWK3 may either lie in an increased accessibility of previously cryptic chitin chains in the lateral cell wall (*i.e.* when the protective polymannan layer is missing), or in an actively increased chitin synthesis and deposition at the cell wall, *i.e.* as a compensatory response to the cell wall stress caused by the impaired barrier function. Such stimulation of counterregulatory pathways upon impairment of cell wall integrity has been observed in several yeast species (44, 45) and involves diverse mechanisms and signaling cascades (46), which are believed to be directly or indirectly connected to the deletion of Och1p activity (36). Especially the osmotic stress exerted on the cell as a result of the impaired cell wall integrity is known to present an important factor for the induction of counterregulatory pathways (47). Due to the persistence of bud scar specific binding of WGA in methanol treated *Pp*MutS cells, we concluded that the strong affinity of WGA to the overall cell wall of *Pp*FWK3 cells traced back to a *de novo* deposition of carbohydrate epitopes (most probably chitin) in this *och1* knockout strain, and not an increased exposure of

constitutive cell wall glycans that are invariably present but usually shielded by an outer chain hypermannan structure in wildtype. The somewhat reduced STL/FM® 4-64 ratio compared to the WGA/FM® 4-64 ratio may be connected to the minor differences regarding the preferential binding ligand. Based on the similarity between STL and WGA staining patterns, it is unlikely, that any GlcNAc motifs other than chitin (*e.g.* in the core glycan of mannoproteins) were the primary binding epitopes detected by either of the two lectins. As a side aspect of the current work, we were able to demonstrate the use of fluorescence labeled lectins as convenient and versatile probes for visualizing stress responses derived from impaired cell wall integrity in yeast.

The decreased GNL/FM® 4-64 ratio of *Pp*FWK3 compared to *Pp*MutS could be explained by the minimized amount of high mannose N-glycans and the therefore inherently lower amount of potential GNL target ligands (*i.e.* α-1,3- and α-1,6-Man residues) of *Pp*FWK3 compared to *Pp*MutS. Nevertheless, the remaining core glycan provided sufficient GNL targets for a distinct signal. The increased LCA/FM® 4-64 signal of *Pp*FWK3 on the other hand, may be explained by the preference of this lectin for short chain X-α-1,2-Man–Man motifs, with X representing either α-Man or β-GlcNAc (48). In mannoproteins, such short motifs may be found in the core glycans, the accessibility of which may be enhanced in absence of the usually highly branched polymannan structures of a wildtype strain (44, 45).

When we analyzed the HRP isoenzymes produced by either a *Pp*MutS^{HRP} strain or the *och1* knockout strain *Pp*FWK3^{HRP}, we found the enzyme preparation from *Pp*FWK3^{HRP} to be significantly more homogenously glycosylated. By performing SEC, both HRP1 and HRP2 eluted approximately at the same size when produced in a *Pp*FWK3^{HRP} strain, in contrast to production in a *Pp*MutS^{HRP} strain, pointing out a clear benefit of using this *och1* knockout *P. pastoris* platform strain.

Enzymatic characterizations of HRP2 revealed decreased stability at 60°C for the homogeneously glycosylated HRP2 compared to the more heterogeneously hyperglycosylated glycovariant. However, catalytic activity was not impaired, indicating that the common yeast type hyperglycosylation only had a thermostabilizing effect on the tested HRP isoenzyme.

The ability of recombinant protein production in *P. pastoris* with a uniform glycosylation pattern not only goes along with Quality by Design (QbD) principles but also allows the development of specific purification and application strategies and thus constitutes a major advantage over wildtype based production.

Conclusions

In conclusion, we irreversibly eliminated the *OCH1* encoded α-1,6-mannosyltransferase activity of *P. pastoris*. The phenotype of the generated *och1* knockout platform strain resembled the phenotype described for *S. cerevisiae*. Nevertheless, the strain was successfully employed for the production of recombinant HRPs as reporter enzymes. Strain specific parameters were determined in comparative bioreactor cultivations. Recombinant HRP from either an unaltered *P. pastoris* strain or the *och1* knockout strain were purified and enzymatically characterized. In summary, the main findings are:

● The *och1* knockout strains were characterized by slow growth, temperature sensitivity and formation of cell clusters. The altered N-glycosylation pathway and resultant structural impacts in the *Pp*FWK3 strain triggered the dynamic reorganization of surface mannose residues and other glycan structures. The cellular response seemed to be more diverse than just a simple lack of an outer chain hypermannan structure, and may also involve secondary counterregulatory mechanisms on the metabolic or structural level (36, 40). Our results in this regard go in direct agreement with previous work on *och1* deletion strains of *S. cerevisiae* (35,

49). Lectin based glycoprofiling represented a rapid and reliable method to provide functional proof for successful deletion of Och1p activity in *P. pastoris*.

● During the consecutive methanol pulses, the *och1* knockout strains lost their metabolic activity due to the formation of cell clusters, thus making the adaption of current production processes necessary.

● The produced recombinant enzyme exhibited a more homogeneous surface glycosylation which is beneficial for subsequent downstream processing and applications.

● Despite the reduced stability at 60°C of the homogeneously glycosylated HRP, its catalytic activity remained unimpaired, rendering the enzyme suitable for most applications.

Here, we report the thorough biotechnological characterization of a *P. pastoris* platform strain that allows the production of recombinant proteins with significantly increased homogeneity in their glycosylation pattern due to an irreversible knockout of the *OCH1* gene. Currently, efforts are driven forward to elucidate the potential benefits of the cell morphological changes in glycoengineered *P. pastoris* strains for the expression of recombinant proteins (50), in addition to the widely established significance for the product itself (*e.g.* (51)), which could be further underlined in this study. Also, future studies will focus on rescuing the growth impaired phenotype to generate a strain that shares the favorable growth phenotype of a wildtype strain but still allows for the production of homogeneously glycosylated secreted proteins.

Acknowledgments

The authors are very grateful to the Austrian Science Fund (FWF): project P24861-B19 and FWF W901 DK Molecular Enzymology for financial support. We would like to thank

Michaela Gerstmann, Astrid Weninger and Karl Metzger for excellent technical assistance in the lab.

References

1. Hasslacher, M., Schall, M., Hayn, M., Bona, R., Rumbold, K., Lückl, J., Griengl, H., Kohlwein, S. D., and Schwab, H. (1997) High-level intracellular expression of hydroxynitrile lyase from the tropical rubber tree Hevea brasiliensis in microbial hosts. *Protein expression and purification* **11**, 61–71 [online] http://www.ncbi.nlm.nih.gov/pubmed/9325140.

2. Werten, M. W., Van den Bosch, T. J., Wind, R. D., Mooibroek, H., and De Wolf, F. A. (1999) High-yield secretion of recombinant gelatins by Pichia pastoris. *Yeast (Chichester, England)* **15**, 1087–1096 [online] http://www.ncbi.nlm.nih.gov/pubmed/10455232.

3. Jahic, M., Rotticci-Mulder, J. C., Martinelle, M., Hult, K., and Enfors, S.-O. (2002) Modeling of growth and energy metabolism of Pichia pastoris producing a fusion protein. *Bioprocess and Biosystems Engineering* **24**, 385–393 [online] http://www.springerlink.com/openurl.asp?genre=article&id=doi:10.1007/s00449-001-0274-5 (Accessed February 4, 2013).

4. Lin-Cereghino, G. P., Lin-Cereghino, J., Ilgen, C., and Cregg, J. M. (2002) Production of recombinant proteins in fermenter cultures of the yeast Pichia pastoris. *Current*

opinion in biotechnology **13**, 329–332 [online] http://www.ncbi.nlm.nih.gov/pubmed/12323354 (Accessed February 8, 2011).

5. Parekh, R. B. (1991) Effects of glycosylation on protein function. *Current Opinion in Structural Biology* **1**, 750–754 [online] http://linkinghub.elsevier.com/retrieve/pii/0959440X9190174R (Accessed March 29, 2013).

6. Ryckaert, S., Martens, V., De Vusser, K., and Contreras, R. (2005) Development of a S. cerevisiae whole cell biocatalyst for in vitro sialylation of oligosaccharides. *Journal of biotechnology* **119**, 379–388 [online] http://www.ncbi.nlm.nih.gov/pubmed/15982773 (Accessed March 29, 2013).

7. Wildt, S., and Gerngross, T. U. (2005) The humanization of N-glycosylation pathways in yeast. *Nature reviews. Microbiology* **3**, 119–128 [online] http://www.ncbi.nlm.nih.gov/pubmed/15685223 (Accessed October 25, 2012).

8. Hamilton, S. R., and Gerngross, T. U. (2007) Glycosylation engineering in yeast: the advent of fully humanized yeast. *Current opinion in biotechnology* **18**, 387–392 [online] http://www.ncbi.nlm.nih.gov/pubmed/17951046.

9. De Pourcq, K., De Schutter, K., and Callewaert, N. (2010) Engineering of glycosylation in yeast and other fungi: current state and perspectives. *Applied microbiology and biotechnology* **87**, 1617–1631 [online] http://www.ncbi.nlm.nih.gov/pubmed/20585772 (Accessed May 25, 2012).

10. Vervecken, W., Kaigorodov, V., Callewaert, N., Geysens, S., De Vusser, K., and Contreras, R. (2004) In vivo synthesis of mammalian-like, hybrid-type N-glycans in Pichia pastoris. *Applied and environmental microbiology* **70**, 2639–2646 [online]

http://www.pubmedcentral.nih.gov/articlerender.fcgi?artid=404441&tool=pmcentrez&rendertype=abstract (Accessed March 15, 2012).

11. Nagasu, T., Shimma, Y., Nakanishi, Y., Kuromitsu, J., Iwama, K., Nakayama, K., Suzuki, K., and Jigami, Y. (1992) Isolation of new temperature-sensitive mutants of Saccharomyces cerevisiae deficient in mannose outer chain elongation. *Yeast (Chichester, England)* **8**, 535–547 [online] http://www.ncbi.nlm.nih.gov/pubmed/1523886.

12. Nakayama, K., Nagasu, T., Shimma, Y., Kuromitsu, J., and Jigami, Y. (1992) OCH1 encodes a novel membrane bound mannosyltransferase: outer chain elongation of asparagine-linked oligosaccharides. *The EMBO journal* **11**, 2511–2519 [online] http://www.pubmedcentral.nih.gov/articlerender.fcgi?artid=556726&tool=pmcentrez&rendertype=abstract (Accessed February 6, 2013).

13. Choi, B.-K., Bobrowicz, P., Davidson, R. C., Hamilton, S. R., Kung, D. H., Li, H., Miele, R. G., Nett, J. H., Wildt, S., and Gerngross, T. U. (2003) Use of combinatorial genetic libraries to humanize N-linked glycosylation in the yeast Pichia pastoris. *Proceedings of the National Academy of Sciences of the United States of America* **100**, 5022–5027 [online] http://www.pubmedcentral.nih.gov/articlerender.fcgi?artid=2872472&tool=pmcentrez&rendertype=abstract.

14. Mille, C., Bobrowicz, P., Trinel, P.-A., Li, H., Maes, E., Guerardel, Y., Fradin, C., Martínez-Esparza, M., Davidson, R. C., Janbon, G., Poulain, D., and Wildt, S. (2008) Identification of a new family of genes involved in beta-1,2-mannosylation of glycans in Pichia pastoris and Candida albicans. *The Journal of biological chemistry* **283**,

9724–9736 [online] http://www.ncbi.nlm.nih.gov/pubmed/18234669 (Accessed February 5, 2013).

15. Nett, J. H., Stadheim, T. A., Li, H., Bobrowicz, P., Hamilton, S. R., Davidson, R. C., Choi, B., Mitchell, T., Bobrowicz, B., Rittenhour, A., Wildt, S., and Gerngross, T. U. (2011) A combinatorial genetic library approach to target heterologous glycosylation enzymes to the endoplasmic reticulum or the Golgi apparatus of Pichia pastoris. *Yeast (Chichester, England)* **28**, 237–252 [online] http://www.ncbi.nlm.nih.gov/pubmed/21360735 (Accessed March 15, 2012).

16. Hamilton, S. R., Bobrowicz, P., Bobrowicz, B., Davidson, R. C., Li, H., Mitchell, T., Nett, J. H., Rausch, S., Stadheim, T. A., Wischnewski, H., Wildt, S., and Gerngross, T. U. (2003) Production of complex human glycoproteins in yeast. *Science (New York, N.Y.)* **301**, 1244–1246 [online] http://www.ncbi.nlm.nih.gov/pubmed/12947202 (Accessed October 7, 2012).

17. Jacobs, P. P., Geysens, S., Vervecken, W., Contreras, R., and Callewaert, N. (2009) Engineering complex-type N-glycosylation in Pichia pastoris using GlycoSwitch technology. *Nature protocols* **4**, 58–70 [online] http://www.ncbi.nlm.nih.gov/pubmed/19131957 (Accessed October 5, 2012).

18. Hamilton, S. R., Davidson, R. C., Sethuraman, N., Nett, J. H., Jiang, Y., Rios, S., Bobrowicz, P., Stadheim, T. a, Li, H., Choi, B.-K., Hopkins, D., Wischnewski, H., Roser, J., Mitchell, T., Strawbridge, R. R., Hoopes, J., Wildt, S., and Gerngross, T. U. (2006) Humanization of yeast to produce complex terminally sialylated glycoproteins. *Science (New York, N.Y.)* **313**, 1441–1443 [online] http://www.ncbi.nlm.nih.gov/pubmed/16960007 (Accessed February 19, 2013).

19. Veitch, N. C. (2004) Horseradish peroxidase: a modern view of a classic enzyme. *Phytochemistry* **65**, 249–59 [online] http://www.ncbi.nlm.nih.gov/pubmed/14751298 (Accessed January 20, 2011).

20. Ausubel, F. M., Brent, R., Kingston, R. E., Moore, D. D., Seidman, J. G., Smith, J. A., and Struhl, K. (eds.) (2001) *Current Protocols in Molecular Biology*, John Wiley & Sons, Inc., Hoboken, NJ, USA [online] http://doi.wiley.com/10.1002/0471142727 (Accessed February 20, 2013).

21. Näätsaari, L., Mistlberger, B., Ruth, C., Hajek, T., Hartner, F. S., and Glieder, A. (2012) Deletion of the Pichia pastoris KU70 Homologue Facilitates Platform Strain Generation for Gene Expression and Synthetic Biology. *PloS one* **7**, e39720 [online] http://www.ncbi.nlm.nih.gov/pubmed/22768112 (Accessed July 7, 2012).

22. Krainer, F. W., Dietzsch, C., Hajek, T., Herwig, C., Spadiut, O., and Glieder, A. (2012) Recombinant protein expression in Pichia pastoris strains with an engineered methanol utilization pathway. *Microbial cell factories* **11**, 22–35 [online] http://www.microbialcellfactories.com/content/11/1/22 (Accessed March 6, 2012).

23. Küberl, A., Schneider, J., Thallinger, G. G., Anderl, I., Wibberg, D., Hajek, T., Jaenicke, S., Brinkrolf, K., Goesmann, A., Szczepanowski, R., Pühler, A., Schwab, H., Glieder, A., and Pichler, H. (2011) High-quality genome sequence of Pichia pastoris CBS7435. *Journal of biotechnology* **154**, 312–320 [online] http://www.ncbi.nlm.nih.gov/pubmed/21575661 (Accessed June 20, 2011).

24. Harju, S., Fedosyuk, H., and Peterson, K. R. (2004) Rapid isolation of yeast genomic DNA: Bust n' Grab. *BMC biotechnology* **4:8** [online]

http://www.pubmedcentral.nih.gov/articlerender.fcgi?artid=406510&tool=pmcentrez&rendertype=abstract (Accessed February 3, 2011).

25. Lin-Cereghino, J., Wong, W. W., Xiong, S., Giang, W., Luong, L. T., Vu, J., Johnson, S. D., and Lin-Cereghino, G. P. (2005) Condensed protocol for competent cell preparation and transformation of the methylotrophic yeast Pichia pastoris. *BioTechniques* **38**, 44–48 [online] http://www.pubmedcentral.nih.gov/articlerender.fcgi?artid=2504082&tool=pmcentrez&rendertype=abstract (Accessed October 18, 2011).

26. Gibson, D. G., Young, L., Chuang, R., Venter, J. C., Hutchison, C. A., and Smith, H. O. (2009) Enzymatic assembly of DNA molecules up to several hundred kilobases. *Nature methods* **6**, 343–5 [online] http://www.ncbi.nlm.nih.gov/pubmed/19363495 (Accessed November 24, 2012).

27. Weis, R., Luiten, R., Skranc, W., Schwab, H., Wubbolts, M., and Glieder, A. (2004) Reliable high-throughput screening with Pichia pastoris by limiting yeast cell death phenomena. *FEMS yeast research* **5**, 179–89 [online] http://www.ncbi.nlm.nih.gov/pubmed/15489201 (Accessed November 8, 2010).

28. Morawski, B., Lin, Z., Cirino, P., Joo, H., Bandara, G., and Arnold, F. H. (2000) Functional expression of horseradish peroxidase in Saccharomyces cerevisiae and Pichia pastoris. *Protein engineering* **13**, 377–84 [online] http://www.ncbi.nlm.nih.gov/pubmed/10835112.

29. Abad, S., Kitz, K., Hörmann, A., Schreiner, U., Hartner, F. S., and Glieder, A. (2010) Real-time PCR-based determination of gene copy numbers in Pichia pastoris.

Biotechnology journal **5**, 413–20 [online] http://www.ncbi.nlm.nih.gov/pubmed/20349461 (Accessed August 23, 2010).

30. Dietzsch, C., Spadiut, O., and Herwig, C. (2011) A dynamic method based on the specific substrate uptake rate to set up a feeding strategy for Pichia pastoris. *Microbial cell factories* **10**, 14 [online] http://www.pubmedcentral.nih.gov/articlerender.fcgi?artid=3059269&tool=pmcentrez&rendertype=abstract (Accessed September 6, 2011).

31. Dietzsch, C., Spadiut, O., and Herwig, C. (2011) A fast approach to determine a fed batch feeding profile for recombinant Pichia pastoris strains. *Microbial cell factories* **10**, 85 [online] http://www.pubmedcentral.nih.gov/articlerender.fcgi?artid=3214193&tool=pmcentrez&rendertype=abstract (Accessed March 7, 2013).

32. Spadiut, O., Rossetti, L., Dietzsch, C., and Herwig, C. (2012) Purification of a recombinant plant peroxidase produced in Pichia pastoris by a simple 2-step strategy. *Protein expression and purification* [online] http://www.ncbi.nlm.nih.gov/pubmed/23026679 (Accessed October 5, 2012).

33. Spadiut, O., Leitner, C., Salaheddin, C., Varga, B., Vertessy, B. G., Tan, T.-C., Divne, C., and Haltrich, D. (2009) Improving thermostability and catalytic activity of pyranose 2-oxidase from Trametes multicolor by rational and semi-rational design. *The FEBS journal* **276**, 776–792 [online] http://www.ncbi.nlm.nih.gov/pubmed/19143837 (Accessed March 28, 2013).

34. Zalai, D., Dietzsch, C., Herwig, C., and Spadiut, O. (2012) A dynamic fed batch strategy for a Pichia pastoris mixed feed system to increase process understanding.

Biotechnology progress **28**, 878–86 [online] http://www.ncbi.nlm.nih.gov/pubmed/22505140 (Accessed March 7, 2013).

35. Zhou, J., Zhang, H., Liu, X., Wang, P. G., and Qi, Q. (2007) Influence of N-glycosylation on Saccharomyces cerevisiae morphology: a golgi glycosylation mutant shows cell division defects. *Current microbiology* **55**, 198–204 [online] http://www.ncbi.nlm.nih.gov/pubmed/17661134 (Accessed March 14, 2013).

36. Lee, B. N., and Elion, E. A. (1999) The MAPKKK Ste11 regulates vegetative growth through a kinase cascade of shared signaling components. *Proceedings of the National Academy of Sciences of the United States of America* **96**, 12679–84 [online] http://www.pubmedcentral.nih.gov/articlerender.fcgi?artid=23046&tool=pmcentrez&rendertype=abstract.

37. Weiler, F., and Schmidt, M. J. (2003) *Non-conventional yeasts in genetics, biochemistry and biotechnology* (Wolf, K., Breunig, K., and Barth, G., eds.), Springer Berlin Heidelberg, Berlin, Heidelberg [online] http://www.springerlink.com/index/10.1007/978-3-642-55758-3 (Accessed April 16, 2013).

38. Shibuya, N., Goldstein, I. J., Van Damme, E. J., and Peumans, W. J. (1988) Binding properties of a mannose-specific lectin from the snowdrop (Galanthus nivalis) bulb. *The Journal of biological chemistry* **263**, 728–734 [online] http://www.ncbi.nlm.nih.gov/pubmed/3335522 (Accessed April 25, 2013).

39. Fouquaert, E., Smith, D. F., Peumans, W. J., Proost, P., Balzarini, J., Savvides, S. N., and Damme, E. J. M. Van (2009) Related lectins from snowdrop and maize differ in their carbohydrate-binding specificity. *Biochemical and biophysical research*

communications **380**, 260–5 [online] http://www.pubmedcentral.nih.gov/articlerender.fcgi?artid=2681488&tool=pmcentrez&rendertype=abstract (Accessed April 25, 2013).

40. Hirayama, H., and Suzuki, T. (2011) Metabolism of free oligosaccharides is facilitated in the och1Δ mutant of Saccharomyces cerevisiae. *Glycobiology* **21**, 1341–8 [online] http://www.ncbi.nlm.nih.gov/pubmed/21622726 (Accessed April 11, 2013).

41. Cabib, E., and Bowers, B. (1971) Chitin and yeast budding. Localization of chitin in yeast bud scars. *The Journal of biological chemistry* **246**, 152–9 [online] http://www.ncbi.nlm.nih.gov/pubmed/5541754 (Accessed March 14, 2013).

42. Chen, C., Dewaele, S., Braeckman, B., Desmyter, L., Verstraelen, J., Borgonie, G., Vanfleteren, J., and Contreras, R. (2003) A high-throughput screening system for genes extending life-span. *Experimental gerontology* **38**, 1051–63 [online] http://linkinghub.elsevier.com/retrieve/pii/S0531556503001864 (Accessed April 11, 2013).

43. Chaudhari, R. D., Stenson, J. D., Overton, T. W., and Thomas, C. R. (2012) Effect of bud scars on the mechanical properties of Saccharomyces cerevisiae cell walls. *Chemical Engineering Science* **84**, 188–196 [online] http://linkinghub.elsevier.com/retrieve/pii/S0009250912005222 (Accessed April 11, 2013).

44. Lesage, G., and Bussey, H. (2006) Cell wall assembly in Saccharomyces cerevisiae. *Microbiology and molecular biology reviews : MMBR* **70**, 317–43 [online] http://www.pubmedcentral.nih.gov/articlerender.fcgi?artid=1489534&tool=pmcentrez&rendertype=abstract (Accessed March 2, 2013).

45. De Groot, P. W. J., Ram, A. F., and Klis, F. M. (2005) Features and functions of covalently linked proteins in fungal cell walls. *Fungal genetics and biology : FG & B* **42**, 657–75 [online] http://www.ncbi.nlm.nih.gov/pubmed/15896991 (Accessed March 6, 2013).

46. Klis, F. M., Boorsma, A., and De Groot, P. W. J. (2006) Cell wall construction in Saccharomyces cerevisiae. *Yeast (Chichester, England)* **23**, 185–202 [online] http://www.ncbi.nlm.nih.gov/pubmed/16498706 (Accessed February 27, 2013).

47. Kapteyn, J. C., Ram, A. F., Groos, E. M., Kollar, R., Montijn, R. C., Van Den Ende, H., Llobell, A., Cabib, E., and Klis, F. M. (1997) Altered extent of cross-linking of beta1,6-glucosylated mannoproteins to chitin in Saccharomyces cerevisiae mutants with reduced cell wall beta1,3-glucan content. *Journal of bacteriology* **179**, 6279–84 [online] http://www.pubmedcentral.nih.gov/articlerender.fcgi?artid=179540&tool=pmcentrez&rendertype=abstract (Accessed March 22, 2013).

48. Maupin, K. A., Liden, D., and Haab, B. B. (2012) The fine specificity of mannose-binding and galactose-binding lectins revealed using outlier motif analysis of glycan array data. *Glycobiology* **22**, 160–9 [online] http://www.pubmedcentral.nih.gov/articlerender.fcgi?artid=3230281&tool=pmcentrez&rendertype=abstract (Accessed April 11, 2013).

49. Nakanishi-Shindo, Y., Nakayama, K., Tanaka, A., Toda, Y., and Jigami, Y. (1993) Structure of the N-linked oligosaccharides that show the complete loss of alpha-1,6-polymannose outer chain from och1, och1 mnn1, and och1 mnn1 alg3 mutants of Saccharomyces cerevisiae. *The Journal of biological chemistry* **268**, 26338–26345 [online] http://www.ncbi.nlm.nih.gov/pubmed/8253757.

50. Jacobs, P. P., Ryckaert, S., Geysens, S., De Vusser, K., Callewaert, N., and Contreras, R. (2008) Pichia surface display: display of proteins on the surface of glycoengineered Pichia pastoris strains. *Biotechnology letters* **30**, 2173–2181 [online] http://www.ncbi.nlm.nih.gov/pubmed/18679585 (Accessed June 10, 2011).

51. Solá, R. J., and Griebenow, K. (2010) Glycosylation of therapeutic proteins: an effective strategy to optimize efficacy. *BioDrugs : clinical immunotherapeutics, biopharmaceuticals and gene therapy* **24**, 9–21 [online] http://www.pubmedcentral.nih.gov/articlerender.fcgi?artid=2805475&tool=pmcentrez&rendertype=abstract (Accessed April 22, 2013).